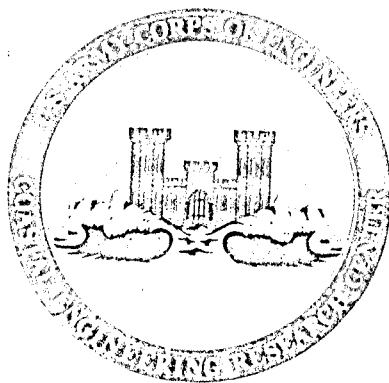# Hydrodynamic Damping
and "Added Mass" for
Flexible Offshore Platforms

by
Charles Petrauskas

TECHNICAL PAPER NO. 76-18
OCTOBER 1976

Prepared for

U.S. ARMY, CORPS OF ENGINEERS

COASTAL ENGINEERING
RESEARCH CENTER

Kingman Building
Fort Belvoir, Va. 22060

Reprint or republication of any of this material shall give appropriate credit to the U.S. Army Coastal Engineering Research Center.

Limited free distribution within the United States of single copies of this publication has been made by this Center. Additional copies are available from:

> *National Technical Information Service*
> *ATTN: Operations Division*
> *5285 Port Royal Road*
> *Springfield, Virginia 22151*

Contents of this report are not to be used for advertising, publication, or promotional purposes. Citation of trade names does not constitute an official endorsement or approval of the use of such commercial products.

The findings in this report are not to be construed as an official Department of the Army position unless so designated by other authorized documents.

REPORT DOCUMENTATION PAGE		READ INSTRUCTIONS BEFORE COMPLETING FORM
1. REPORT NUMBER TP 76-18	2. GOVT ACCESSION NO.	3. RECIPIENT'S CATALOG NUMBER
4. TITLE (and Subtitle) HYDRODYNAMIC DAMPING AND "ADDED MASS" FOR FLEXIBLE OFFSHORE PLATFORMS		5. TYPE OF REPORT & PERIOD COVERED Technical Paper
		6. PERFORMING ORG. REPORT NUMBER HEL 9-23
7. AUTHOR(s) Charles Petrauskas		8. CONTRACT OR GRANT NUMBER(s) DACW72-69-C-0001
9. PERFORMING ORGANIZATION NAME AND ADDRESS Department of the Army Coastal Engineering Research Center Kingman Building, Fort Belvoir, Va. 22060		10. PROGRAM ELEMENT, PROJECT, TASK AREA & WORK UNIT NUMBERS F31234
11. CONTROLLING OFFICE NAME AND ADDRESS Department of the Army Coastal Engineering Research Center (CERRE-OC) Kingman Building, Fort Belvoir, Va. 22060		12. REPORT DATE October 1976
		13. NUMBER OF PAGES 110
14. MONITORING AGENCY NAME & ADDRESS(If different from Controlling Office)		15. SECURITY CLASS. (of this report) UNCLASSIFIED
		15a. DECLASSIFICATION/DOWNGRADING SCHEDULE

16. DISTRIBUTION STATEMENT (of this Report)

17. DISTRIBUTION STATEMENT (of the abstract entered in Block 20, If different from Report)

Approved for public release, distribution unlimited.

18. SUPPLEMENTARY NOTES

19. KEY WORDS (Continue on reverse side if necessary and identify by block number)

"Added Mass"   Structural dynamics
Hydrodynamic damping   Wave forces
Offshore platforms   Wave-structure interaction

20. ABSTRACT (Continue on reverse side If necessary and identify by block number)

The dynamic response of deepwater flexible platforms due to wind-generated ocean waves appears to be an important design consideration; therefore, a theoretical and experimental study was made of hydrodynamic damping and "added mass."

Classical potential theory with linearized boundary conditions was used to study the hydrodynamic damping due to wavemaking and the coefficient of

(continued)

DD FORM 1473   EDITION OF 1 NOV 65 IS OBSOLETE
1 JAN 73

added mass on a vertical surface-piercing cylinder as a function of oscillation frequency, σ, cylinder diameter, D, water depth, h, and mode shape. The parameters, $\sigma^2 h/g$ and D/h, and the mode shape completely defined the nondimensionalized wavemaking and added-mass forces. It was found that for practical purposes the wavemaking force may be assumed to be localized in the near-surface zone and therefore dependent on only the parameter $\sigma\sqrt{D/g}$. The coefficient of added mass, in general, depends on both parameters and the mode shape. It also varies with elevation, but for practical purposes a uniform value of one can be used if D/h < 0.01. Damping for a number of proposed platforms was found negligible because the diameters in the near-surface zone were too small. To attain damping of 2 to 4 percent of critical would require, e.g., diameters greater than 30 feet in a 600-foot water depth for a platform with a natural period of 4 seconds.

Experiments were conducted to verify the results of potential theory. Rigid vertical cylinders were oscillated with simple-harmonic motion in calm water. Total forces and radiated waves were measured. They compared very well with theoretical values. Other investigators' data also verified the theory.

A small experimental study was made in an attempt to verify the hydrodynamic damping implied by the quasi-steady drag-force interaction term of the presently used modified Morison equation to represent the drag force on an oscillating cylinder in waves. Damping was measured for an elastically supported circular cylinder in a steady current. The measured values were up to 4 times lower than the theoretical values. The disagreement appears to be that the experiments were outside the range for which the quasi-steady assumption is valid. Coefficients of added mass were also measured and were found equal to the potential theory value irrespective of the velocity of the current.

PREFACE

This report is published to assist coastal engineers in the study of wave forces on structures. The work was carried out under the coastal construction research program of the U.S. Army Coastal Engineering Research Center (CERC).

This report is published, with only minor editing, as received from the contractor; results and conclusions are those of the author and do not necessarily represent those of CERC or the Corps of Engineers.

Comments on this publication are invited.

Approved for publication in accordance with Public Law 166, 79*th* Congress, approved 31 July 1945, as supplemented by Public Law 172, 88*th* Congress, approved 7 November 1963.

JOHN H. COUSINS
Colonel, Corps of Engineers
Commander and Director

CONTENTS

CONTENTS

FIGURES--Continued

CONTENTS

FIGURES--Continued

CONVERSION FACTORS, U. S. CUSTOMARY TO METRIC (SI) UNITS OF MEASUREMENT

U.S. customary units of measurement used in this report can be converted to metric (SI) units as follows:

Multiply	by	To obtain
inches	25.4	millimeters
	2.54	centimeters
square inches	6.452	square centimeters
cubic inches	16.39	cubic centimeters
feet	30.48	centimeters
	0.3048	meters
square feet	0.0929	square meters
cubic feet	0.0283	cubic meters
yards	0.9144	meters
square yards	0.836	square meters
cubic yards	0.7646	cubic meters
miles	1.6093	kilometers
square miles	259.0	hectares
acres	0.4047	hectares
foot-pounds	1.3558	newton meters
ounces	28.35	grams
pounds	453.6	grams
	0.4536	kilograms
ton, long	1.0160	metric tons
ton, short	0.9072	metric tons
degrees (angle)	0.1745	radians
Fahrenheit degrees	5/9	Celsius degrees or Kelvins[1]

[1] To obtain Celsius (C) temperature readings from Fahrenheit (F) readings, use formula: $C = (5/9)(F - 32)$. To obtain Kelvin (K) readings, use forumla: $K = (5/9)(F - 32) + 273.15$.

SYMBOLS AND DEFINITIONS

A	projected area of horizontal cylinder and flanges; equation (76)
a	cylinder radius
C_{am}	coefficient of "added mass"
C_D	coefficient of drag
C_I	coefficient of inertia
C_g	nondimensional amplitude of the total force on vertical cylinder due to a periodic incident wave; equation (60)
C_w	nondimensional amplitude of the total wavemaking force for translational mode of oscillation; equation (40)
$\widehat{C}_{am}$	C_{am} averaged over the water depth
C_w^*	generalized damping coefficient; equation (23)
C_s^*	generalized structural damping coefficient
D	cylinder diameter
DMF	dynamic magnification factor; equation (61)
F_o	$\sigma\sqrt{D/g}$
F_w	amplitude of the total wavemaking force for the translational mode of oscillation
F_v	amplitude of the total viscous force for the translational mode of oscillation
F_D	steady-state drag force
F^*	generalized hydrodynamic force acting on cylinder; equation (8)
F_G^*	generalized force due to incident wave; equation (20)
f	distributed hydrodynamic force acting on vertical cylinder
f_{am}	distributed "added-mass" force
f_w	distributed wavemaking force

8

f_g	distributed force due to incident wave
G	function of αmh and $\psi(y)$; equation (35)
G_0	function of kh and $\psi(y)$; equation (33)
g	acceleration of gravity
H	wave height
$H_1^{(1)}$, $H_1^{(1)'}$	Hankel function of the first kind of order one and its first derivative
$H_1^{(2)}$, $H_1^{(2)'}$	Hankel function of the second kind of order one and its first derivative
h	water depth
$Im(b)$	imaginary part of a complex number, b
I_1	modified Bessel function of the first kind of order one
i	integer; also the complex number $\sqrt{-1}$
J_1, J_1'	Bessel function of the first kind of order one and its first derivative
K_1, K_1'	Modified Bessel function of the second kind of order one and its first derivative
K_S^*	generalized structural stiffness
k	wave number
L	wavelength
M_i	lumped structural mass at elevation y_i where i is an integer
M_{am}	total added mass
M^*	generalized total mass
M_S^*	generalized structural mass
m	integer
N	number of vertical legs supporting platform
n	integer

SYMBOLS AND DEFINITIONS--Continued

P_1, P_2, P_3 functions of Bessel functions; defined in Appendix A

p dynamic pressure acting on cylinder

p_B dynamic pressure acting on cylinder due to its motion

p_{B_w} dynamic pressure acting on cylinder due to wavemaking; equation (36)

$p_{B_{am}}$ dynamic pressure acting on cylinder due to added mass; equation (37)

$Re(b)$ real part of the complex number b

R_{am}^* effective coefficient of added mass for mode-shape $\psi(y)$; equation (55)

r radial coordinate; Figure 2

S_o oscillation Strouhal number, $\sigma_n D/2\pi\bar{U}$

T period of oscillation

t time

$\bar{U}$ velocity of the current at the centerline of the channel averaged over time

u, $\dot{u}$ horizontal component of the wave water particle velocity and acceleration, respectively, at $x = o$ as if the structure were not present

X, $\dot{X}$, $\ddot{X}$ displacement, velocity and acceleration, respectively, of vertical cylinder at the mean water line; also, the displacement, velocity, and acceleration, respectively, of horizontal cylinder

X_0 oscillation amplitude at the mean water line for the vertical cylinder; also, the initial displacement of the horizontal cylinder

X_{0d} amplitude of dynamic response

X_{0s} amplitude of static response

x horizontal coordinate and the displacement of the vertical cylinder at elevation y with respect to its mean position; also, the argument of the functions P_1, P_2 and P_3

SYMBOLS AND DEFINITIONS--Continued

$\dot{x}$, $\ddot{x}$ velocity and acceleration, respectively, at elevation y, of the vertical cylinder

Y_0 amplitude of radiated wave

Y_1, Y_1' Bessel function of the second kind of order one and its first derivative

y vertical coordinate; Figure 2

y_i i^{th} elevation

z horizontal coordinate; Figure 2

α_m m^{th} root of the equation $\sigma^2 h/g = -\alpha_m h \tan \alpha_m h$, where $\alpha_m h > 0$ and $m = 1, 2, \ldots \infty$

θ angular coordinate; Figure 2

ν kinematic viscosity

ξ fraction of critical damping

ξ_s fraction of critical damping due to structural effects

ξ_w fraction of critical damping due to wavemaking

ξ_{vi} fraction of critical damping due to viscous effects

ρ mass density of water

σ radian frequency

σ_n natural frequency in water

σ_s natural frequency in air

Φ velocity potential

Φ_I, Φ_D, Φ_B velocity potential due to the incident wave, due to the diffracted wave and due to the motion of the body, respectively

$\Phi_B = \Phi_I + \Phi_D$ velocity potential due to the interaction of the incident wave with a motionless vertical cylinder

φ_B spatial part of Φ_B; equation (26)

$\psi(y)$ mode shape of the vertical cylinder

HYDRODYNAMIC DAMPING AND "ADDED MASS" FOR FLEXIBLE OFFSHORE PLATFORMS

by
Charles Petrauskas

I. INTRODUCTION

The discovery of oil in water depths up to 1,000 feet is one of the primary factors that has stimulated research on the problem of dynamic response of fixed offshore platforms. In water depths less than 400 feet a static design based on the force due to an expected maximum wave during the lifetime of the platform is usually sufficient to guarantee a stiff platform whose first-mode frequency is sufficiently high so that dynamic response due to waves can be neglected. However, in deeper water economical static designs will tend to decrease the first-mode frequencies. For example, Burke and Tighe (1972) cite first-mode frequencies of 2.6, 1.7, 1.4, and 1.0 radians per second for proposed platforms in water depths of 400, 600, 800, and 1,000 feet, respectively.

Wind-generated waves are a major source of frequency-dependent energy for the dynamic excitation of these platforms. The energy of these waves is usually specified by a spectral density function (wave spectrum) that defines its distribution as a function of frequency σ, and direction, θ. The one-dimensional (integrated over θ) spectrum that was developed by Pierson and Moskowitz (1964) is commonly used. It is a unimodal function, defined either in terms of windspeed or the significant wave height. The effect of increasing windspeed is to increase the energy level at the peak and shift the peak to lower frequencies. The wave energy for frequencies above the peak has been measured by many investigators (Phillips, 1966) and postulated by Phillips (1958) on the basis of dimensional analysis to be proportional to σ^{-5}. These same measurements appear to show that the factor of proportionality is a universal constant. However, this has been recently disputed by measurements of Barnett (1972) that show the factor to be dependent on fetch in such a way that for short fetches the factor and consequently the wave energy can be up to 10 times higher.

The combination of decreasing first-mode frequencies and the variation of wave energy with respect to frequency implies that dynamic response could be a significant factor in the design of these platforms in deep water.

1. <u>Present Representation of Hydrodynamic Forces on Flexible Platforms</u>.

To study the effect of surface waves on dynamic response requires an equation that defines the forces on the members of the platform. The presently used representation of hydrodynamic forces on flexible platforms,

as defined by the horizontal force, df(y,t), on an element, dy, of a vertical structural member whose motion is constrained in the x-y plane (Fig. 1(a)) is given by the following equation:

$$df(y,t) = \left\{ C_I \, \rho \, \frac{\pi D^2}{4} \, \dot{u}(y,t) - C_{am} \, \rho \, \frac{\pi D^2}{4} \, \ddot{x}(y,t) \right.$$

$$\left. + C_D \, \frac{\rho D}{2} \, \left| u(y,t) - \dot{x}(y,t) \right| \, [u(y,t) - \dot{x}(y,t)] \right\} dy, \qquad (1)$$

where

C_I = coefficient of inertia,

C_{am} = coefficient of "added mass,"

C_D = drag coefficient,

$u, \dot{u}$ = horizontal components of the wave water particle velocity and acceleration at x = 0 as if the structure were not present,

and

$\dot{x}, \ddot{x}$ = velocity and acceleration of structural member.

The equation as written applies to unidirectional waves traveling in the x-direction that are either periodic or random. If random, the equation is assumed valid for a realization of the stochastic process defining the surface waves. For a nonvertical member and multidirectional seas the equation may be used to define the force in the direction of the member's motion, assumed to take place in the plane that is normal to the member's undeflected orientation, provided the component of the fluid's motion is also in the same direction.

The equation is a modification of one that was developed by Morison, et al. (1950) for wave forces on a rigid vertical piling. The modification attempts to take into account the forces due to the velocity and acceleration of the structural members. The equation will be referred to as the "modified Morison equation."

a. Rationale. The first two terms of the equation represent the effect of the relative acceleration between the structural member and the fluid. Their appearance as additive terms proportional to $\dot{u}$ and $\ddot{x}$, respectively, can be explained by use of potential theory if each differential element, dy, of the vertical cylinder is considered moving with an acceleration $\ddot{x}$ in a two-dimensional uniform flow field having an acceleration $\dot{u}$ (Fig. 1(b)). Batchelor (1967) derives the force on an arbitrary body in an inviscid fluid by selecting an accelerating frame of reference such that the velocity of the fluid in this frame of reference is zero far away from the body. Then the force on the body is found to

(a)

(b)
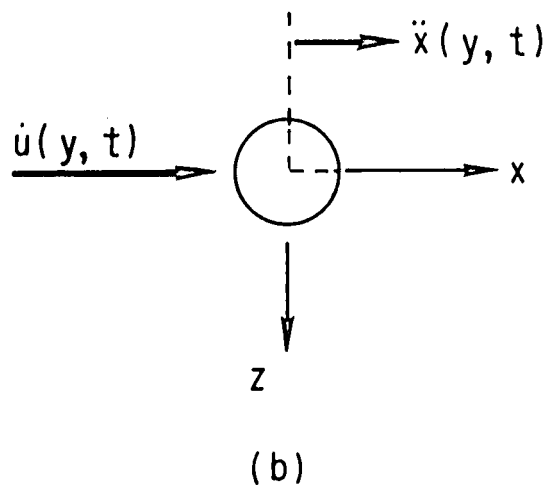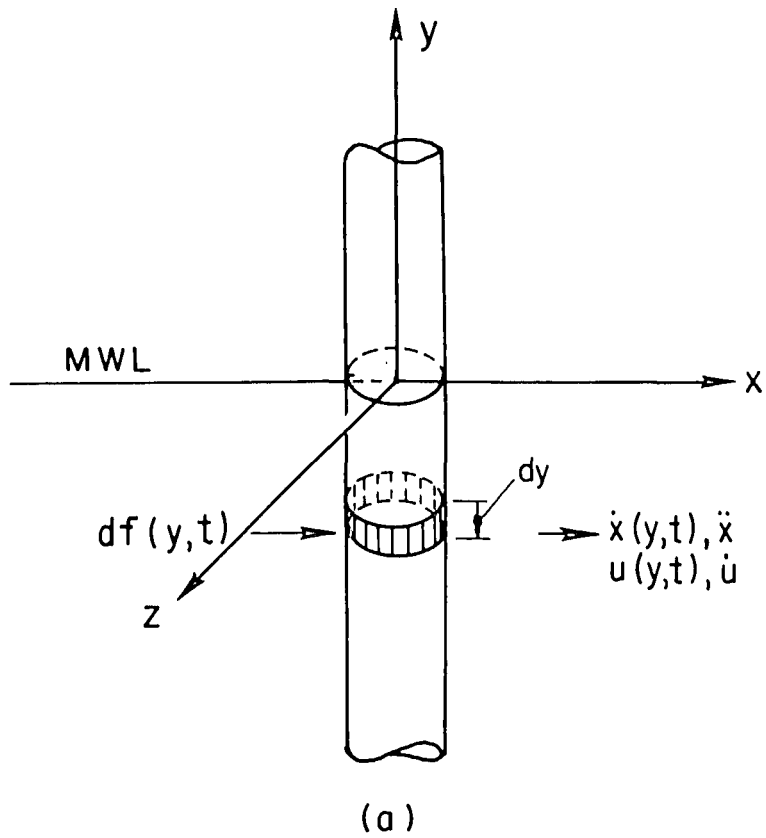
Figure 1. Definition sketch for modified
Morison force equation.

consist of two parts. The first part is an effective "buoyancy" force due to the pressure gradient needed to accelerate the fluid. The second part is identical to the "added-mass" force on a body moving in a still fluid with an acceleration $\ddot{x}$ - $\dot{u}$. The net force on the circular cylinder in Figure 1(b) can then be expressed by:

$$df = \left[\rho \, \frac{\pi D^2}{4} \, \dot{u} - C_{am} \, \rho \, \frac{\pi D^2}{4} \, (\ddot{x} - \dot{u}) \right] dy, \qquad (2)$$

where C_{am} = 1. Comparing this result with the first two terms of equation (1) shows that they are identical provided $C_I = C_{am} + 1$.

The effect of relative velocity is represented by the third term of equation (1), defined here as the drag-force interaction term. Its form is that of the drag force on a circular cylinder in a steady flow of viscous fluid at high Reynolds number. At each instant of time the drag force is assumed to be the same as in a steady flow of velocity u - $\dot{x}$. This quasi-steady approach has been used successfully to predict transverse oscillations due to a steady wind of elastically supported prismatic cylinders for the situation where the vortex shedding frequency is much higher than the natural frequency of the cylinder (Parkinson and Modi, 1967; Novak, 1969).

b. <u>Implications</u>. The present force equation implies two effects due to platform motion. The added-mass force, being proportional to $\ddot{x}$, implies an increase in the effective mass of the platform and therefore lowers the modal frequencies. Because of the rate at which wave energy decays with increasing frequency, any lowering of the first-mode frequency provides a large increase in the amount of wave energy that is available for dynamic excitation.

The assumed form of the drag force interaction term implies the existence of hydrodynamic damping. This can be clearly seen by imagining that the platform is excited by random waves such that on the average $\dot{x}$ << u and sgn(u - $\dot{x}$) ≈ sgn u. Then the following approximation can be made to the drag-force interaction term to isolate the damping effect:

$$C_D \, \frac{\rho D}{2} \, |u - \dot{x}| \, (u - \dot{x}) \approx C_D \, \frac{\rho D}{2} \, |u| u - C_D \, \rho D \, |u| \dot{x} . \qquad (3)$$

The term $C_D \, \rho D |u| \dot{x}$ is a positive damping force because being proportional to $|u|$ it always opposes the velocity of the platform members. Its proportionality to $|u|$ also implies that the damping increases with increasing wave height.

c. <u>Applications in the Literature</u>. The present equation has been used in a number of theoretical studies to evaluate the importance of dynamic response and the hydrodynamic damping implied by the drag-force interaction

term (Shubinski, Wilson, and Selna, 1967; Selna and Cho, 1972; Foster, 1970; Burke and Tighe, 1972; Malhotra and Penzien, 1970; Penzien, Kaul, and Berge, 1972). The coefficients C_I and C_{am} used by the investigators, usually have corresponded to the two-dimensional values of 2 and 1, respectively. In instances where specific values were not cited the authors assumed that $C_{am} = C_I - 1$. C_D ranged from 0.7 to 1.4; in some cases specific values were not given. The most informative studies were made by the latter three groups of investigators. They show that a dynamic analysis is important for deepwater fixed platforms, and that the hydrodynamic damping can be significant.

The equation has also been used to predict dynamic response of platform models in the laboratory. Nath and Harleman (1969, 1970) studied the response of vertical cylinders and multileg platforms to incident periodic and random unidirectional waves. Measured response compared well with the theoretical predictions based on the equation without the drag-force interaction term and C_I and C_{am} equal to 2 and 1, respectively. The good comparison was in part fortuitous for the following three reasons: (a) Use of cylinders whose diameters were sufficiently large compared with the wave heights so that inertial forces predominated, (b) use of plastic cylinders whose damping was large so that hydrodynamic damping was masked, and (c) use of structural mass that was large compared with the added mass so that results were insensitive to free-surface effects on added mass.

2. Objectives and Scope of Research.

In view of the possible importance of dynamic response, research was undertaken to develop information on added mass and hydrodynamic damping.

The major part of the research was directed toward developing quantitative information on the effects of the existence of a free surface which causes the coefficient of added mass to vary with elevation and permits the generation of waves by the oscillation of structural members that are located in the near-surface zone. This latter effect acts as a damping mechanism because energy of the generated waves radiates away from the platform. A vertical surface-piercing circular cylinder was chosen as an idealization of the platform because the vertical members forming the legs of the platform are usually larger in diameter than the horizontal and diagonal bracing. Consequently the forces due to wavemaking and effects of the free surface on the added mass will be most important for these vertical members. In some cases the platform itself may consist of a single vertical column.

In Section II, classical potential theory with linearized boundary conditions is used to derive the differential equation of motion for the dynamic response of the circular cylinder to incident waves. The mode shape of the cylinder is assumed known *a priori* in order that the response could be considered from the point of view of a single-degree-of-freedom

system. The wavemaking and added mass forces are derived and studied as
a function of cylinder diameter, water depth, oscillation frequency, and
mode shape. Energy dissipation due to wavemaking is examined and its
importance evaluated for fixed offshore platforms.

Section III discusses the experimental program to verify the results
of the potential theory. Rigid vertical circular cylinders were oscil-
lated with simple-harmonic motion in a translational mode. The resulting
external hydrodynamic forces and the generated waves were measured and
then compared with the theoretical results.

The oscillations were performed in stillwater and consequently the
verification is a limited one because a prototype structure in nature
oscillates in an incident wave field. However, for the linearized
boundary conditions the velocity potential and consequently the forces
due to the incident waves are theoretically independent of the motion
of the structure. Some experimental evidence of this independence for
models of ship hulls is given by Vugts (1968).

A smaller part of the research is devoted to an experimental study
aimed at verifying the hydrodynamic damping implied by the drag-force
interaction term in the modified Morison equation (Sec. IV). An elas-
tically supported horizontal cylinder was positioned within an open
channel so that its axis was normal to the direction of a steady current.
The motion of a cylinder was constrained so that the oscillations were
in the direction of the current. It was located deep enough so that
the free-surface effects were considered unimportant. Dynamic response
to an initial displacement was measured for a range of current speeds.
The measurements are compared with the damping predicted by the drag-
force interaction term. Added mass was also measured as a function of
current speed. The experiment was designed so that the natural frequency
of the elastically mounted cylinder was much higher than the highest
frequency of vortex shedding. This was done to avoid any possible feed-
back due to vortex shedding.

Vortex shedding was not studied although it could be an important
mechanism for providing additional excitation energy at the modal fre-
quencies of the platform. Bidde (1970) and Wiegel and Delmonte (1972)
present laboratory measurements of transverse forces on rigid vertical
circular cylinders subjected to unidirectional periodic waves. They
show transverse forces up to 60 percent of the inline forces. Bidde's
results for deepwater waves appear to show that the ratio of transverse
force to inline force depends on the ratio of wave height, H, to
cylinder diameter, D. This dependence on H/D seems reasonable because
Keulegan and Carpenter (1958) show that the initiation of vortex shedding
and the number of vortices shed depends on the excursion of the water
particle relative to D. The frequency of vortex shedding in waves is
not well known. The data of these investigators show average frequencies
of 2 to 6 times the wave frequency. For large values of H/D, such that
a large number of vortices are shed, an estimate of frequency can be made

by using the Strouhal number of 0.25 measured by Roshko (1961) for steady flow at supercritical Reynolds number. Then for deepwater waves, if the maximum water particle velocity at the mean water line (MWL) is used, the vortex shedding frequency is approximately 2(H/D) times the wave frequency. In that case vortex shedding may act as a mechanism for transferring energy from low-frequency waves to the structure at high frequency. The level of this energy at the first-mode frequency could be much higher than that available directly from the surface waves because most of it would be supplied by the larger waves with frequencies centered about the peak of the wave spectrum. It seems that such a mechanism of energy transfer would be important for unidirectional waves, but it is not clear if it could be effective in random multidirectional seas.

II. POTENTIAL THEORY MODEL FOR DYNAMIC RESPONSE OF PLATFORMS

Classical potential theory with linearized boundary conditions is used to formulate the steady-state dynamic response problem for a platform idealized by a vertical cylinder. The hydrodynamic forces due to wave-making and added mass are investigated in detail and used in the equation of motion to study the importance of wavemaking as a damping mechanism for idealized and actual platforms.

1. Idealization of Offshore Platform.

The platform is idealized by a single vertical surface-piercing circular cylinder of diameter, D, with the deck mass, M_1, concentrated at an arbitrary distance, y_1, above the MWL. It is assumed to respond dynamically predominantly with a mode shape $\psi(y)$ only in the x-y plane. $\psi(y)$ is defined such that $\psi(0) = 1.0$. The deflection of the platform is assumed infinitesimal so that the platform behaves as a linear system. Figure 2 is a definition sketch and presents the coordinate system that is used.

2. Differential Equation of Motion.

With the above assumptions the dynamic system can be simplified to an equivalent single-degree-of-freedom linear system with a generalized structural mass, M_s^*, generalized structural stiffness, K_s^*, and generalized structural damping, C_s^*, excited by a generalized force, $F^*(t)$. The generalized displacement is $X(t)$, the deflection of the cylinder at the MWL. The differential equation of motion for $X(t)$ is then given by:

$$\ddot{X}(t) + 2\xi_s \sigma_s \dot{X}(t) + \sigma_s^2 X(t) = F^*(t)/M_s^* , \qquad (4)$$

where

$$\sigma_s = \sqrt{K_s^*/M_s^*} = \text{radian natural frequency of the system in air,} \qquad (5)$$

$$\xi_s = C_s^*/2M_s^*\sigma_s = \text{fraction of critical damping in air.} \qquad (6)$$

19
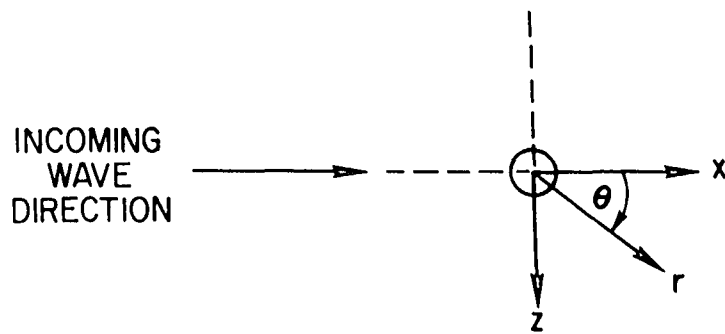
PLAN VIEW OF COORDINATE SYSTEM
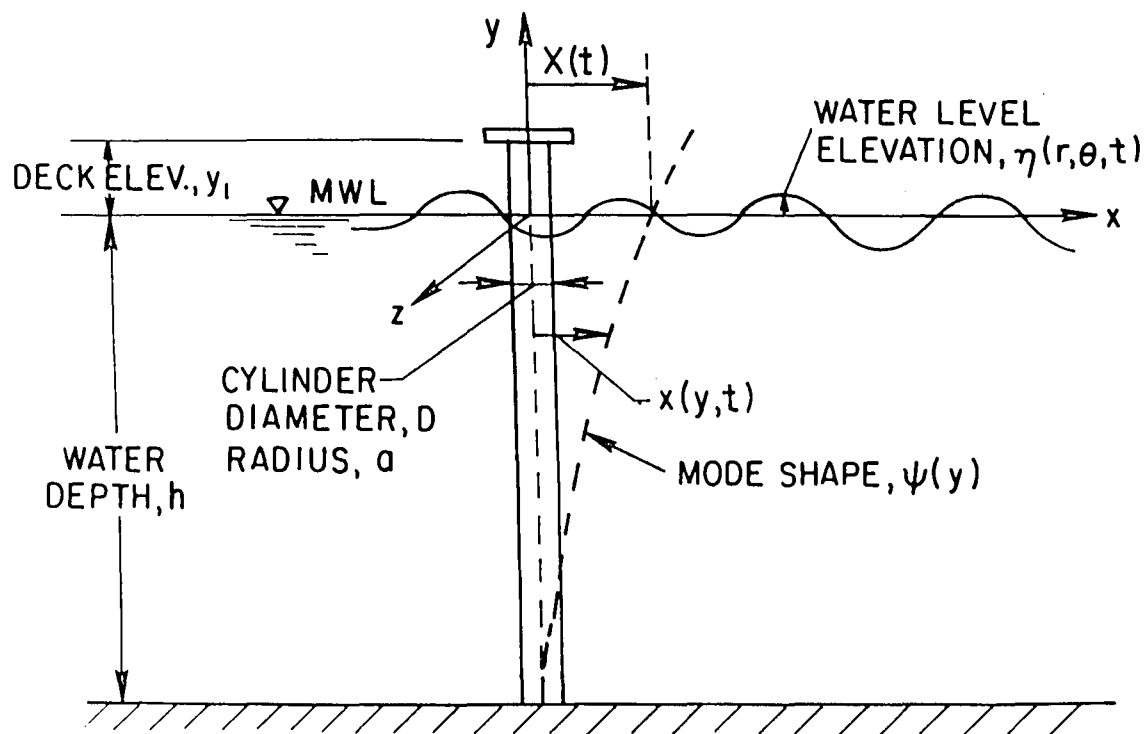
Figure 2. Definition sketch and coordinate system.

The structural damping of the platform in air is specified in terms of a single quantity, ξ_s. This representation of damping is commonly used in the modal method of dynamic response analysis where ξ_s is specified for each mode. A more detailed representation of structural damping is not used or warranted because there is at present no method for specifying in detail the energy dissipation capabilities of all the members and connections in a structure. The values of ξ_s used in practice are based on experience and on the few data that are available from shaking tests of land structures, such as reported by Hoerner and Jennings (1969). In this study the specification by ξ_s is particularly convenient because the hydrodynamic damping due to wavemaking can be specified in equivalent terms and thereby comparisons can be made.

The generalized quantities M_s^* and $F^*(t)$ are derived by the application of the principle of virtual displacement, first formulated by Jean Bernoulli in 1717. In essence it states the following: If forces acting on a structural system are in equilibrium, and if the system is subjected to a virtual displacement compatible with the geometric arrangement or kinematic constraints, then the total virtual work done is zero. Application of this principle to the dynamic system of Figure 2 yields the following:

$$M_s^* = \int_{-h}^{y_1} m_s(y)\ \psi^2(y)\,dy + \sum_i M_i\ \psi^2(y_i), \qquad (7)$$

where

$m_s(y)$ = distributed structural mass per unit length,

M_i = concentrated mass at elevation y_i,

and

$$F^*(t) = \int_{-h}^{y_1} f(y,t)\ \psi(y)\,dy, \qquad (8)$$

where

$f(y,t)$ = distributed hydrodynamic force per unit length.

$F^*(t)$ is the generalized hydrodynamic force acting on an oscillating cylinder in the presence of surface waves. The water is assumed inviscid so that $f(y,t)$ is derivable from a velocity potential $\Phi(r,\theta,y,t)$. With the further assumption of linearized theory, $f(y,t)$ can be calculated by integrating the pressure, $p(r,\theta,y,t)$, corresponding to Φ, around

the circumference of the cylinder at its mean position, r = a. The following equation results:

$$f(y,t) = -a \int_0^{2\pi} p(a,\theta,y,t) \cos\theta \, d\theta. \tag{9}$$

The relationship between p and Φ according to linear theory is given by:

$$p = -\rho \, \partial\Phi/\partial t - \rho g y. \tag{10}$$

This relationship is derived by integrating the Euler equations of motion, yielding Bernoulli's Law, and then neglecting the higher order terms that are due to convective acceleration. Then,

$$F^*(t) = \int_{-h}^{0} \int_0^{2\pi} \rho a \, \partial\Phi/\partial t \Big|_{r=a} \, \psi(y) \cos\theta \, d\theta \, dy. \tag{11}$$

Consistent with linear theory, the integration with respect to y extends only to the MWL, and consequently the hydrostatic pressure in equation (10) has no net effect.

According to linear theory (Wehausen and Laitone, 1960) Φ can be represented as the sum of three velocity potentials:

$$\Phi = \Phi_I + \Phi_D + \Phi_B, \tag{12}$$

where Φ_I is the potential of the incident waves, Φ_D is the potential of the diffracted waves, and Φ_B is the potential due to the motion of the cylinder. The physical interpretation is that $\Phi_I + \Phi_D \equiv \Phi_G$ is the velocity potential due to the interaction of the incoming wave with a motionless vertical cylinder and Φ_B is the velocity potential due to the motion of the cylinder in a disturbance-free fluid. Substitution of equation (12) into equation (11) then yields:

$$F^*(t) = \int_{-h}^{0} \int_0^{2\pi} a \rho \partial(\Phi_B + \Phi_G)/\partial t \Big|_{r=a} \, \psi(y) \cos\theta \, d\theta \, dy. \tag{13}$$

For the steady-state case of simple-harmonic motion defined by:

$$\dot{X}(t) = X_0 \sigma e^{i\sigma t}, \tag{14}$$

where

$\quad X_0$ = amplitude of the cylinder oscillation at y = 0,

$\quad \sigma$ = radian frequency of oscillation,

the dynamic pressure, p_B, due to the motion of the cylinder can be decomposed into two parts that are proportional to $\dot{X}(t)$ and $\ddot{X}(t)$, respectively, as follows:

$$p_B = -\rho \partial \phi_B / \partial t \big|_{r=a} = q_0(a,\theta,y) e^{i\sigma t}$$

$$= q_1(a,\theta,y)\, \dot{X}(t) + q_2(a,\theta,y)\, \ddot{X}(t), \qquad (15)$$

where q_0 is complex but q_1 and q_2 are real. Then the generalized force becomes:

$$F^*(t) = \int_{-h}^{0} \int_{0}^{2\pi} a[\rho \partial \phi_G / \partial t \big|_{r=a}$$

$$- q_1 \dot{X}(t) - q_2 \ddot{X}(t)] \cos\theta\, \psi(y)\, d\theta\, dy, \qquad (16)$$

where

$$- \int_{0}^{2\pi} a\, q_1 \cos\theta\, \dot{X}(t)\, d\theta , \qquad (17)$$

is the distributed wavemaking force, $f_w(y,t)$, per unit length of the cylinder. It is an energy dissipation term because it opposes the cylinder velocity. The term:

$$- \int_{0}^{2\pi} a\, q_2 \cos\theta\, \ddot{X}(t)\, d\theta , \qquad (18)$$

is the distributed added-mass force, $f_{am}(y,t)$, per unit length of the cylinder. It has the same effect as the inertial force due to structural mass.

Incorporating equation (16) into the equation of motion yields:

$$\ddot{X}(t) + 2\sigma_n [\xi_s M_s^* / (M_s^* + M_{am}^*) + \xi_w]\, \dot{X}(t)$$

$$+ \sigma_n^2 X(t) = F_G^*(t) / (M_s^* + M_{am}^*), \qquad (19)$$

23

where

$F_G^*(t)$ = generalized force due to the diffraction of the incident wave on a motionless cylinder

$$= a \int_{-h}^{0} \int_{0}^{2\pi} \rho \, \partial \Phi_G / \partial t \big|_{r=a} \cos\theta \, \psi(y) \, d\theta dy , \qquad (20)$$

M_{am}^* = generalized added mass

$$= \int_{-h}^{0} \int_{0}^{2\pi} a \, q_2 \cos\theta \, \psi(y) d\theta dy , \qquad (21)$$

σ_n = radian natural frequency in water

$$= \sqrt{ K_s^* / (M_s^* + M_{am}^*) } , \qquad (22)$$

C_W^* = generalized wavemaking damping coefficient

$$= \int_{-h}^{0} \int_{0}^{2\pi} a \, q_1 \cos\theta \, \psi(y) \, d\theta dy , \qquad (23)$$

ξ_W = fraction of critical damping due to wavemaking

$$C_W^* / [2 \sigma_n (M_s^* + M_{am}^*) . \qquad (24)$$

3. <u>Hydrodynamic Forces Due to Motion.</u>

The hydrodynamic forces on the cylinder due to its motion are derivable from the velocity potential Φ_B and in linear theory are independent of the forces due to the incident waves. In this section Φ_B is derived and a theoretical investigation is made of the wavemaking and added-mass forces.

a. <u>Derivation of Velocity Potential.</u> Φ_B is derived for the steady-state simple-harmonic motion of a vertical cylinder in an incompressible inviscid fluid of constant depth, h, and of infinite radial extent. The motion of the cylinder is specified by its velocity

$$\dot{x}(y,t) = X_0 \sigma \psi(y) e^{i\sigma t} .$$

Figure 2 is the definition sketch.

24

The derivation of Φ_B is similar to that for a flap-type wave maker in finite depth for which the velocity potential was derived by Havelock (1929) and rederived and its mathematical aspects discussed by Biesel and Suquet (1952). In both instances separation of variables is used to solve the Laplace equation with linearized boundary conditions. The main difference is that Φ_B is here three-dimensional and requires a solution in cylindrical coordinates, (r, θ, y), whereas the flap-type wavemaker problem is two-dimensional. This difference is important because it results in a vertical variation of added mass that is very different from that of the two-dimensional problem.

It is also similar to the derivation of the diffracted potential for the case of a vertical cylinder in an incident wave field as solved for finite depth by MacCamy and Fuchs (1954). Here the difference is in the boundary condition on the surface of the cylinder. For the diffracted potential the velocity on the boundary in the radial direction must be such that no flow crosses the boundary. The solution results in outwardly radiating waves. But for Φ_B the boundary condition is specified by the motion of the cylinder. This results not only in radiated waves but also in a nonprogressive disturbance that is maximum at the cylinder and decays exponentially with distance. This latter disturbance contributes to the added mass.

The potential for the case of a circular cylinder in infinite water depth has been derived by Havelock (1929). Although his solution could have been used for obtaining the wavemaking forces in deep water, the added-mass forces required a finite-depth solution. Consequently all derived forces are based on the following solution in finite depth.

(1) Partial Differential Equation and Boundary Conditions.
Φ_B must satisfy the Laplace equation in cylindrical coordinates, that is,

$$\nabla^2 \Phi_B = 0 = \left(\frac{\partial^2}{\partial y^2} + \frac{\partial^2}{\partial r^2} + \frac{1}{r^2} \frac{\partial^2}{\partial \theta^2} \right) \Phi_B \tag{25}$$

in the region $a \le r < \infty$; $-h \le y \le 0$; and $0 \le \theta \le 2\pi$.

Because Φ_B is sought for steady-state simple-harmonic motion the time factor can be separated out, yielding:

$$\Phi_B = \varphi_B (r, \theta, y) e^{i\sigma t} , \tag{26}$$

where φ_B also must satisfy Laplace's equation, the following linearized boundary conditions,

25

(a) $\left(\dfrac{\partial}{\partial y} - \dfrac{\sigma^2}{g}\right) \varphi_B = 0$ on $y = 0$,

(b) $\dfrac{\partial \varphi_B}{\partial y} = 0$ on $y = -h$,

(c) $\dfrac{\partial \varphi_B}{\partial r} = X_0 \, \sigma \, \psi(y) \cos\theta$ on $r = a$,

and the radiation condition that:

$$\lim_{r \to \infty} r^{\frac{1}{2}} (\partial \varphi_B / \partial r + i k \varphi_B) = 0 ,$$

where k is the wave number. The radiation condition guarantees that the solution for Φ_B is unique and implies that the generated wave is outgoing and its amplitude decays as $r^{-\frac{1}{2}}$ (Wehausen, 1971).

(2) <u>Elementary Solutions</u>. Using the standard separation-of-variables technique, the elementary solutions for φ_B that satisfy the boundary conditions are as follows:

(a) $\cosh k(y+h) [A_0 H_1^{(1)}(kr) + B_0 H_1^{(2)}(kr)] \cos\theta$,

(b) $\cos\alpha_m (y+h) [A_m I_1(\alpha_m r) + B_m K_1(\alpha_m r)] \cos\theta$, \qquad (27)

where kh and $\alpha_m h$ satisfy the following transcendental equations:

$$\sigma^2 h/g = kh \tanh kh , \qquad (28)$$

$$\sigma^2 h/g = -\alpha_m h \tan \alpha_m h$$

for

$$\alpha_m h > 0 \text{ and } m = 1,2,\ldots,\infty . \qquad (29)$$

The first equation is the classical relationship between wavelength and frequency that is derivable from the free-surface condition for small amplitude plane surface waves. In this case it is simply a functional relationship between $\sigma^2 h/g$ and kh and has the classical meaning only for the radiated waves far from the cylinder. The second equation has no simple physical interpretation. The solutions $\alpha_m h$ can be interpreted geometrically as shown in Figure 3.
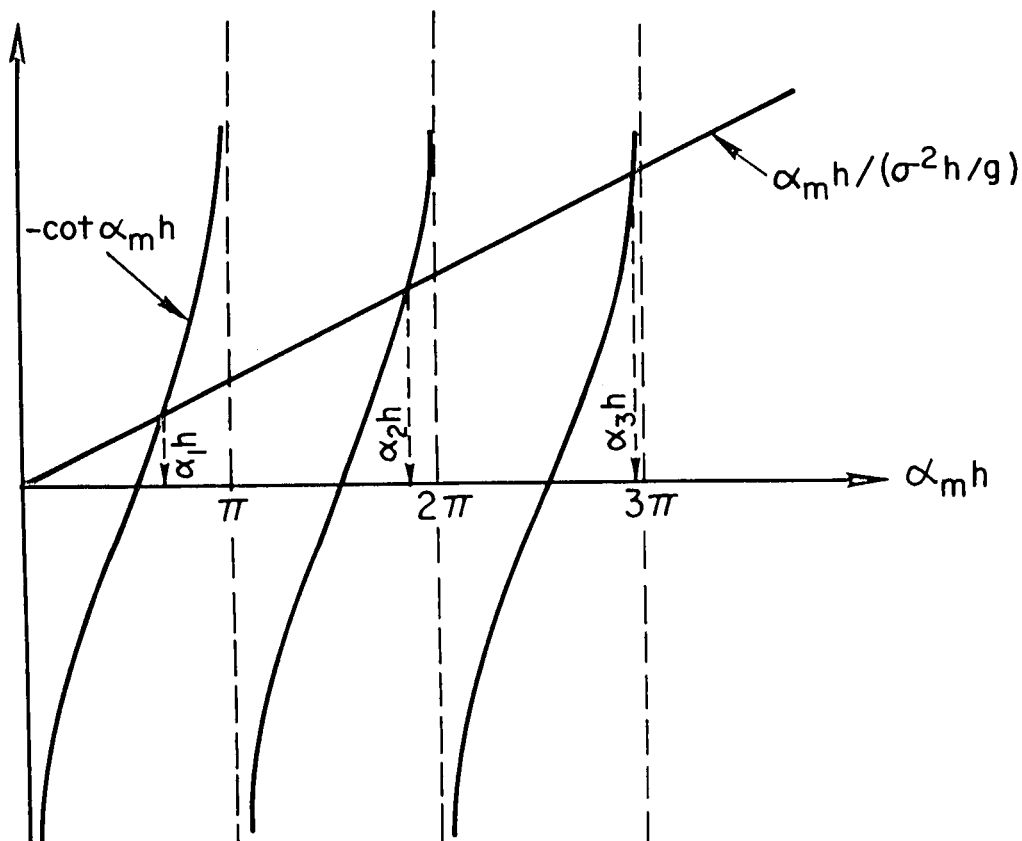
Figure 3. Geometrical interpretation for the roots of
$\sigma^2 h/g = -\alpha_m h \tan \alpha_m h$.

$H_1^{(1)}$ and $H_1^{(2)}$ are the Hankel functions of the first and second kind of order one. Their asymptotic behavior, as represented by the first term of their asymptotic expansions (Dwight, 1961), are:

$$H_1^{(1)} (kr) = (2/\pi kr)^{\frac{1}{2}} e^{i(kr-3\pi/4)},$$

$$H_1^{(2)} (kr) = (2/\pi kr)^{\frac{1}{2}} e^{-i(kr-3\pi/4)}.$$

If they are multiplied by the time factor, $e^{i\sigma t}$, the products represent an incoming and an outgoing wave, respectively, with an amplitude that decays like $r^{-\frac{1}{2}}$.

I_1 and K_1 are the modified Bessel functions of the first and second kind, respectively, of first order. The first terms of their asymptotic series (Dwight, 1961) are:

$$I_1(\alpha_m r) = e^{\alpha_m r} / (2\pi \alpha_m r)^{\frac{1}{2}},$$

$$K_1(\alpha_m r) = e^{-\alpha_m r} (\pi/2\alpha_m r)^{\frac{1}{2}}.$$

These functions are analogous to the exponential functions that result from the solution of the flap-type wavemaker. They represent a non-progressive disturbance that decays rapidly with the radial distance.

(3) Expansion of Boundary Condition on Surface of Cylinder in Terms of Elementary Functions. φ_B is a linear combination of the elementary solutions, but to satisfy the radiation condition the coefficients A_m: $m = 0,1,2,...,\infty$ must be identically zero. Consequently,

$$\varphi_B = B_0 H_1^{(2)}(kr) \cosh k(y+h) \cos\theta$$

$$+ \sum_{m=1}^{\infty} B_m K_1(\alpha_m r) \cos\alpha_m(h+y) \cos\theta. \qquad (30)$$

The constants B : $m = 0,1,2,...,\infty$ are determined from boundary condition (c) for the normal velocity on the surface of the cylinder. Substitution of into the boundary condition yields:

$$X_0 \sigma \psi(y) = B_0 k H_1^{(2)\,\prime}(ka) \cosh k(y+h)$$

$$+ \sum_{m=1}^{\infty} B_m K_1'(\alpha_m a) \cos\alpha_m(y+h). \qquad (31)$$

The functions in equation (31) form a complete orthogonal set over the interval $-h \leq y \leq 0$ and therefore the coefficients are given by:

$$B_0 = \frac{X_0 \sigma}{kH_1^{(2)}(ka)} \left(\int_{-h}^{0} \psi(y)\cosh k(y+h)\,dy \Big/ \int_{-h}^{0} \cosh^2 k(y+h)\,dy \right),$$

$$B_m = \frac{X_0 \sigma}{k K_1'(\alpha_m a)} \left(\int_{-h}^{0} \psi(y)\cos\alpha_m(h+y)\,dy \Big/ \int_{-h}^{0} \cos^2\alpha_m(h+y)\,dy \right).$$

28

Then

$$\Phi_B = \varphi_B(r,\theta,y)e^{i\sigma t} = X_0\,\text{ch}[\,G_0(kh)\cosh k(y+h)\,H_1^{(2)}(kr)/H_1^{(2)\prime}(ka)$$

$$+ \sum_{m=1} G(\alpha_m h)\cos\alpha_m(h+y)\,K_1(\alpha_m r)/K_1'(\alpha_m a)]\,\cos\theta\,e^{i\sigma t},\qquad (32)$$

where

$$G_0(kh) = \frac{(2/h)\displaystyle\int_{-h}^{0}\psi(y)\cosh k(y+h)\,dy}{\sinh kh\cosh kh + kh},\qquad (33)$$

$$\left.G(\alpha_m h) = \frac{(2/h)\displaystyle\int_{-h}^{0}\psi(y)\cos\alpha_m(h+y)\,dy}{\sin\alpha_m h\cos\alpha_m h + \alpha_m h}\right\}\quad m=1,2,\ldots,\infty \qquad (34)$$

(4) Dynamic Pressures Due to Wavemaking, p_{B_W} and Added Mass, $p_{B_{am}}$. To obtain p_{B_W} and $p_{B_{am}}$, the functions q_1 and q_2 must be related to φ_B. Because φ_B is a complex number it can be written as $\text{Re}(\varphi_B) + i\,\text{Im}(\varphi_B)$. Then:

$$p_B \equiv -\rho\,\partial\Phi_B/\partial t\,\big|_{r=a} = -\rho\sigma[\,i\,\text{Re}(\varphi_B) - \text{Im}(\varphi_B)]\,\big|_{r=a}\,e^{i\sigma t}.\qquad (35)$$

Equating this with equation (15), where $\dot{X} = X_0\sigma e^{i\sigma t}$, yields:

$$q_1 = (\rho/X_0)\,\text{Im}(\varphi_B)\,\big|_{r=a},$$

and

$$q_2 = -(\rho/X\sigma)\,\text{Re}(\varphi_B)\,\big|_{r=a}.$$

Taking the real and imaginary parts of φ_B yields the following results for the dynamic pressures:

$$p_{B_W} = \rho\,\text{ch}\,G_0(kh)\,P_1(ka)\cosh k(y+h)\cos\theta\,\dot{X}(t),\qquad (36)$$

where

$$P_1(ka) = 2/\{\pi ka[J_1'(ka)^2 + Y_1'(ka)^2]\},$$

29

and

$$P_{B_{am}} = \rho h[G_0(kh)P_2(ka)\cosh k(y+h)$$

$$+ \sum_{m=1}^{\infty} G(\alpha_m h) P_3(\alpha_m a) \cos\alpha_m(h+y)] \cos\theta \; \ddot{X}(t), \qquad (37)$$

where

$$P_2(ka) = - [J_1(ka) \; J_1'(ka)$$

$$+ Y_1(ka) \; Y_1'(ka)] / [J_1'(ka)^2 + Y_1'(ka)^2] ,$$

$$P_3(\alpha_m a) = -K_1(\alpha_m a)/K_1'(\alpha_m a). \qquad (38)$$

J_1 and Y_1 are Bessel functions of the first and second kind, respectively, of the first order. Behavior of the functions P_1, P_2, and P_3 is discussed in Appendix A.

   b. <u>Wavemaking Forces</u>. The distributed wavemaking force, $f_w(y,t)$, as defined by equation (17) is given by:

$$f_w(y,t) = -\rho\pi a \, ch \, G_0(kh) P_1(ka) \cosh k(y+h) \dot{X}(t). \qquad (39)$$

f_w is maximum at the MWL and decays with respect to y like the velocity potential of a small amplitude free-surface wave. In non-dimensional form, it is a function of two independent parameters, kh and ka and the mode shape $\psi(y)$. Because k is related to the oscillation frequency σ by equation (28) the wavemaking forces and consequently the damping due to wavemaking are frequency-dependent.

   (1) <u>Total Wavemaking Force for Translation Mode, $\psi(y) = 1$</u>. To gain a better understanding of the wavemaking force, the theoretical result for total force was studied for the case of translational oscillation that would occur, e.g., if a rigid cylindrical structure were excited by simple-harmonic ground motion. This theoretical result, in terms of the nondimensional amplitude C_w of the total force, F_w, defined as the coefficient of the wavemaking force is:

$$C_w = F_w/\rho g\pi a^2 X_0 = (\sigma^2 h/g) \sinh kh \, G_0(kh) P_1(ka)/ka , \qquad (40)$$

where for $\psi(y) = 1$,

$$G_0(kh) = \frac{2\sinh kh}{kh(\sinh kh \cosh kh + kh)} . \qquad (41)$$

It is derived by integrating the amplitude of $f_w(y,t)$ over the water depth.

F_W is solely due to wave generation. This can be shown by considering the limiting case where $kh \to 0$. For small values of kh, such that $h/L < 1/25$, use of the shallow water approximations ($\sinh kh \approx kh$ and $\cosh \approx 1.0$) yields the result:

$$C_w \approx (kh)^2 \, P_1(ka)/ka ; \qquad (42)$$

then

$$\lim_{kh \to 0} C_w = 0,$$

This result is expected because when kh is zero, so is $\sigma^2 h/g$, and therefore the free-surface boundary condition for the velocity potential implies that the vertical velocity is zero. The free surface is in effect a lid so that the flow field is the same as for the two-dimensional case of a cylinder oscillating in an infinite motionless fluid for which the part of the force that is proportional to velocity is zero.

If $kh > 0$, then the free-surface condition permits the existence of waves, resulting in a force that opposes the velocity and consequently net work is done on the fluid over each cycle of oscillation.

For the case of deep water, for practical purposes defined by $h/L > 1/2 (kh > \pi)$, the wavemaking force depends on only one parameter, $F_0 = \sigma\sqrt{D/g}$. This can be shown by using the deepwater approximations ($\sigma^2 h/g \approx kh$, $ka \approx \sigma^2 a/g$ and $\cosh kh \approx \sinh kh \approx e^{kh}/2$) in equation (40), which yield:

$$C_w \quad 4P \, (F_0^2/2)/F_0^2 . \qquad (43)$$

The dependence on one parameter is expected because for $kh > \pi$ the radiated waves are not influenced by the bottom. Then the wavemaking forces do not depend on the water depth. As kh increases, the extent of the zone over which f_w is significant decreases, so that for practical purposes the radiated wave energy is characterized by the motion at the MWL and does not depend on the exact mode shape. This simplifies the estimation of damping for offshore platforms because the wavemaking force can then be assumed to act at the MWL as a point force having an amplitude determined by equation (43). However, the estimate is always on the high side. The magnitude of the error is determined as a function of kh and $\psi(y)$ in the next section.

As stated previously, the wavemaking force is frequency-dependent. This dependence is illustrated in Figure 4 showing C_w plotted versus F_0. The shape of the curve implies that the damping due to wavemaking could be important only for a small range of F_0 values, so that for a given diameter, energy can be effectively dissipated through a small range of frequencies.

MEASURED DATA

	D, ft	h, ft	D/h
○	0.50	1.00	0.50
□	0.50	0.83	0.60
◑	0.50	0.67	0.75
◧	0.75	1.00	0.75
△	0.75	0.83	0.90
◇	0.75	0.67	1.12

$X_0 = 0.025$ ft

$C_W \approx \frac{\pi}{4} F_0^4 \ \text{for} \ F_0 < 1.0$

$C_W \approx 4/F_0^2 \ \text{for} \ F_0 > 2.0$

C_W (vertical axis)

$F_0 = \sigma \sqrt{D/g}$ (horizontal axis)
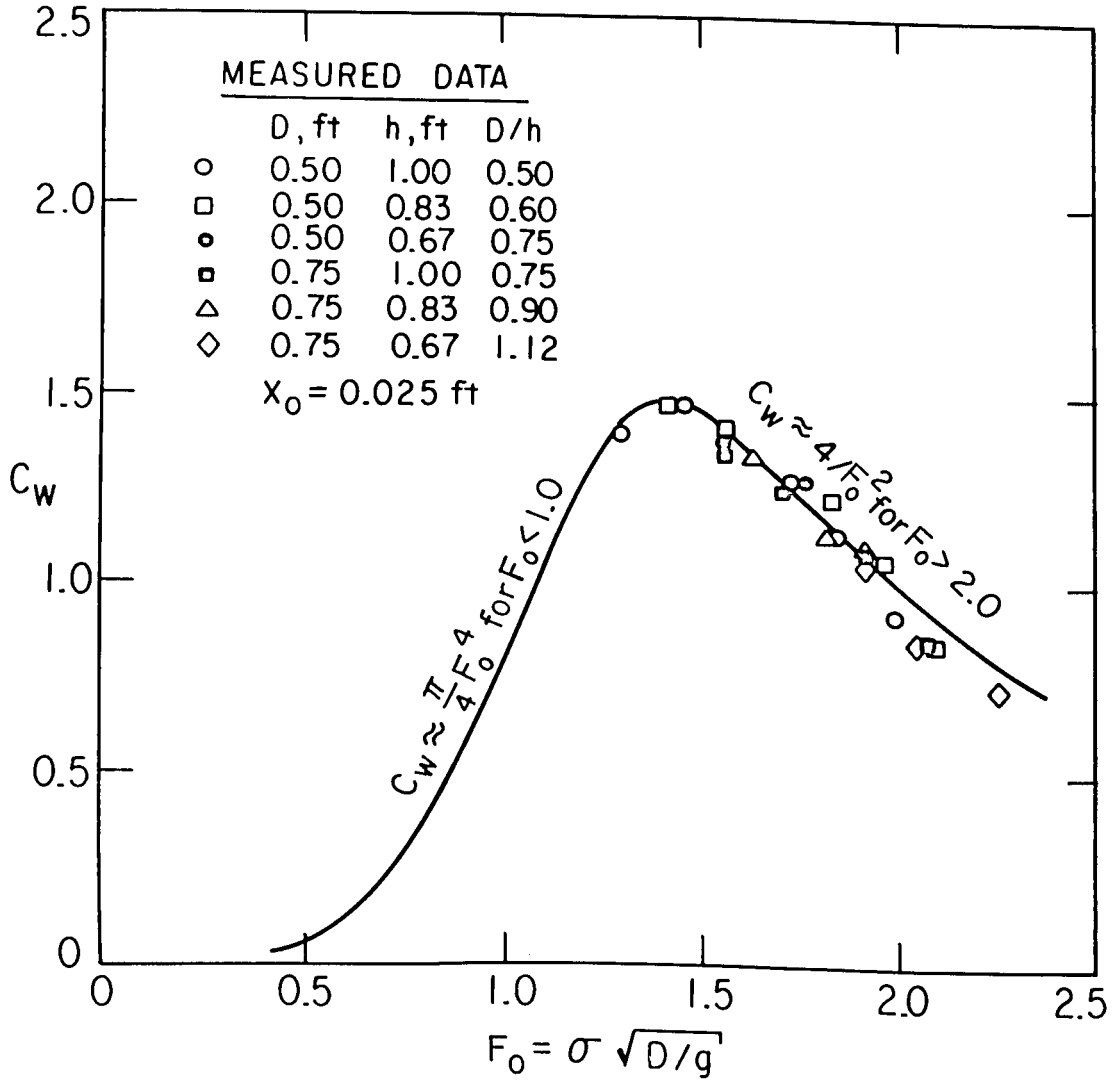
Figure 4. Coefficient of the wavemaking force for $\sigma^2 h/g > \pi$ (data from force measurements).

(2) <u>Effect of Mode Shape</u>. First the mode shape affects the distributed wavemaking force and secondly enters into the calculation of the generalized wavemaking damping coefficient, C_W^*, as defined by equation (23).

In the first case, the effect of the mode shape is included in the function $G_0(kh)$, to which f_w is proportional. Assuming first-mode shapes to be contained within the class of shapes defined by (Fig. 5):

$$\psi(y) = 1 - q(y), \tag{44}$$

where $0 \leq q(y) \leq 1$ such that $q(0) = 0$ and $q(-h) = 1$ yields the result that:

$$G_0(kh) = \frac{2\sinh kh}{kh(\sinh kh \cosh kh + kh)}$$

$$\left[1 - \frac{k}{\sinh kh} \int_{-h}^{0} q(y) \cosh k(y+h) dy\right]. \qquad (45)$$

If $q(y)$ is equal to zero for all y, $G_0(kh)$ corresponds to the translation mode. Otherwise the second term within the brackets is positive, so that the effect of $q(y)$ is to reduce f_w for the translation mode by a factor that depends on kh and the shape of $q(y)$.
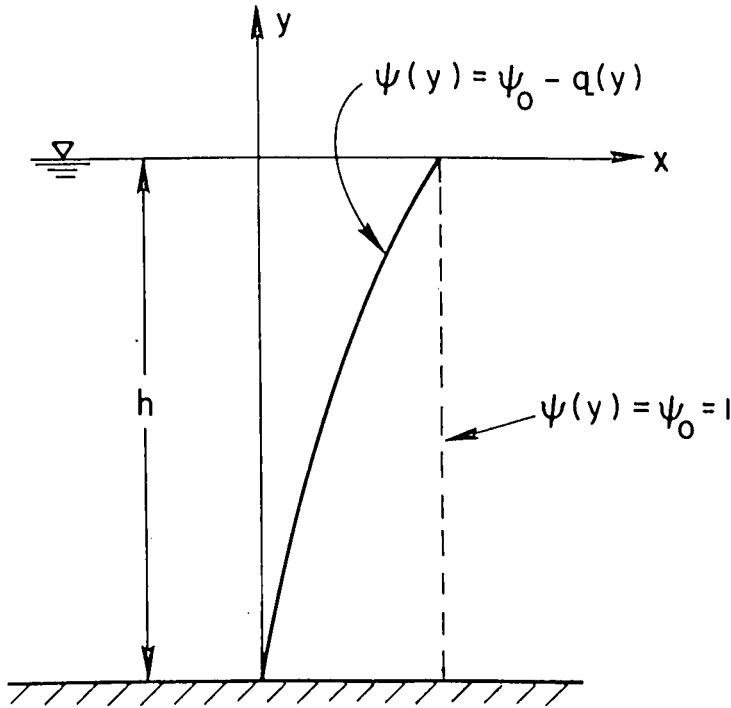
Figure 5. First-mode shapes.

Assuming $q(y)$ can be expanded in a Taylor series about $y = 0$,

$$q(y) = q(0) + q'(0)y + \ldots + q^{(n)}(0)y^n/n!$$

The major contribution to the integral in the above equation will come from the second term of the expansion which is the slope of $q(y)$ at $y = 0$. Substitution of the second term yields the following result for deep water:

$$G_0(kh) \approx \frac{4e^{-kh}}{kh}\left[1 - \frac{q'(0)h}{kh}\right]. \qquad (46)$$

33

A reasonable first-mode shape is given by:

$$\psi(y) = 1 - \cos \frac{\pi}{2} (1 + \frac{y}{h}), \qquad (47)$$

which corresponds approximately to the first mode for a cantilever column having a constant cross section and mass per unit length. Then q'(0) = π/2h and the error made in using the translation mode is approximately (π/2kh). 100 percent.

In the case where C_w^* is calculated, $\psi(y)$ acts as weight function for the amplitude of f_w. Because f_w is distributed with depth like cosh k(y + h),

$$C_w^* \propto \left(1 - \frac{kh}{\sinh kh} \int_{-h}^{0} q(y) \cosh k(y+h) dy\right)^2, \qquad (48)$$

and therefore the result for the translation mode will represent an upper bound for C_w^*. The error made in using C_w^* based on the translation mode will be twice that for f_w.

In most practical situations the error will be small. For example, the platforms analyzed by Burke and Tighe (1972) yield values for $\sigma_n^2 h/g$ (or equivalently kh) ranging from 32 to 84. The corresponding errors range from 9.8 to 3.7 percent. Therefore, for practical purposes C_w^* can be considered independent of $\psi(y)$. Then the deepwater results for C_w as plotted in Figure 4 can be used because

$$C_w^* = C_w \ \rho g (\pi a^2/\sigma). \qquad (49)$$

c. <u>Added-Mass Forces</u>. The distributed added-mass force, $f_{am}(y,t)$, as defined by equation (18), is given by:

$$f_{am}(y,t) = - \rho \pi ah \left[G_0(kh) \ P_2(ka) \cosh k(y+h) \right.$$

$$\left. + \sum_{m=1}^{\infty} G(\alpha_m h) \ P_3(\alpha_m a) \cos \alpha_m(h+y) \right] \ddot{x}(t). \qquad (50)$$

It consists of two components. The first varies with depth in the same way as the distributed wavemaking force so that in deep water it is concentrated in the near-surface zone; it will be referred to as a "local" force. The second component is defined by an infinite series and acts at all elevations even for deep water; it will be referred to as an "overall" force.

In nondimensional form, f_{am} is completely defined by two parameters, ka and kh, and the mode shape $\psi(y)$. This can be clearly seen for the

local force although it is not so obvious for the overall force, which is defined in terms of $\alpha_m h$ and $\alpha_m a$. But because $\alpha_m a \equiv \alpha_m h (ka)/(kh)$ and the set $\{\alpha_m h: m = 1,2,\ldots\infty\}$ are determined uniquely by $\sigma^2 h/g$, which is itself determined by kh, the same two parameters completely define the overall force. For plotting theoretical results, the alternate parameters, $\sigma^2 h/g$ and D/h, were used because they are related directly to the characteristics of the dynamic system, whereas kh and ka require the calculation of k for a given σ and h.

The added-mass force per unit length over a width πa for the two-dimensional flap-type wavemaker is given by

$$\lim_{ka\to\infty} f_{am}$$

for which $P_2(ka) = 0$ and $P_3(\alpha_m a) = 1.0$ (App. A). In this case the local component no longer exists. This results in an added mass distribution that is very different from that for the circular cylinder.

(1) Added-Mass Forces for Translation Mode, $\psi(y) = 1$. The added-mass forces for the translation mode are as simple to obtain as the wave-making forces and provide a better understanding of their nature. Calculations are presented showing the variation of added mass with respect to elevation and its dependence on the parameters $\sigma^2 h/g$ and D/h.

(a) Distributed Coefficient of Added Mass, $C_{am}(y)$. The variation of added mass with respect to elevation is specified by $C_{am}(y)$ defined as follows:

$$C_{am}(y) = \frac{\text{amp}[f_{am}(y,t)]}{\rho\pi a^2 \,\text{amp}[\ddot{x}(y,t)]}, \tag{51}$$

where the term "amp(z)" means amplitude of the quantity z which is assumed to be simple harmonic in time. $\ddot{x}(y,t)$ is the acceleration of the cylinder at elevation y and therefore $\text{amp}[x(y,t)] = \psi(y)X_0\sigma^2$. For $\psi(y) = 1$,

$$C_{am}(y) = \frac{h}{a}\Bigl[G_0(kh)P_2(ka)\cosh k(y+h) $$

$$+ \sum_{m=1}^{\infty} G(\alpha_m h)P_3(\alpha_m a)\cos\alpha_m(h+y)\Bigr], \tag{52}$$

where $G_0(kh)$ is defined by equation (41) and

35

$$G(\alpha_m h) = \frac{2 \sin \alpha_m h}{\alpha_m h (\sin \alpha_m h \cos \alpha_m h + \alpha_m h)} . \qquad (53)$$

$C_{am}(y)$ was evaluated by computer for a series of $\sigma^2 h/g$ values and for $D/h = 0.50$ and 0.10 and are plotted in Figures 6 and 7. The overall component was based on 30 terms, each of which required an iterative solution for $\alpha_m h$.

Certain trends can be noted from the plotted results. As $\sigma^2 h/g$ becomes small, C_{am} approaches a constant value of one. The explanation is identical to that for the wavemaking forces. For $\sigma^2 h/g = 0$, the boundary condition on the free surface implies the existence of an impermeable lid. Consequently, the flow field is identical to the two-dimensional case of a circular cylinder accelerating in a fluid of infinite extent for which the coefficient of added mass is one.

At the other extreme when $\sigma^2 h/g$ becomes very large the local component goes to zero and $\alpha_m h$, as can be inferred from Figure 3, approaches $m\pi/2$ where $m = 1,3,5,\ldots,\infty$. Therefore,

$$\lim_{\sigma^2 h/g \to \infty} C_{am}(y) = \frac{8}{\pi^2} \frac{h}{a} \sum_{m=1,3,5}^{\infty} \sin \frac{m\pi}{2} \frac{P_3 \left(\frac{m\pi}{2} \frac{a}{h}\right)}{m^2} \cos \frac{m\pi}{2}\left(1 + \frac{y}{h}\right), \qquad (54)$$

and consequently $C_{am}(y)$ for larger $\sigma^2 h/g$ can be considered dependent only on a/h. The function P_3 is monotonically increasing and is always less than one. For large a/h, P_3 will be close to one so that the terms of the series decrease approximately as m^{-2}, making the first term dominant. In that case $C_{am}(y)$ will vary approximately as $\cos \pi/2(1 + y/h)$. The result for $\sigma^2 h/g = 50$ and $D/h = 0.50$ in Figure 6 illustrates this case. However, $\sigma^2 h/g$ is apparently not large enough because in the limit C_{am} at $y = 0$ should be zero, whereas a negative value results. (Negative added-mass values have also been derived by Ogilvie (1963) for a submerged horizontal circular cylinder oscillating with simple-harmonic motion in the horizontal direction. He used linear theory and found negative values for some cases of low submergence.) As a/h becomes small, C_{am} approaches a constant value of one. This can be seen by considering the case of $a/h \to 0$ in which

$$P_3 \to \frac{m\pi}{2} \frac{a}{h} ,$$

and therefore,

$$\lim_{\sigma^2 h/g \to \infty, \, a/h \to 0} C_{am}(y) = \frac{4}{\pi} \sum_{m=1,3,5}^{\infty} \frac{\sin(m\pi/2)}{m}$$
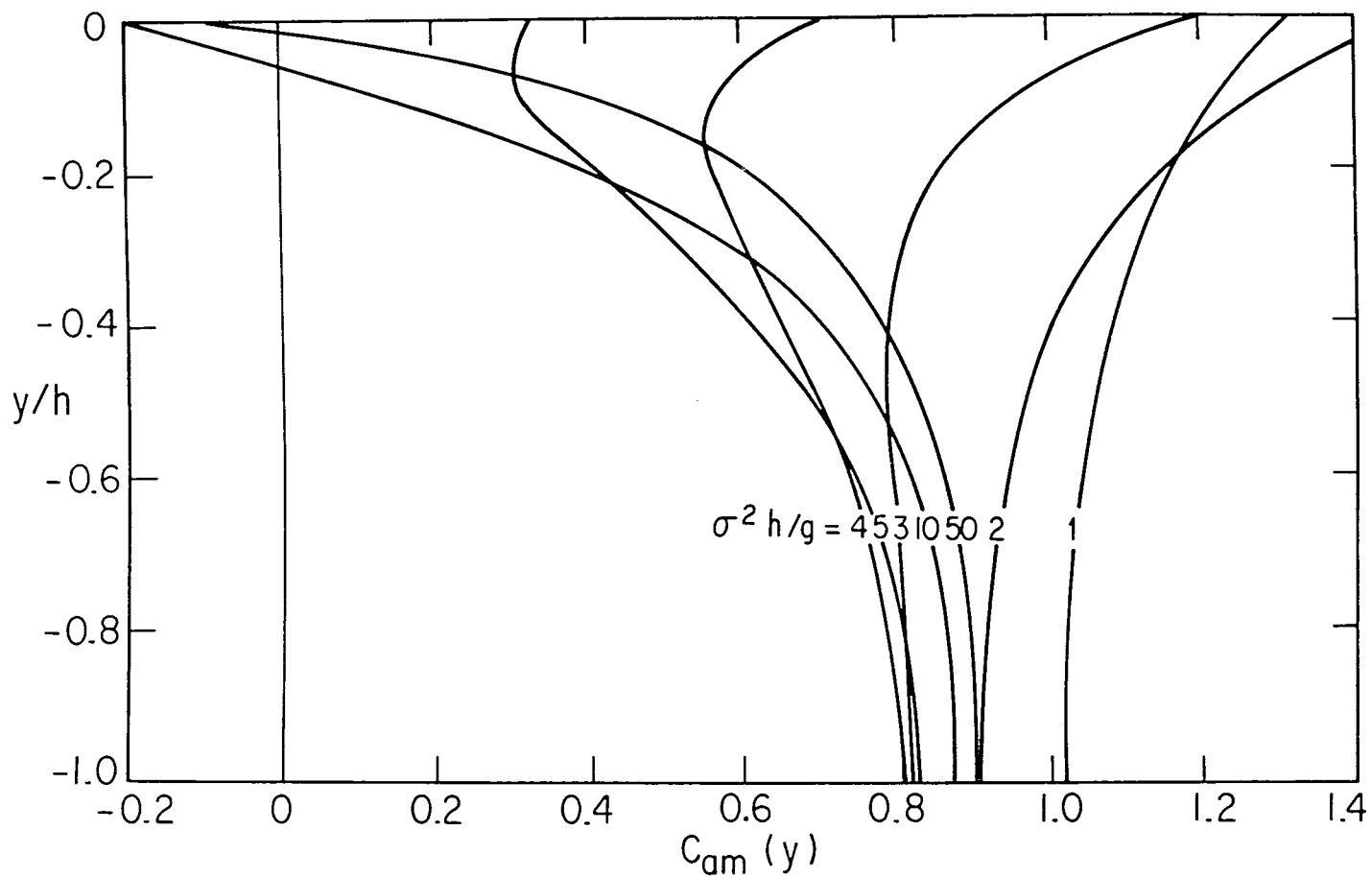
Figure 6.   Variation of the coefficient of "added mass" with respect to elevation
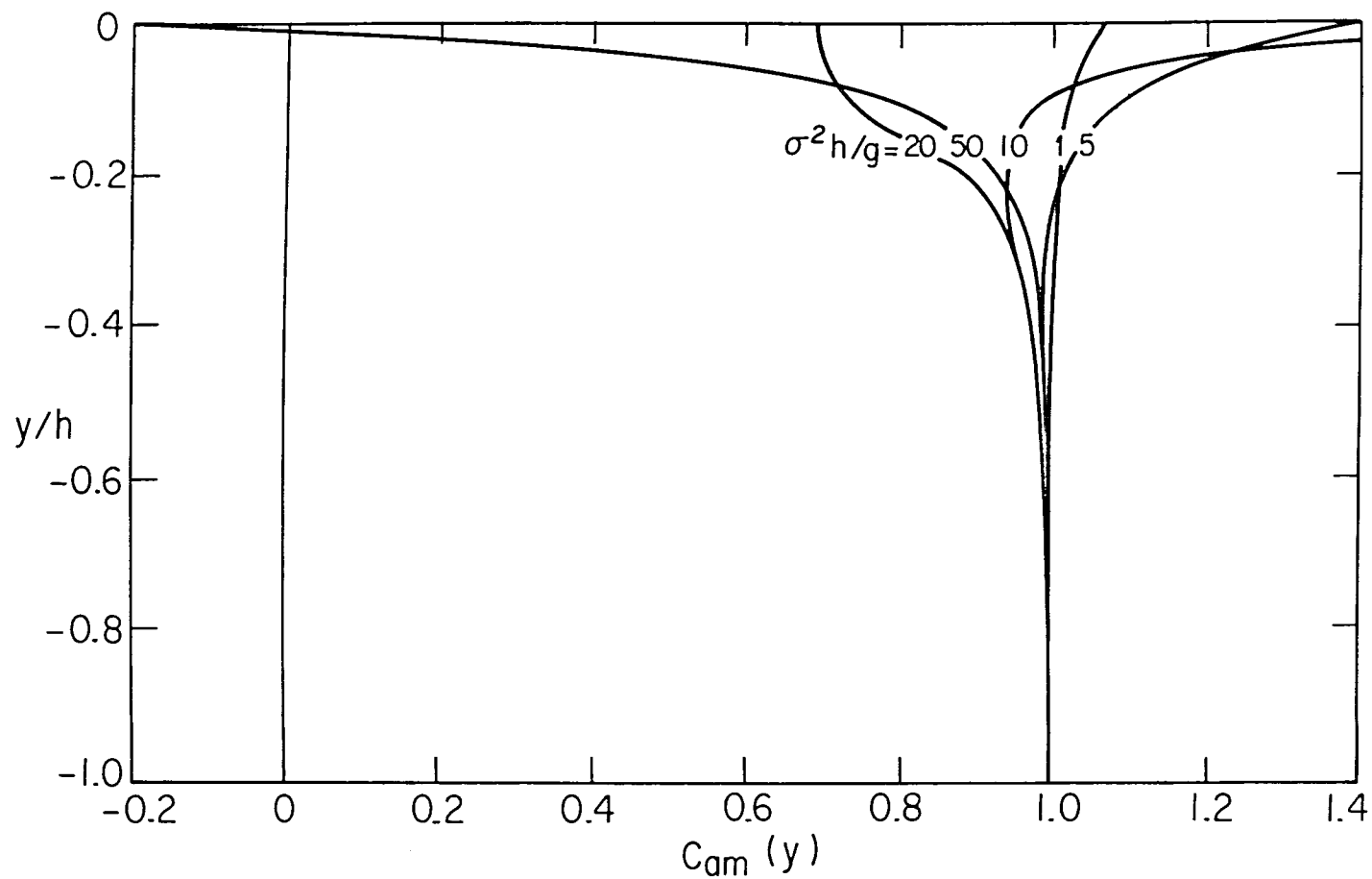for D/h = 0.50; translation mode.

Figure 7. Variation of the coefficient of "added mass" with respect to elevation
for D/h = 0.10; translation mode.

The series converges to the value $\pi/4$ (Dwight, 1961) and consequently, $C_{am}(y) = 1.0$ except at the MWL where it is zero. The tendency toward uniformity can be seen in Figure 7 for $\sigma^2h/g = 50$ and $D/h = 0.10$. In fact, it can be shown theoretically that for all σ^2h/g, C_{am} approaches the value one as a/h becomes small. This tendency can be seen by comparing the results for $D/h = 0.5$ with those for $D/h = 0.1$ where C_{am} is approximately one for a much larger part of the water depth.

The limiting case of $\sigma^2h/g \to \infty$ can also be derived by solving for the velocity potential function with its value equal to zero at $y = 0$. This boundary condition results when $\sigma^2h/g \to \infty$ for the free-surface boundary condition. This approach has been used by other investigators with the intent of applying the results to earthquake-excitation problems. The boundary condition, being homogeneous in time, implies that the added mass is not time-dependent and consequently the added-mass forces are directly proportional to any time function representing the base acceleration. Jacobsen (1949) studied the added mass by this approach for fluid outside and inside rigid circular tanks. He found that the distribution of added mass with respect to elevation for the inside fluid is similar to that outside except that it approaches uniformity more quickly with decreasing a/h. Garrison and Berklite (1973) studied it for fluid outside arbitrarily shaped bodies using a numerical procedure based on the distribution of singularities on the bodies' surface. He included the circular cylinder as a special case for comparison with analytical results based on equation (54). Chopra (1967, 1968, 1970) studied it for vertical-wall dams excited by earthquake-produced ground motion.

At the MWL, C_{am} ranges from values greater than one (up to 1.5 for the plotted results) all the way to negative values. This variation is due to the combined effects of the local and overall components. For small values of σ^2h/g the local component dominates. In fact, for $\sigma^2h/g \to 0$ it can be seen from Figure 3 that $\alpha_m h \to m\pi$ so that $G(\alpha_m h) \to 0$ because $\sin \alpha_m h \to 0$. Consequently, the overall component contributes little. As σ^2h/g increases, the local component becomes concentrated near the surface, but the overall component at $y = 0$ provides a negative contribution because the product $G(\alpha_m h) \cos \alpha_m h$ is always negative. Eventually the overall component dominates, resulting in a negative C_{am} and implying that the force on the cylinder at this level is in the direction of the acceleration rather than opposite to it as is usually the case. As $\sigma^2h/g \to \infty$ the contribution from the local component disappears. At the same time $\alpha_m h \to m\pi/2$ where m is odd so that $G(\alpha_m h) \cos \alpha_m h \to 0$ and consequently $C_{am} \to 0$.

(b) Average Coefficient of Added Mass, $\hat{C}_{am}$. $\hat{C}_{am}$ is the average value of $\overline{C_{am}(y)}$ for the translation mode. The computation of this quantity is simpler than $C_{am}(y)$ because the terms of the infinite series are proportional to m^{-3} rather than m^{-2} and therefore the series converges more rapidly. Calculations were made by computer for many different pairs of σ^2h/g and D/h covering the range of laboratory

experiments and field conditions. The infinite series was assumed to have converged when an additional term caused less than 0.01 percent change in the cumulative sum. The results are plotted in Figure 8 (experimental data are discussed in Section III).

These results illustrate more fully the influence of the two parameters. For practical purposes: (a) $\sigma^2 h/g$ can be considered infinite if it is greater than 100 so that $C_{am}(y)$ as defined by equation (54) can be used, and (b) the influence of D/h is negligible for values less than about 0.01 so that a constant $C_{am}(y)$ of unity can be assumed to act at all depths.

(2) Effect of Mode Shape. The effect of $\psi(y)$ on $C_{am}(y)$ was not studied directly. Instead its integrated effect, as included in the generalized added mass, M_{am}^*, defined by equation (21), was investigated. This choice was made because M_{am}^* is a measure of the kinetic energy component due to hydrodynamic effects and consequently enters into the evaluation of effective energy dissipation due to wavemaking as defined by the fraction of critical damping, ξ_w, in equation (24).

The effect of mode shape was studied in terms of a normalized generalized coefficient of added mass, R_{am}^*, defined by:

$$R_{am}^* = \frac{\dfrac{1}{h}\displaystyle\int_{-h}^{0} C_{am}(y)\, \psi^2(y)\, dy}{\dfrac{1}{h}\displaystyle\int_{-h}^{0} \psi^2(y)\, dy}, \qquad (55)$$

where $C_{am}(y)$ is now a function of $\psi(y)$ as defined by equation (51). The numerator is the average value of $C_{am}(y)$ weighed by $\psi^2(y)$ and is equivalent to $M_{am}^*/\rho\pi a^2 h$. The denominator is the same quantity for the case where $C_{am}(y) = 1.0$. Therefore, R_{am}^* is an overall measure of the deviation of $C_{am}(y)$ from a uniform value of one as influenced by the combination of $\psi(y)$, $\sigma^2 h/g$ and D/h. It is the equivalent constant coefficient of added mass, applied at all elevations, that yields the correct natural frequency in a fluid for a prescribed mode shape.

The four mode shapes studied were the cantilever mode, defined by equation (47), and approximations to three higher modes defined by:

$$\psi(y) = \sin n\frac{\pi}{2}(1 + y/h); \quad n = 3, 5, \text{ and } 7. \qquad (56)$$

The results are plotted in Figures 9 and 10; equations used to obtain results are given in Appendix B.

The significant result for the cantilever mode is the increased sensitivity of R_{am}^* to D/h when compared with results for the
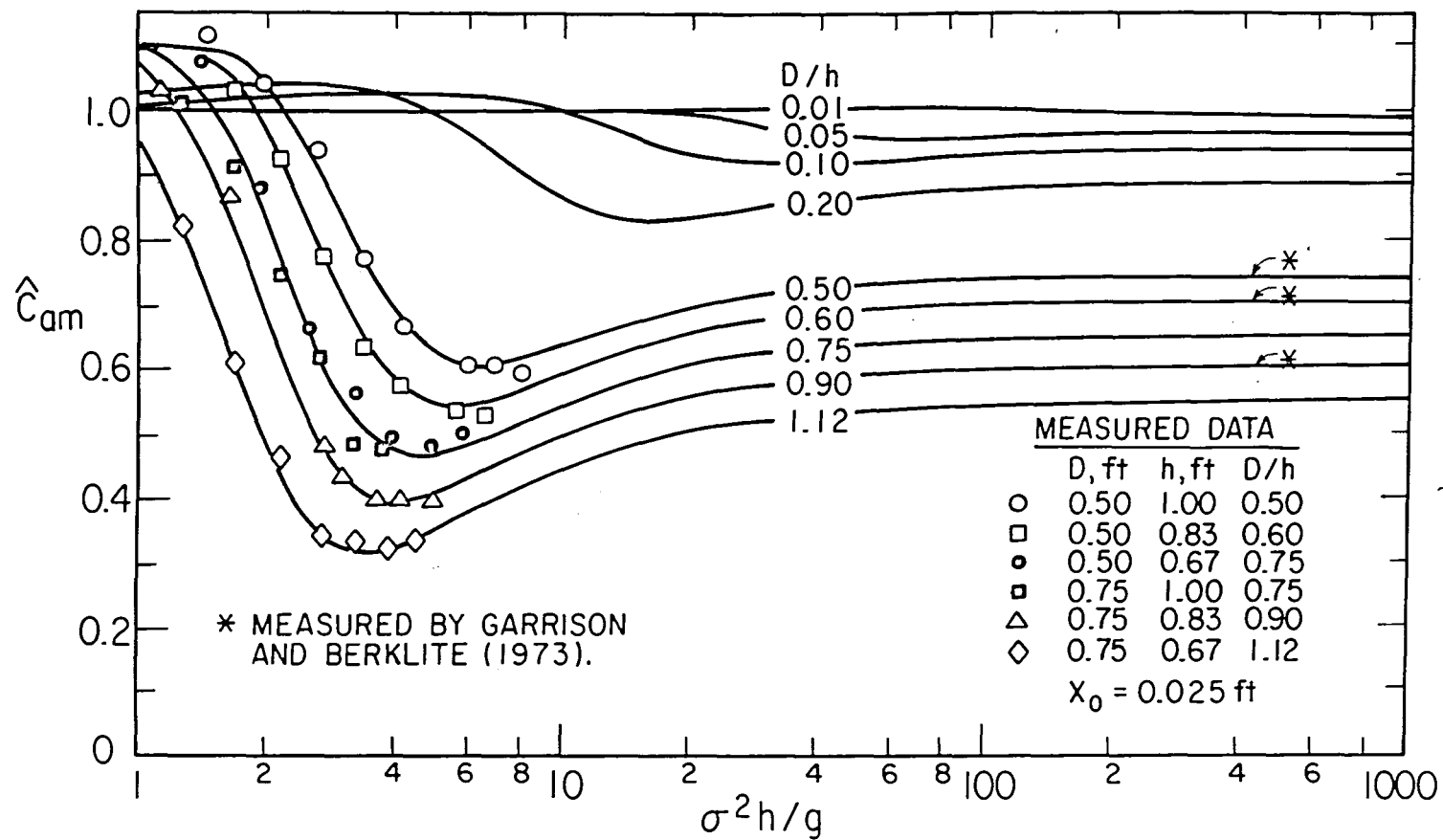
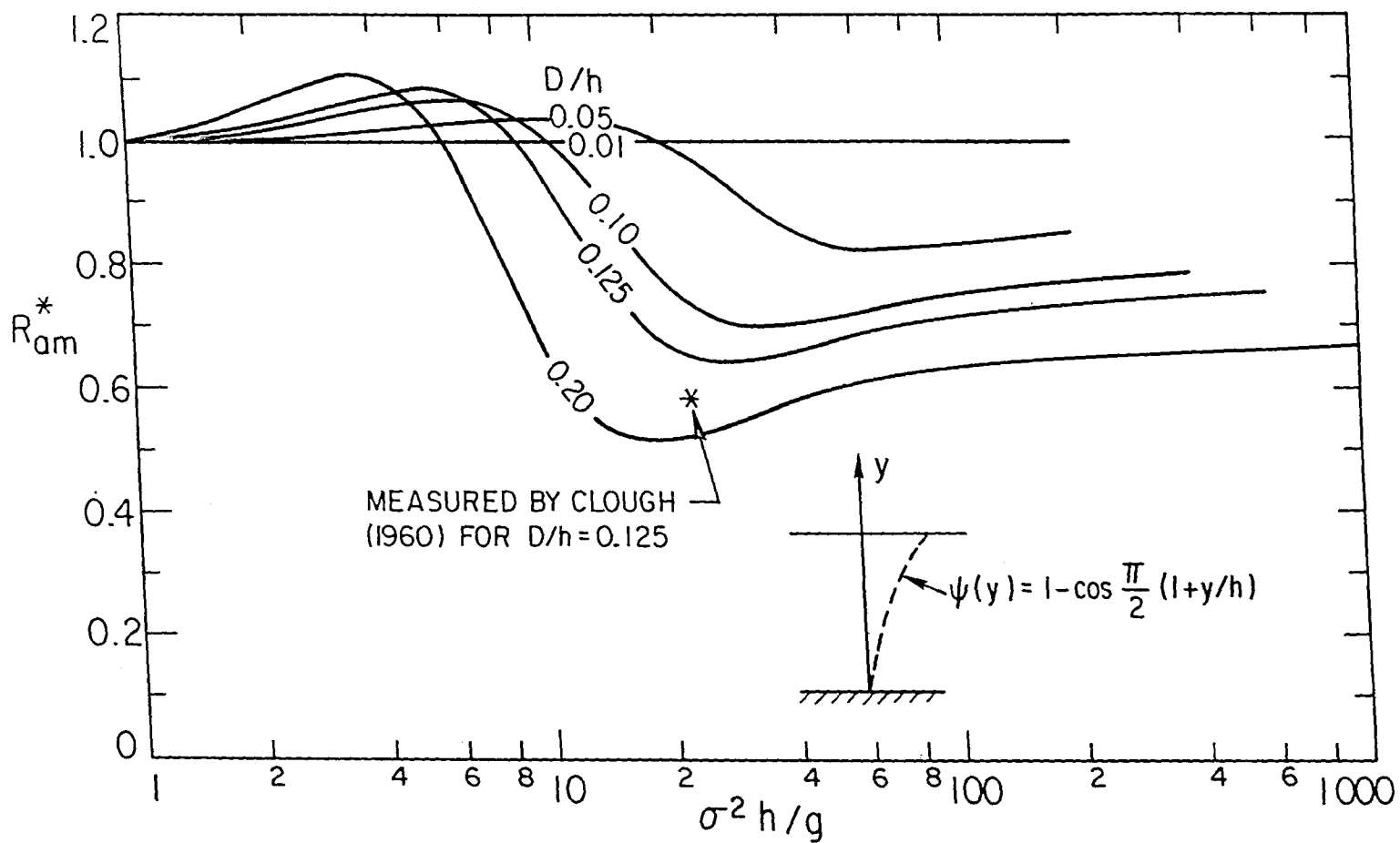Figure 8. Average coefficient of "added mass" for translation mode.

Figure 9. Effective coefficient of "added mass" for cantilever mode.
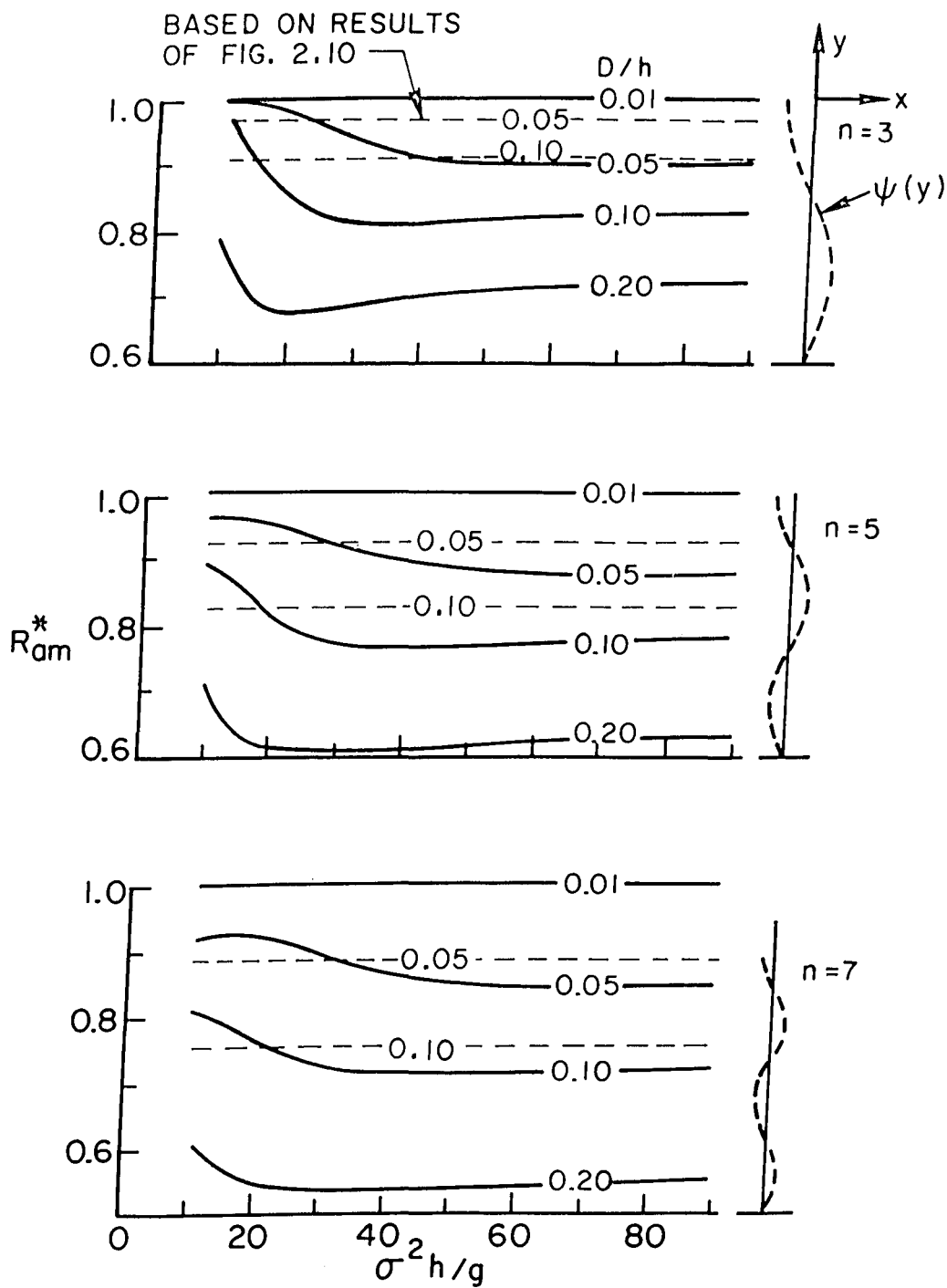
Figure 10. Effective coefficient of "added mass" for
$\psi(y) = \sin n \pi/2(1 + y/h)$; n = 3, 5, and 7.

43

translation mode. This effect is primarily due to the weight function $\psi^2(y)$ being applied to the variation of $C_{am}(y)$, as exhibited in Figures 6 and 7, rather than due to effects of $\psi(y)$ on $C_{am}(y)$. This was clarified by study of the higher mode shapes.

Figure 10 shows that as the number of nodes increases for the higher modes, R_{am}^* for a given D/h and $\sigma^2 h/g$ decreases. The results are a combination of effects due to $\psi(y)$ and the presence of a free surface and an impermeable bottom. As n increases, the effect of the free surface and bottom contribute less and less to R_{am}^*. The primary contribution comes from $\psi(y)$. The resulting R_{am}^* approaches that for $\psi(y)$ in a fluid of infinite extent in the y-direction. Evidence for this is shown by the dotted lines that correspond to the infinite fluid result plotted in Figure 11, calculated from the velocity potential derived by Landweber (1967). The dotted lines were obtained from Figure 11 by the relationship $\pi D/S = \pi/4 \, n \, D/h$, where S is the wavelength of the deflected shape.

Figure 11. Effective added mass for flexible cylinder in infinite fluid.

4. Hydrodynamic Forces Due to the Incident Waves.

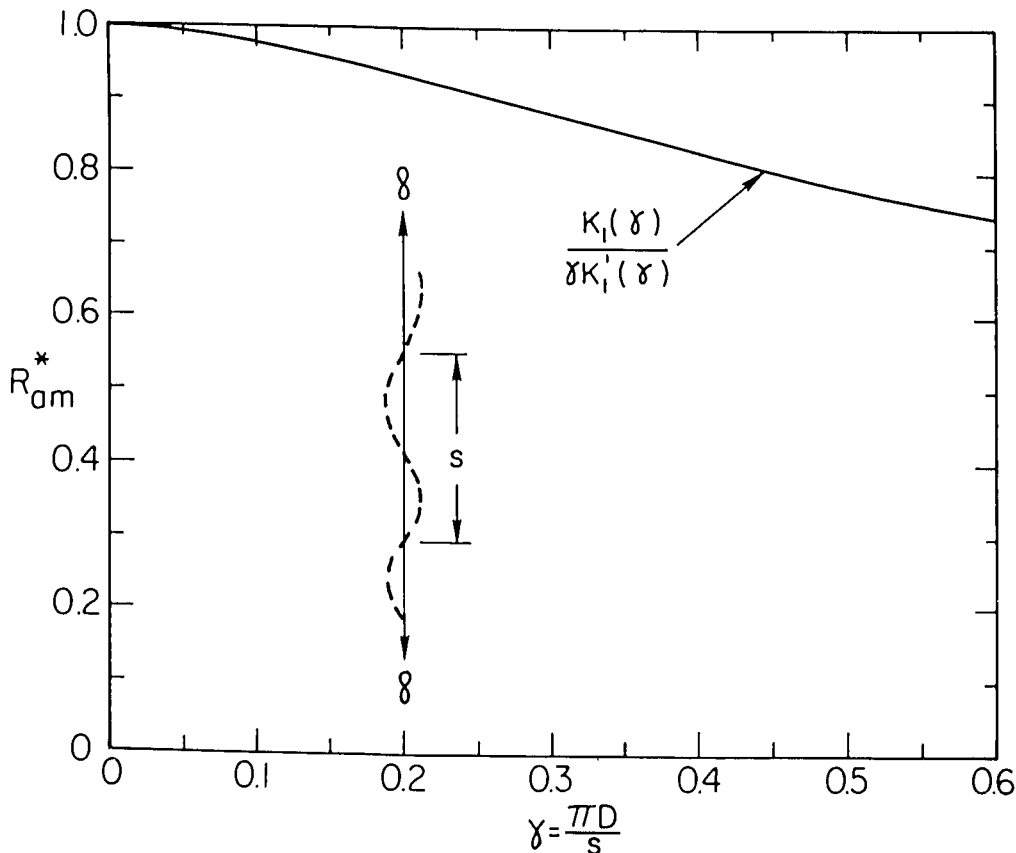The velocity potential, ΦG, for the diffraction of a plane surface wave about a rigid vertical cylinder has been derived by Havelock (1940) for infinite depth and by MacCamy and Fuchs (1954) for finite depth.

a. Distributed Force. For a wave of height H traveling in a positive x-direction, defined by:

$$\eta = \frac{H}{2} \sin(kx - \sigma t),$$

where η is the surface elevation, the force per unit length is given by:

$$f_g(y,t) = - \frac{2\rho g H}{k} \frac{\cosh k(y+h)}{\cosh kh} P_4(ka) \cos(\sigma t + \gamma), \tag{57}$$

where

$$P_4(ka) = 1/[J_1'(ka)^2 + Y_1'(ka)^2]^{\frac{1}{2}} = [\pi ka\, P_1(ka)/2]^{\frac{1}{2}}, \tag{58}$$

$$\gamma = \text{arc} \tan[J_1'(ka)/Y_1'(ka)], \tag{59}$$

f_g is maximum at the MWL and decays with respect to y like the wave-making forces. In nondimensional form it is a function of two parameters kh and ka. Unlike the forces due to the motion of the cylinder, the incident-wave forces do not depend on $\psi(y)$; this is a consequence of linearization.

b. Total Force and its Relationship to the Generalized Force. Although $\psi(y)$ has no direct influence on f_g, it does enter into the calculation of dynamic response as a weight function applied to f_g, yielding $F_G^*(t)$ as defined by equation (20). The force magnitude at the first-mode frequency will be of most importance for the dynamic response problem. This frequency will usually be sufficiently high that f_g will be concentrated in the near-surface zone and $\psi(y)$ will have little influence. For practical purposes the generalized force will then be equal to the total deepwater force. The error made will be identical to that made in the calculation of f_w based on the translation mode.

The amplitude of total force, F_G, in nondimensional form is defined by C_g. For deep water (kh > π) it is given by:

$$C_g = F_G/\rho g \pi a^2 (H/2) = \frac{8}{F_0^3} \left[\frac{P_1(F_0^2/2)}{\pi} \right]^{\frac{1}{2}}. \tag{60}$$

It is plotted in Figure 12; the limiting values were derived using the limiting values for the function P_1 in Appendix B.

The plotted results show that the nondimensional force decreases rapidly beyond $F_0 = 1$. This decrease is important because the effective exciting force can be decreased by increasing the first-mode frequency.

45
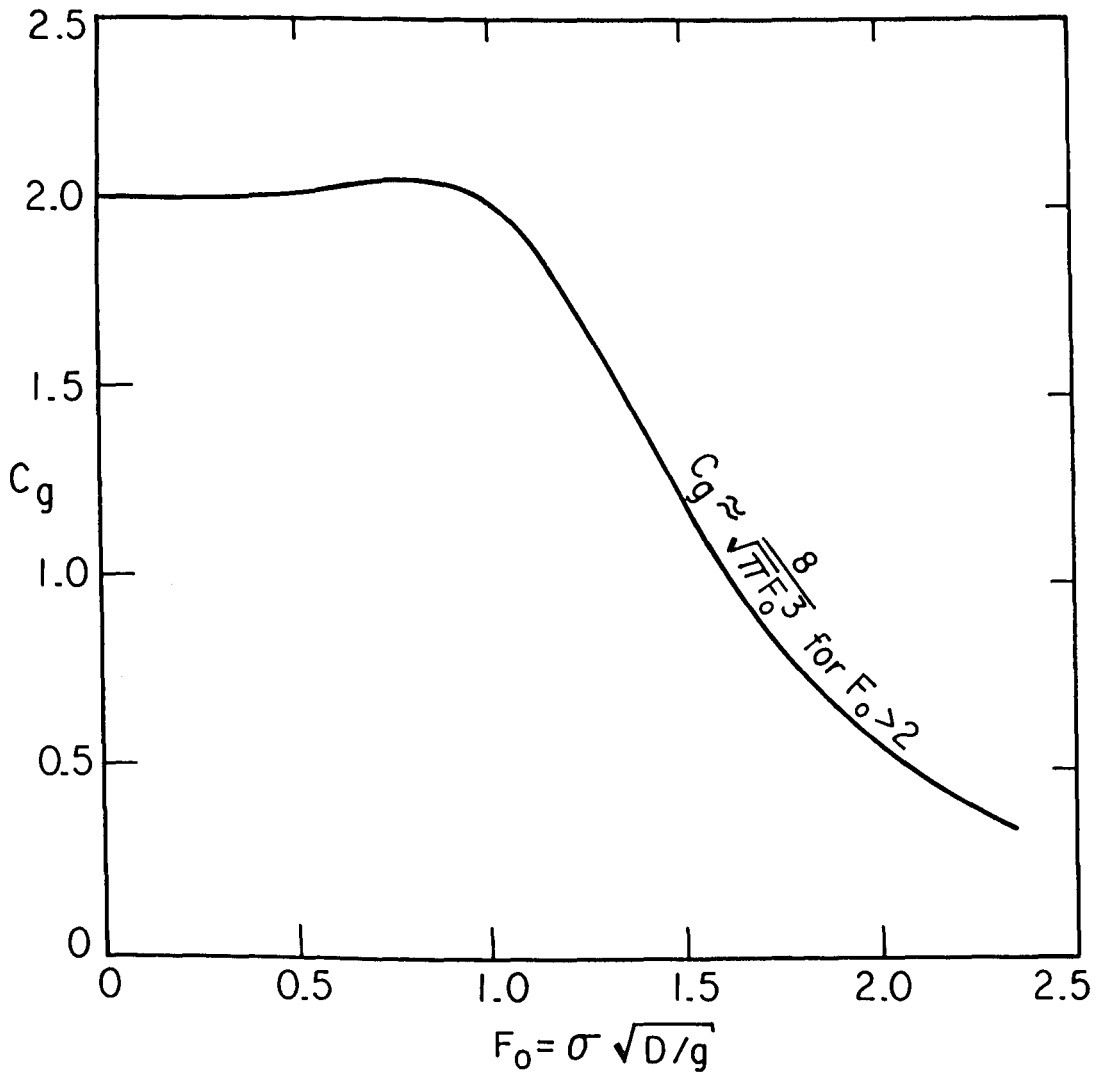
Figure 12. Coefficient of the force due to the incident wave
for $\sigma^2 h/g > \pi$.

5. Dynamic Response and Damping.

The wavemaking and added-mass forces of the previous sections show
that the coefficients of the differential equation of motion (equation 19)
are frequency-dependent. This implies that the dynamic system is actually
represented by an integral equation in the time domain (Tick, 1959).
Consequently, the transient part of the well known general solution of
the equation with constant coefficients is not valid in this case. To
obtain the transient part requires the solution of an initial value
problem. However, the steady-state part of the general solution is valid
and can be used to obtain the response due to either periodic waves or
random waves specified by a wave spectrum.

The steady-state solution for the amplitude of dynamic response, X_{0d}, due to a periodic input of frequency σ is given by the following equation:

$$X_{0d} = (DMF) \; X_{0s} , \tag{61}$$

where

X_{0s} = amplitude of static response,

DMF = dynamic magnification factor,

$$= 1/\{[1 - (\sigma/\sigma_n)^2]^2 + [2\xi(\sigma/\sigma_n)]^2\}^{\frac{1}{2}} .$$

The DMF for constant values of ξ is plotted in Figure 13. It is a unimodal function of σ/σ_n peaking at 1.0 for ξ values less than about 0.20 (20 percent of critical damping). The value at resonance is inversely proportional to ξ; equal to $1/2\xi$. Static response occurs when σ/σ_n becomes small because then $DMF \approx 1.0$. The $DMF \to 0$ as $\sigma/\sigma_n \to \infty$.

In the case of damping due to wavemaking, equation (24), gives:

$$\xi = \xi_w = C_w^* / 2\sigma_n (M_s^* + M_{am}^*) , \tag{62}$$

where C_w^* and M_{am}^* are functions of $\sigma^2 h/g$, D/h and $\psi(y)$. In deep water this reduces to:

$$\xi_w \approx \frac{C_w(F_0) \, \rho g \pi \, D^2/4}{2\sigma_n^2 (M_s^* + M_{am}^*)} . \tag{63}$$

F_0 and $\sigma^2 h/g$ can be written by $(\sigma/\sigma_n) \, \sigma_n \, \sqrt{D/g}$ and $(\sigma/\sigma_n)^2 \, \sigma^2 h/g$, respectively, and consequently ξ in equation (61) will be a function of σ/σ_n. Therefore, the DMF will have a different shape from that shown in the figure and this would have to be taken into account when calculating the dynamic response spectrum to random waves. Nevertheless, the DMF for constant ξ is very useful for understanding the importance of damping. Its inverse proportionality to ξ at resonance implies that even very small amounts of damping are important in reducing the dynamic response. For example, if the forcing function is simple-harmonic with $\sigma = \sigma_n$ then $X_{0d} = (1/2\xi) \, X_{0s}$. Wave energy is usually spread over a band of frequencies so that the effectiveness of ξ in reducing the overall response, defined by the rms $[X(t)]$, will depend to a great extent on how far removed is the frequency σ_p at the peak of the wave spectrum from the natural frequency of the structure. For example, under lifetime design storm conditions, such that $\sigma_p \ll \sigma_n$, the static response may dominate; but under the more frequently occurring moderate conditions such that $\sigma_p \approx \sigma_n$, the dynamic response will be inversely proportional to ξ.
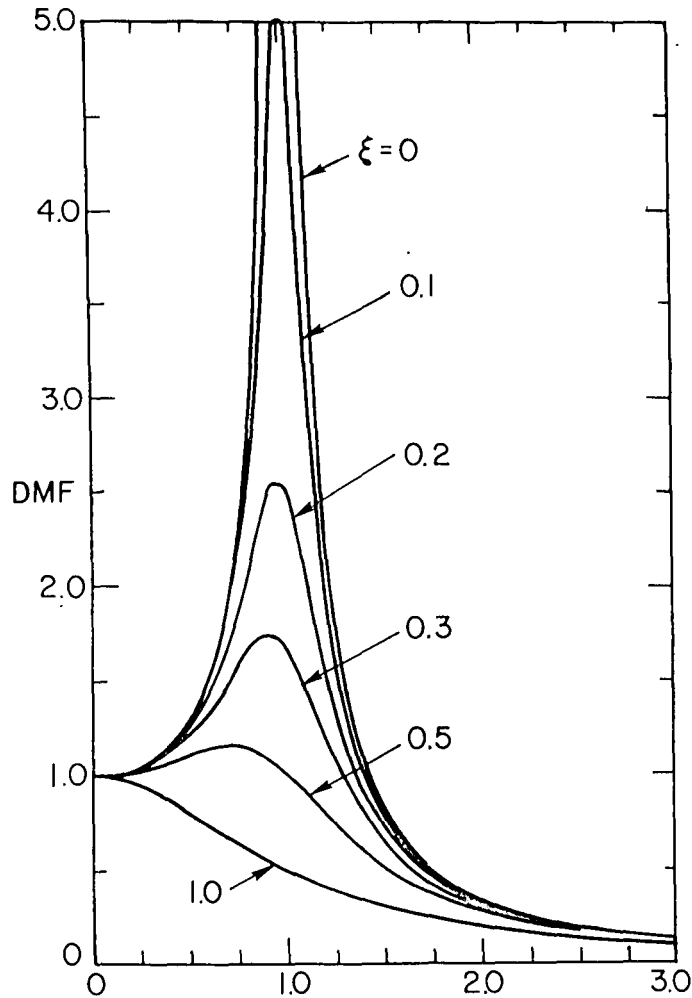
Figure 13. Effect of damping on dynamic
response (Biggs, 1964).

Consequently, the effectiveness of ξ must be evaluated on a statistical basis taking into consideration the occurrence probabilities of lifetime and moderate conditions.

a. Idealized Platforms. ξ_w and dynamic response were studied theoretically as a function of diameter for three idealized platforms having natural periods of 3, 4, and 5 seconds in a water depth of 600 feet. The objective was to determine the level of damping that can be obtained from this mechanism and the conditions under which it is of significance.

The idealized platforms are described with reference to Figure 2. The first platform is a single vertical cylinder extending to the MWL having a wall thickness of 2 inches and no deck. The second platform is the same except that it extends some distance above the MWL and supports a deck. Both the mass of the deck and mass of the steel above the MWL are assumed

lumped at the deck level so that the generalized mass, M_1^*, is 400 k-slugs. This value was obtained from the mass at deck level used by Burke and Tighe (1972) for proposed deepwater drilling platforms. The third platform is the same as the second except that M_1^* is assumed to be shared by four legs. Consequently each of the legs contributes to wavemaking; interaction between legs was neglected. In all cases the shell was considered full of water adding a mass per unit length of $\rho \pi D^2/4$ to the structural mass. The cantilever mode shape was used for $\psi(y)$.

(1) <u>Effect of Diameter and Natural Frequency on ξ_w.</u> ξ_w was calculated by using equation (62) with the assumption that $\sigma = \sigma_n$. The total generalized mass, M^*, for the cantilever mode shape was given by:

$$M^* = M_s^* + M_{am}^* = [(\rho A_w + \rho_s A_s) + \rho A_w \, R_{am}^*] \int_{-h}^{0} \psi^2(y)\,dy + M_1^*/N \qquad (64)$$

where

A_w = area of enclosed water $\approx \pi D^2/4$

A_s = area of shell $\approx \pi D d$ where d = wall thickness

ρ_s = mass density of steel

$$\int_{-h}^{0} \psi^2(y)\,dy = 0.228h$$

N = number of legs

R_{am}^* is defined by equation (55).

C_w^* was calculated exactly, although the use of the deepwater approximation, defined by equation (49), would have resulted in an error no higher than 10 percent. ξ_w is shown plotted versus diameter in Figure 14.

The plotted results show that ξ_w will be most important for the larger cylinders. However, the diameter for which it becomes significant will depend on σ_n. The results also indicate that ξ_w generally increases with decreasing σ_n but the relationship is complicated because for a given diameter ξ_w may sometimes be greater for the platform having a higher σ_n. The following explains the theoretical results in terms of the wavemaking forces and their dependence on the parameter, $F_0 = \sigma_n \sqrt{D/g}$.

The first case (one leg; no deck) represents an approximate upper bound on the available ξ_w because the structural mass of this idealized
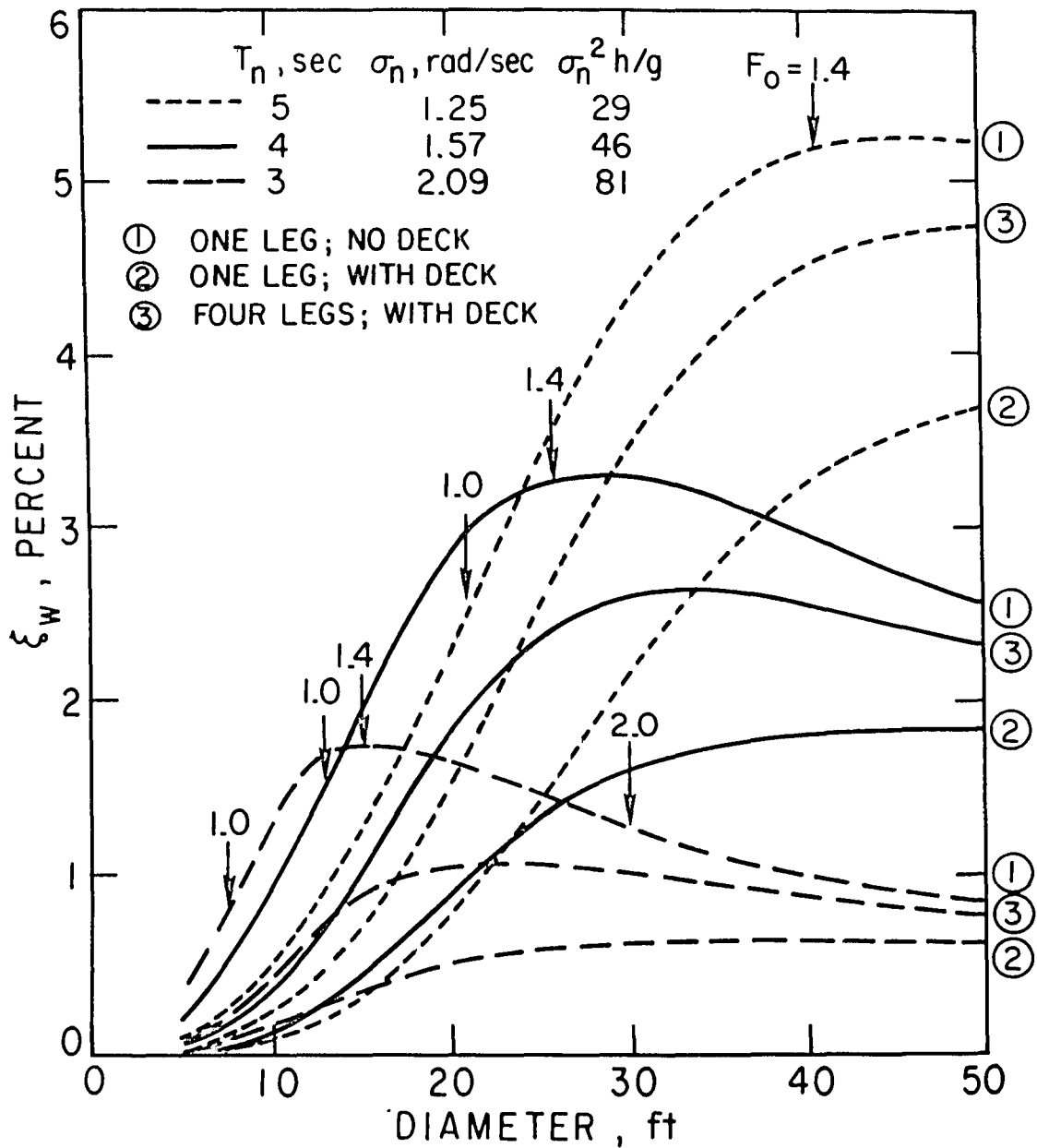
Figure 14. Effect of natural frequency and diameter on percent of critical damping for idealized platforms in water depth of 600 feet.

platform for diameters larger than 20 feet is less than 15 percent of the combined added mass and mass of the internal water. The effect of diameter on ξ_w can be understood from the deepwater approximation for C_w^* defined by equation (63). When F_0 is less than one, this equation implies that $\xi_w \propto D^2$ because both C_w^* and $M_{am}^* \propto D^2$. This quadratic increase of ξ_w with increasing diameter is portrayed by the left limbs of the plotted curves. When F_0 is greater than about two, $\xi_w \propto D^{-1}$ because then $C_w \propto D^{-1}$ but $M_{am}^* \propto D^{-2}$. Consequently, ξ_w decays more slowly with increasing diameter than it rises. The rise and decay imply that there must be a diameter for which ξ_w is maximum. This diameter is defined by $F_0 = 1.4$ at which C_w is a maximum.

The effect of decreasing the natural frequency is to increase the peak ξ_w and shift it to larger diameters. The shift of the peak results from the requirement that $F_0 = 1.4$. An increase in the peak ξ_w occurs because both C_w^* and $M_{am}^* \propto D^2$; consequently $\xi_w \propto \sigma_n^{-2}$. For a given diameter monotonic relationships exist only in the limiting situations where F_0 is less than one and greater than two, respectively. When $F_0 < 1$, $\xi_w \propto \sigma_n^2$ because $C_w \propto \sigma_n^{-4}$ and Figure 9 implies that M_{am}^* is practically independent of σ_n for the range of values that are considered here. When $F_0 > 2$, $\xi_w \propto \sigma_n^{-4}$ because $C_w \propto \sigma_n^{-2}$. These results are valid only for the range of σ_n satisfying the criteria on F_0. In general, for a given diameter, ξ_w need not be monotonically related to D and requires a series of plots as shown here to evaluate the conditions under which maximum damping can be achieved.

Similar trends exist for the other cases. The major difference is the decrease of ξ_w and the shift of the peak values to larger diameters. These effects are due to the contribution of the deck mass and can be similarly explained by a study of equation (63).

The behavior of ξ_w for prototype structures will be approximately represented by the region between the plots for the second and third cases. ξ_w for the smaller diameters (but not < 15 feet) will correspond more closely to the second case because one column will probably not be sufficient to provide the necessary stiffness. In this case, ξ_w will range from 0.5 to 1.0 percent of critical. For the larger diameters it will correspond more closely to the third case. Consequently, ξ_w will be higher, on the order of 2 to 3 percent of critical.

Decreasing the water depth would increase ξ_w because M_{am}^* is proportional to h. However, σ_n will likely be larger because stiffer platforms can be constructed in shallower water. This will tend to decrease ξ. The net effect requires an analysis for each depth.

(2) <u>Effect of Diameter and Diffraction on Dynamic Response.</u> The dynamic response at resonance is given by:

$$X_{0d} = \frac{amp[F_G^*(t)]}{\sigma_n \, C_w^*} .$$ (65)

Using the deepwater approximations for the amplitude of $F_G^*(t)$, defined by equation (60), and C_w^* yields the result:

$$X_{0d}/(H/2) = \frac{C_g(F_0)}{C_w(F_0)} .$$ (66)

This is plotted in Figure 15 as a function of diameter for the idealized platforms. Because at resonance X_{0d} is independent of mass, all the idealized platforms have the same response provided the same incident-wave force acts on all legs.

The dynamic response, as shown in the figure, decreases with increasing diameter due to the combined effects of diffraction and wavemaking. This can be shown theoretically for $F_0 > 2$ where $C_w \approx 4/F_0^2$ and $C_g \approx 8/(\sqrt{\pi} F_0^3)$ yielding $X_{0d}/(H/2) \propto 1/D^{1/2}$. Diffraction acts as a low-pass filter significantly reducing the response of large-diameter platforms as illustrated for the 4-second natural period. The "no diffraction" curve was calculated by assuming $C_g = 2$, which is the limiting value as F_0 becomes small.

b. <u>Damping for Actual Platforms.</u> The Table below represents ξ_w for proposed deepwater oil drilling platforms that were studied by Burke and Tighe (1972) and Malhotra and Penzien (1969) and for the Texas Tower No. 4

Table. Damping due to wavemaking for actual platforms.

Source	h (ft)	σ_n (rad/s)	k-slugs[1]	N [2]	D (ft)	F_0	$C_w(F_0)$	ξ_w (pct)
Burke and Tighe (1972)	400	2.59	560	4	5.0	1.02	0.66	0.05
	600	1.67	900	4	5.0	0.66	0.18	0.02
	800	1.42	1,000	4	5.0	0.56	0.08	----
	1,000	1.01	1,800	4	5.0	0.40	0.02	----
Malhotra and Penzien (1969)	1,270	0.57	1,800	3	18.0	0.43	0.02	0.08
Brewer Engineering Laboratories, Inc. (1959)	180	2.20	330	3	12.5	1.37	1.48	0.56

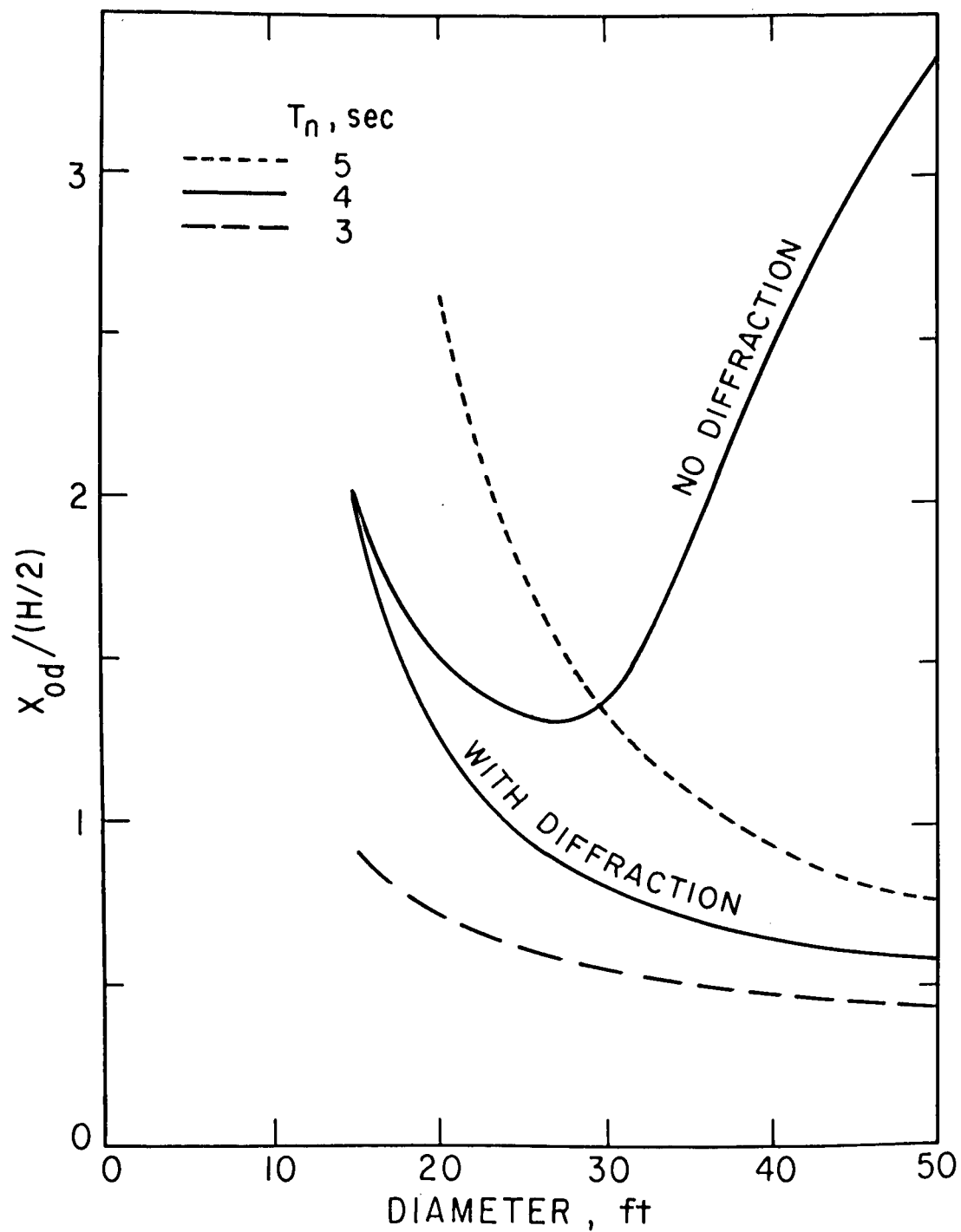[1]$M^* = \sum_i M_i \psi^2(y_i)$.

[2]Number of legs.

Figure 15. Effect of diameter and diffraction on the dynamic response at resonance for idealized platforms in water depth of 600 feet.

that was studied by Brewer Engineering Laboratories, Inc. (1959). ξ_W for the first five platforms in the Table is insignificant. Member diameters of the first four platforms are much too small for this damping mechanism to be effective, while the natural frequency is too low and the water too deep for the fifth platform. Only for the Texas Tower is ξ_W of some significance because the natural frequency and diameter combine to produce a maximum value for C_W. However, due to the predominance of the deck mass, the diameter is still too small to provide appreciable damping. For example, according to equation (63), assuming $M_s^* >> M_{am}^*$, a diameter of 25 feet could provide ξ_W close to 3 percent. Of course the design static load, being predominantly due to inertial forces, would be quadrupled. This would have to be considered in conjunction with any possible reduction in dynamic response.

The mode shapes and frequencies used to compute ξ_W for the oil drilling platforms were calculated from the mass and stiffness matrices published by the investigators. The mode shapes are shown in Figure 16.

III. EXPERIMENTAL VERIFICATION OF THE POTENTIAL MODEL

The objective of the experimental program was to verify the wavemaking and added-mass forces predicted by the potential model. The tests consisted of oscillating rigid surface-piercing vertical cylinders in a translation mode and measuring the total forces and the generated waves. These oscillations were performed in stillwater and therefore the verification is a limited one because a prototype structure in nature oscillates in an incident wave field. However, the test is valid within the scope of potential theory with linearized boundary conditions for which the forces due to the incident waves and those due to the motion of the structure are independent.

This section discusses the experimental equipment, important factors in their design, and the experimental program and its results.

1. Experimental Equipment and Important Factors in Their Design.

A general view of the experimental equipment and arrangement is shown in Figure 17. Some of the relevant dimensions are given in the schematic diagram of Figure 18. A four-legged platform of welded steel structural members supports the carriage used to transmit a translational oscillation to the test cylinders and the necessary power transmission equipment to impart to them an approximately simple-harmonic motion. It is placed in a rectangular basin (63 by 150 feet) so that the shortest distance from the test cylinders to the nearest wall is about 24 feet. The system is capable of oscillation frequencies up to 2.8 cycles per second and amplitudes of carriage displacement, X_0, up to 0.5 foot. An array of five gages is positioned along a circular arc to measure the surface waves in one quadrant.

a. Platform. The theoretical results of the previous section imply that the amplitude of the generated wave will be proportional to cos θ.
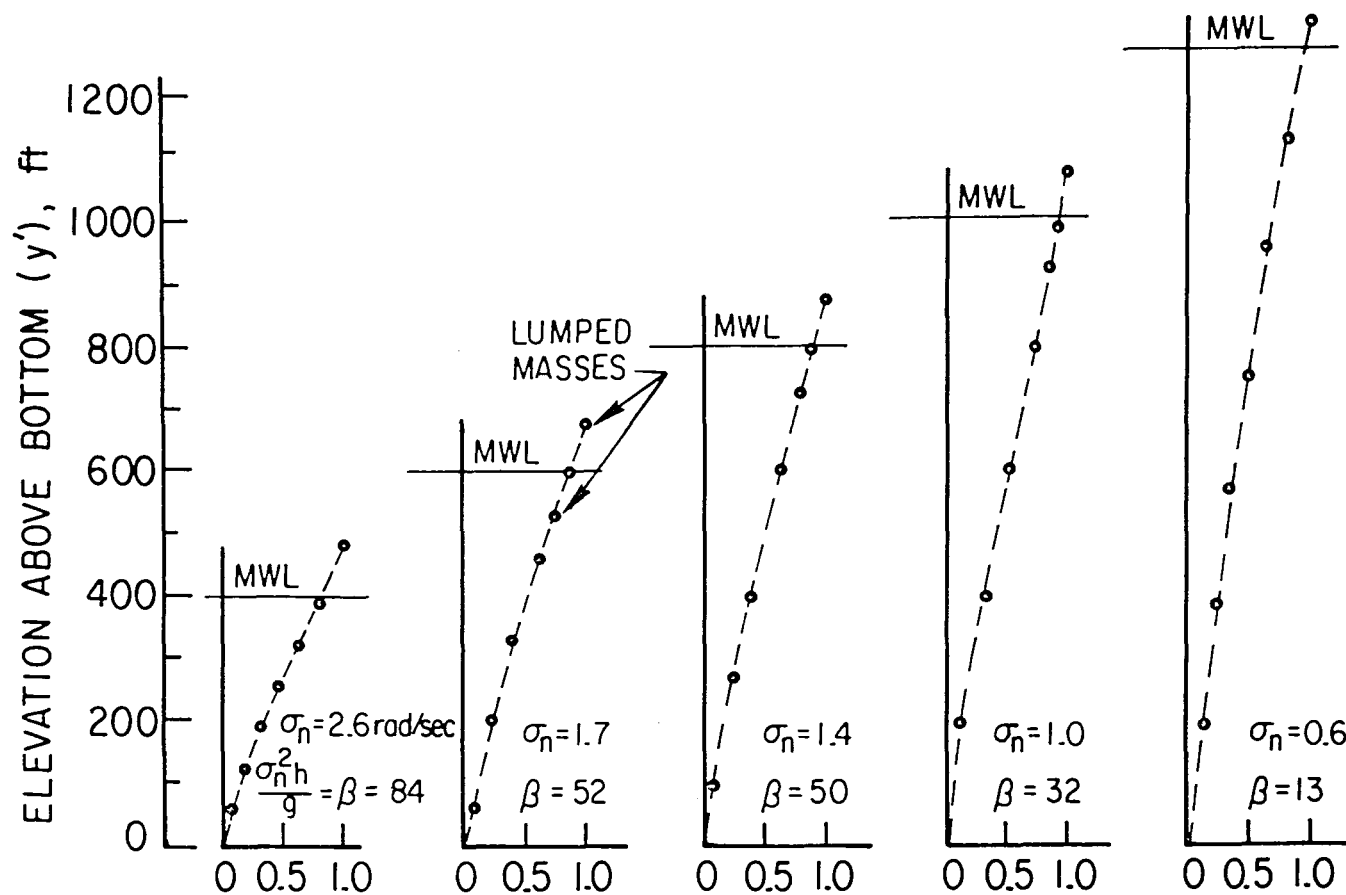
Figure 16. First-mode shapes and frequencies for lumped mass idealizations of five proposed deepwater oil drilling platforms (Burke and Tighe, 1972; Malhotra and Penzien, 1969).
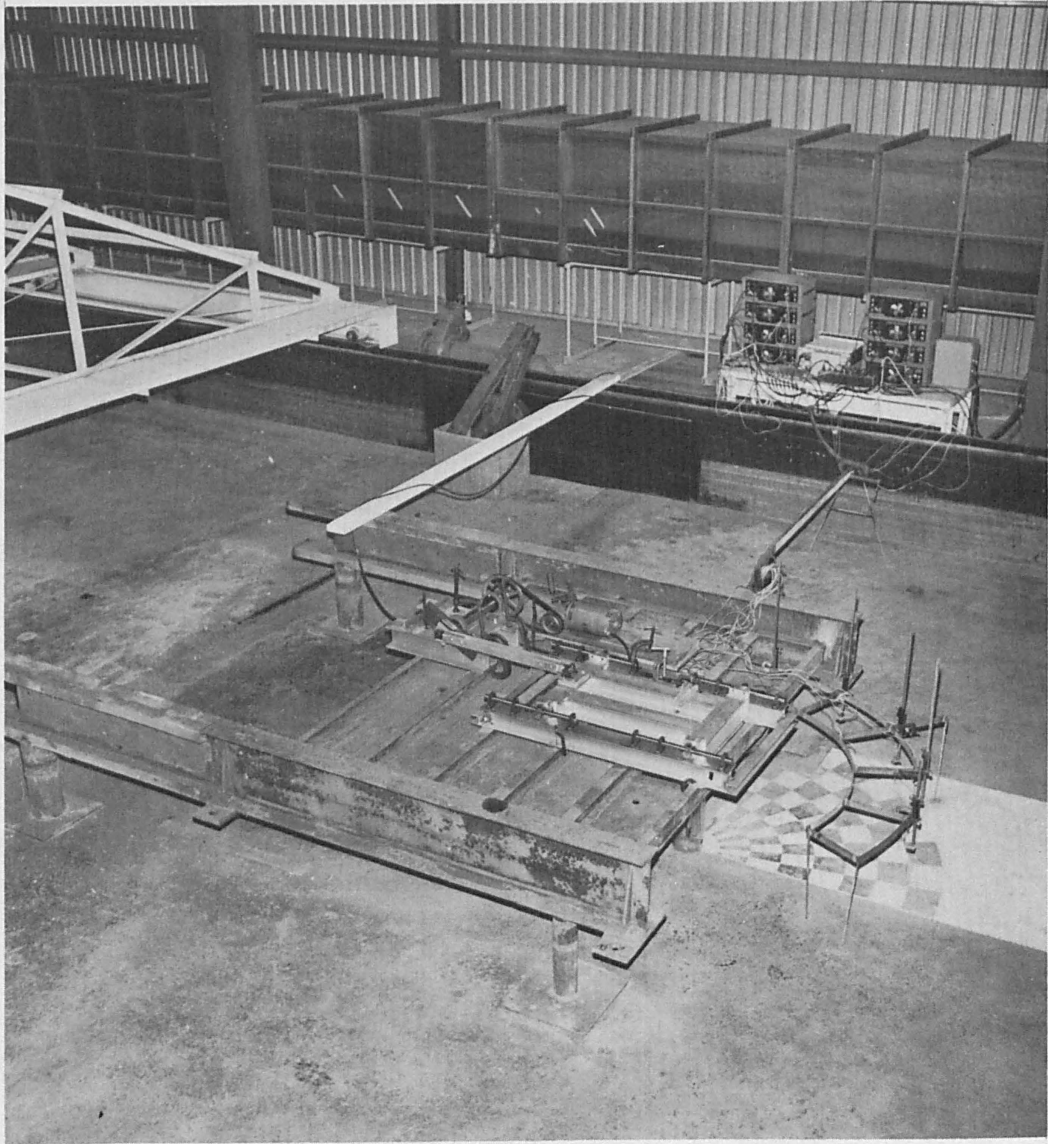
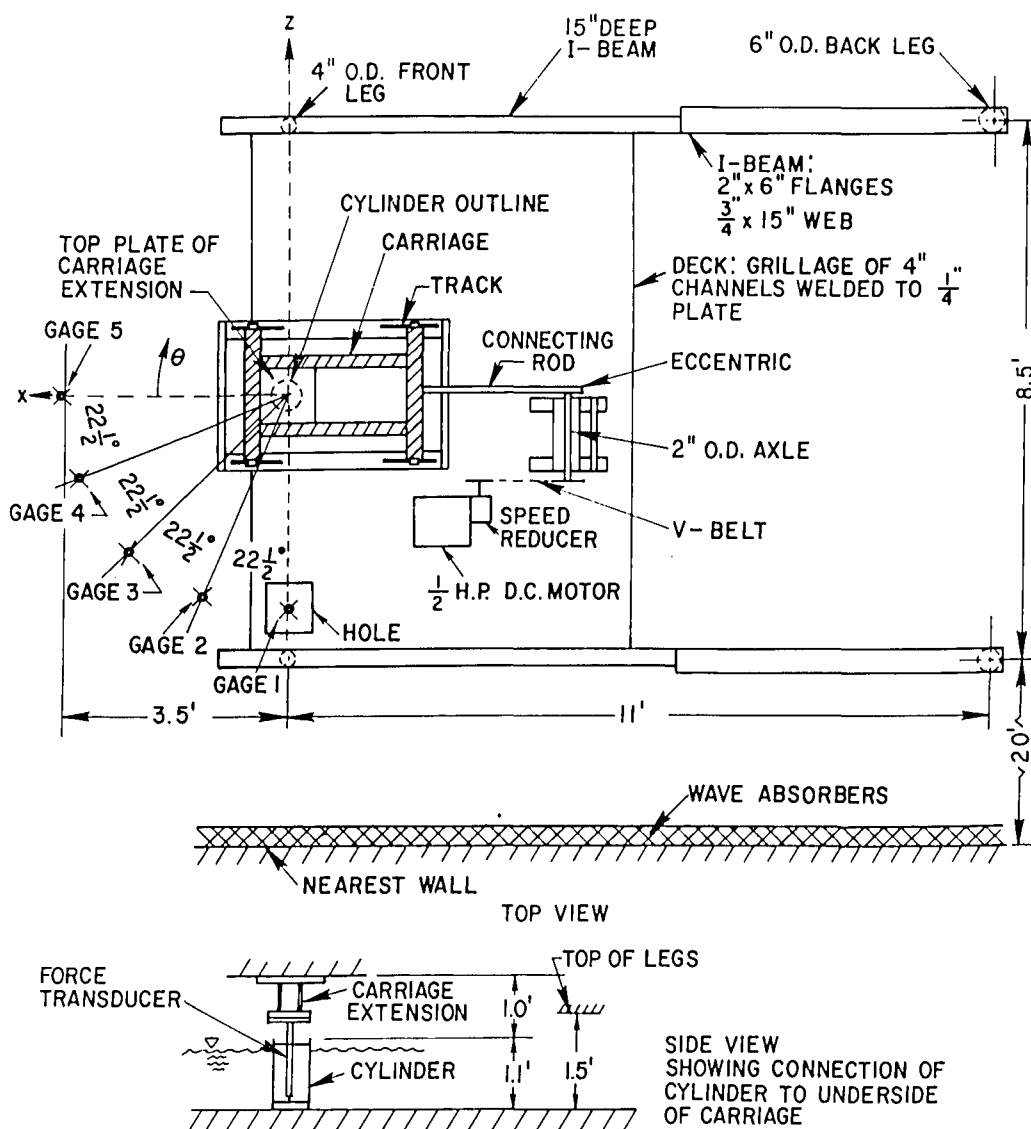Figure 17.   General view of experimental equipment.

Figure 18. Schematic diagram of experimental arrangement.

Consequently, to minimize the effect of wave reflection it was necessary to perform the experiments off a platform situated near the middle of a wide basin; existing two-dimensional flumes could not be used. This necessitated the construction of a platform for supporting the carriage and power transmission equipment.

The main design considerations were rigidity and wave reflectivity. It was very important for the platform to be rigid (have a large stiffness and high modal frequencies) because frequency-dependent energy sources dynamically excite the platform and the resulting vibrations could contaminate the force measurements. The simple-harmonic motion of the carriage at a maximum frequency of 2.8 cycles per second induces horizontal loads on the platform at the same frequency and vertical loads and torque on the axle of the eccentric and speed-reducer shaft at double the frequency. Energy at higher frequencies is supplied by motor noise and impact forces due to backlash in the speed-reducer gears and clearances in other moving parts. Based on the experience of using a trial platform it was determined that a very rigid platform would be required; one for which the lowest natural frequency wouldn't be less than about 40 to 50 cycles per second. To minimize wave reflection the legs had to be of small diameter and located as far away as possible from the oscillating cylinder. However, this makes the platform more flexible so that a compromise had to be made between rigidity needs and minimization of wave reflection.

The present platform satisfied the natural frequency criteria for the following assumed modes of vibration: (a) a vertical mode in the z-y plane (the y-axis points out of the page in Figure 18.) where the deck bends as a beam assumed simply supported by the I-beams; (b) a vertical mode in the x-y plane where the beams supporting the deck bend as if simply supported by the legs; and (c) a horizontal mode where the deck and the supporting beams translate in the x-z plane, the stiffness being provided by the legs which are assumed fixed to the underside of the beams and pinned at the basin floor.

Wave reflection from the front legs was minimized by locating the carriage so that the mean position of the cylinder axis intersected a line connecting the two front legs. Although according to linear theory no energy should radiate perpendicular to the direction of oscillation, measurements showed a small amount at twice the oscillation frequency. This was too small to affect the force measurements and could be neglected in the calculation of radiated energy from the measured surface waves. Reflections from the back legs were also small and in most cases sufficient force and wave data were obtained before the reflected wave arrived.

b. _Carriage._ The purpose of the carriage is to transmit a translational motion to the cylinder along a line. Consequently, it was essential that all elements of the carriage and supports be rigid and the motion restrained laterally and vertically. At the same time the carriage had to be light to reduce the inertial loads on the platform and on the mechanical linkages. The restraints had to be low-friction devices

for which the difference between dynamic and static friction was small so that impact forces due to stick-slip would be minimized. Welded aluminum construction was used for the carriage to meet the rigidity and weight requirements and special roller-bearing devices were used to meet the friction and restraint requirements.

The carriage that was used is a welded aluminum frame of four 4- by 4- by 5/16-inch H-beams (Figs. 17, 18, and 19) supported on four tracks of 1-inch O.D. solid stainless steel 60 Case-hardened and ground shafting of material 440C. The supports and restraints are provided by the SKF linear-motion assemblies shown in Figure 20. These assemblies solved the difficult problem of providing a frictionless four-point support and complete lateral and vertical restraint without the alinement problems that usually occur in such cases. Each assembly consists of two rollers enclosed within a housing; each roller is supported by two completely sealed ball bearings. On one side of the carriage the rollers within the housings can move along their axes, thereby preventing jamming due to any misalinement in the tracks. Each assembly can be rotated so that the rollers can be preloaded in place onto the shafting thereby eliminating any play in the vertical direction. Each of the tracks is rigidly connected to a lower aluminum frame by means of three shaft-support blocks (Fig. 19). The blocks are movable to allow a maximum travel of 1 foot. The lower frame acts as a rigid base for the carriage. A rigid vertical extension of the carriage, consisting of an H-beam whose ends are butt-welded to aluminum plates, connects to the underside of the carriage (Fig. 18). The H-beam passes through a hole cut in the platform and the lower welded plate provides a flat surface for attaching the force transducers and cylinders (Fig. 21). The use of four clamps as shown in the figure provided a sufficiently rigid connection.

c. Power Transmission Equipment. The power transmission equipment is illustrated in Figure 19. The basic elements are the connecting rod, eccentric and its axle, and the V-belt and pulleys.

The connecting rod transforms the constant rotational speed of the eccentric into a periodic translation of the carriage. The motion is approximately simple-harmonic if X_0 is sufficiently small compared to the length of the connecting rod and if the center of the eccentric's axle is at the same elevation as the center of the pin at the carriage connection point. The design length of the rod was 2.5 feet and X_0 was 0.25 foot for the force measurements. This resulted in the second harmonic of the carriage displacement and acceleration that was 0.25 and 1 percent, respectively, of the first harmonic. The corresponding values for the radiated wave measurements based on a maximum X_0 of 0.094 foot reached 0.9 and 3.7 percent. To reduce impact loads it was essential that the clearance between the pins and the bearing surface of the connecting rod ends be as small as possible. Commercially available bushing-type rod ends were found unsuitable because the initial wear was too great and ball bearing rod ends produced too much noise in the measured force
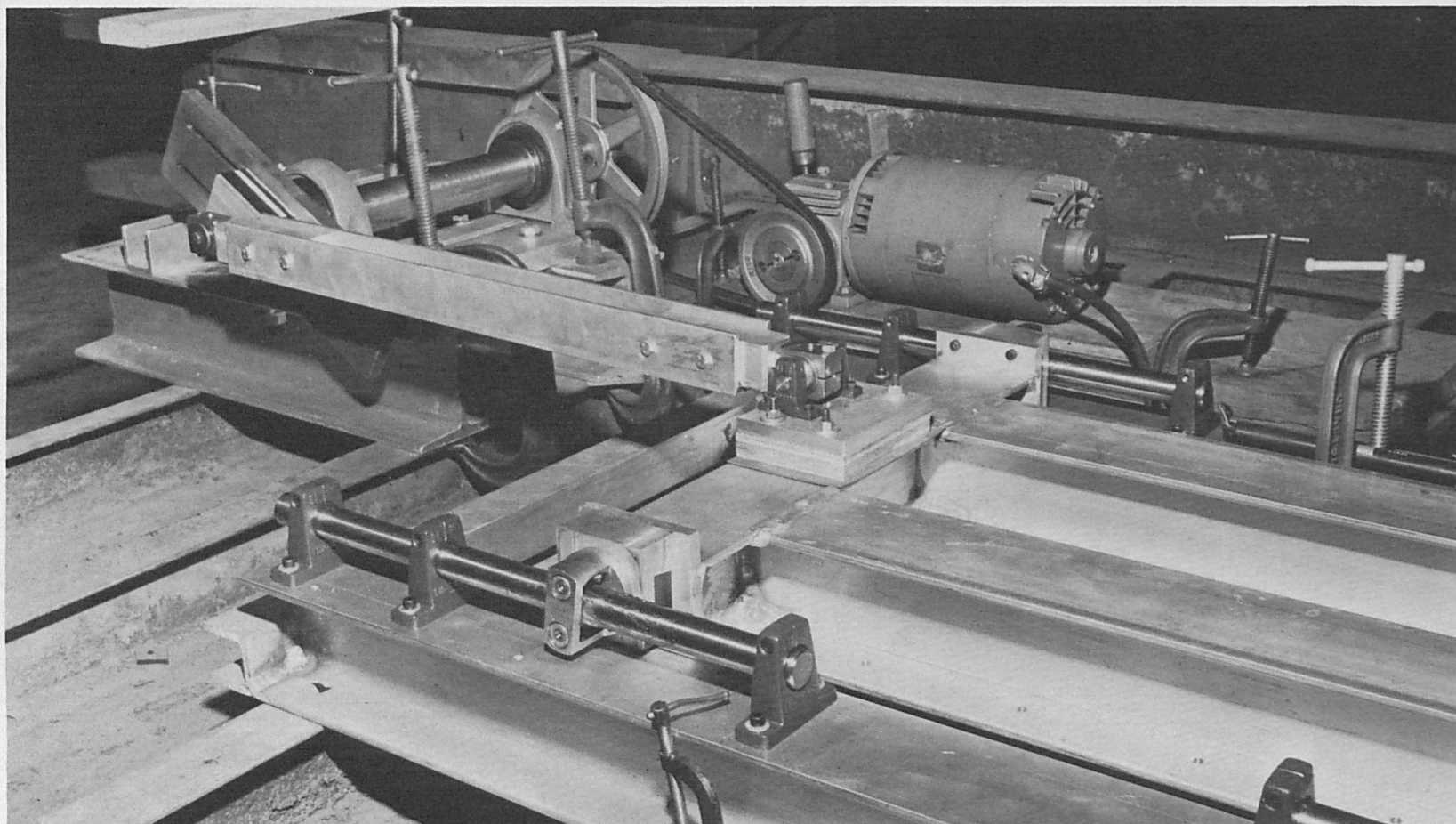
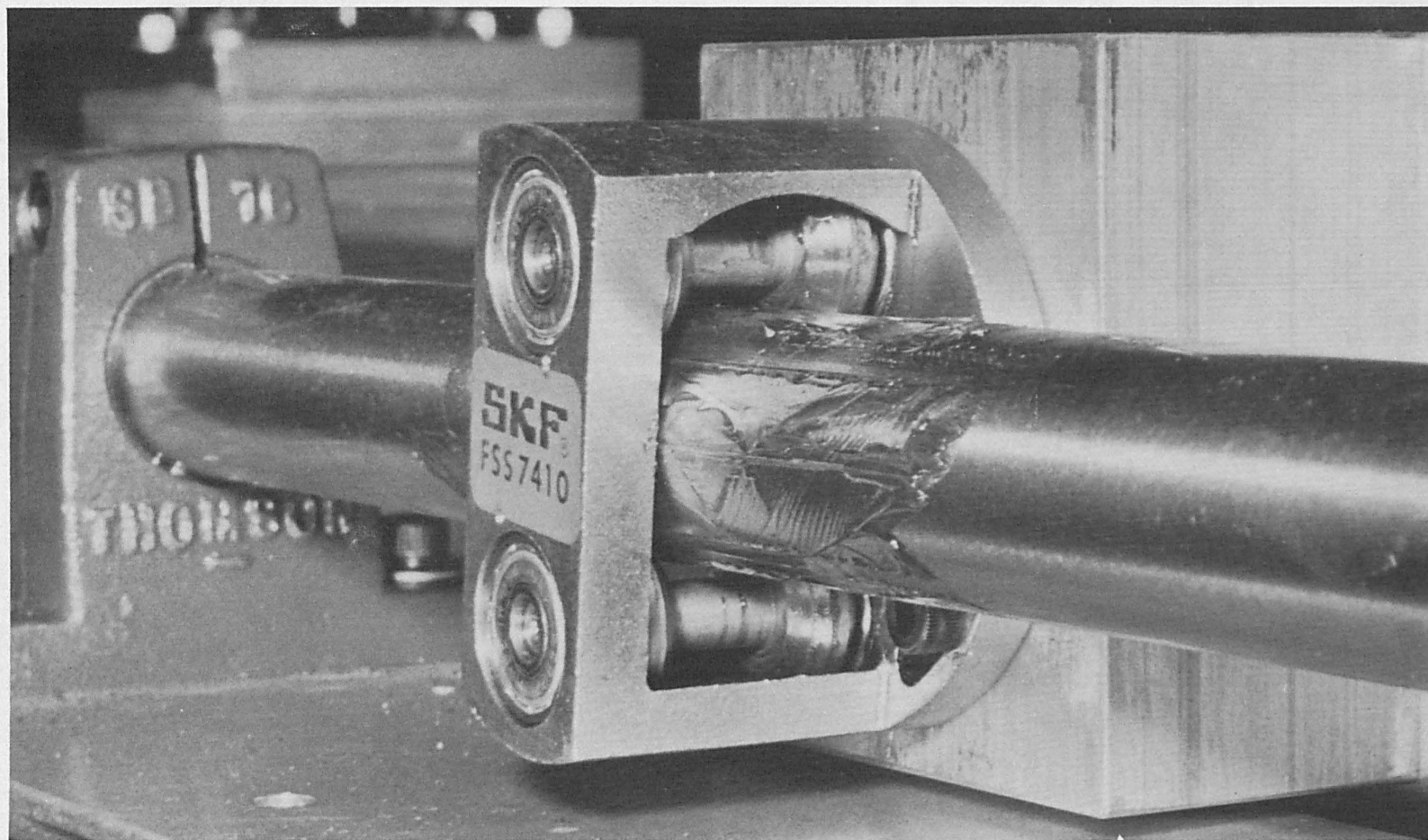Figure 19. Power transmission equipment.

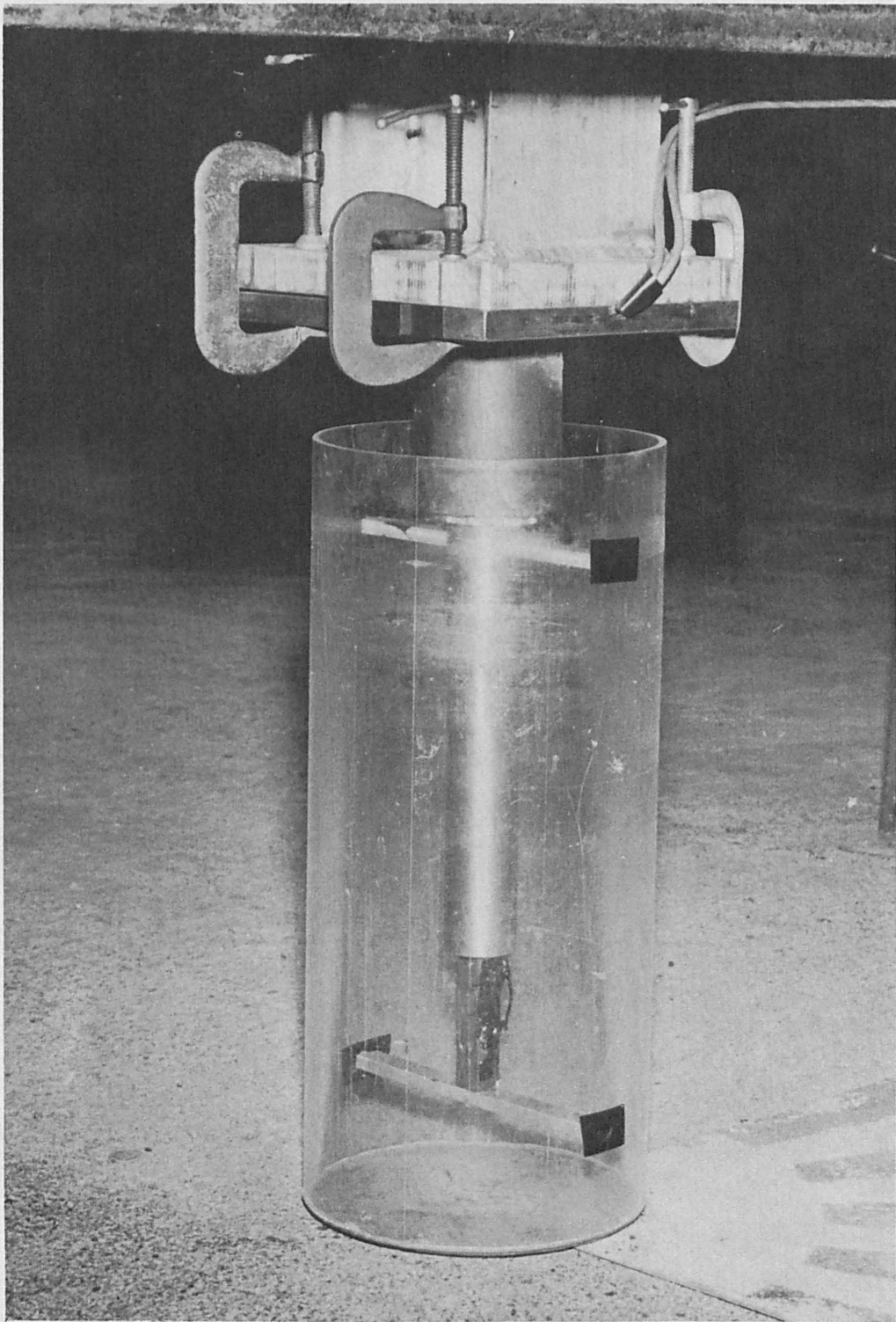Figure 20. Linear-motion assembly for supporting carriage on track.

Figure 21. Attachment of cylinder and force transducer to carriage extension.

records. Consequently, split-ring type rod ends of bronze-bearing material were designed and built. These were made with an adjustable bore thereby providing a method for controlling the clearance.

The eccentric is a device for adjusting X_0. It consists of a 3/4-inch thick steel plate butt-welded to a 2-inch O.D. axle. An aluminum block with an attached pin that connects to the rod end can freely slide along two slots that are cut in the plate. This allows a maximum X_0 of 0.5 foot. The important design consideration was the rigidity of the axle because the axle acts as a spring for the carriage mass and the added mass. After a 1-inch O.D. axle proved to be too flexible, the 2-inch O.D. axle was chosen. The noise content of the force measurements was reduced and its frequency increased.

Commercially available cast iron pulleys and a rubber V-belt were used to transmit the rotary motion from the speed-reducer shaft to the eccentric's axle. The noise level in the force measurements was sensitive to the tension of the belt. Although lowering the tension reduced the noise level, it had to be maintained at a high enough tension to prevent belt slippage and corresponding distortion of the simple-harmonic carriage displacement. An optimum tension was found and used throughout the force measurement experiments.

d. _Power_. The power was supplied by a combination of 1/2 horsepower direct-current motor and speed reducer. The motor speed could be varied over a continuous range by a variable transformer-type control. The 1/2 horsepower was sufficient because the dominant forces are inertial so that very little net work has to be done. A d.c. motor was particularly suitable because of its low noise level compared to an a.c. motor. The speed reducer was a worm-gear type. Because of clearance between the gear teeth impact forces occurred on torque reversal and contaminated the force records. However, enough control over the noise level was provided by the V-belt tension that special devices, such as a brake on the eccentric's axle, for preventing torque reversal were not necessary.

e. _Cylinders and Force Transducer_. Two cylinders, approximately 1.1 feet in height and having diameters of 0.50 and 0.75 foot, respectively, were used in the experimental program. These are illustrated together with the force transducer in Figure 22.

The cylinders had to be watertight containers constructed of light material in order to isolate the added-mass forces due to the outside water from the total force measurements. Plastic material was suitable for this purpose. Each cylinder was constructed of tubing having a wall thickness of 1/8 inch. A disk was welded to one end to provide a watertight fit.

The force transducer was designed to measure the total force on the cylinders by summing the forces transmitted to the upper and lower struts (Figure 22). The forces from the struts are transmitted to the upper-force and lower-force load cells that consist of flexible aluminum
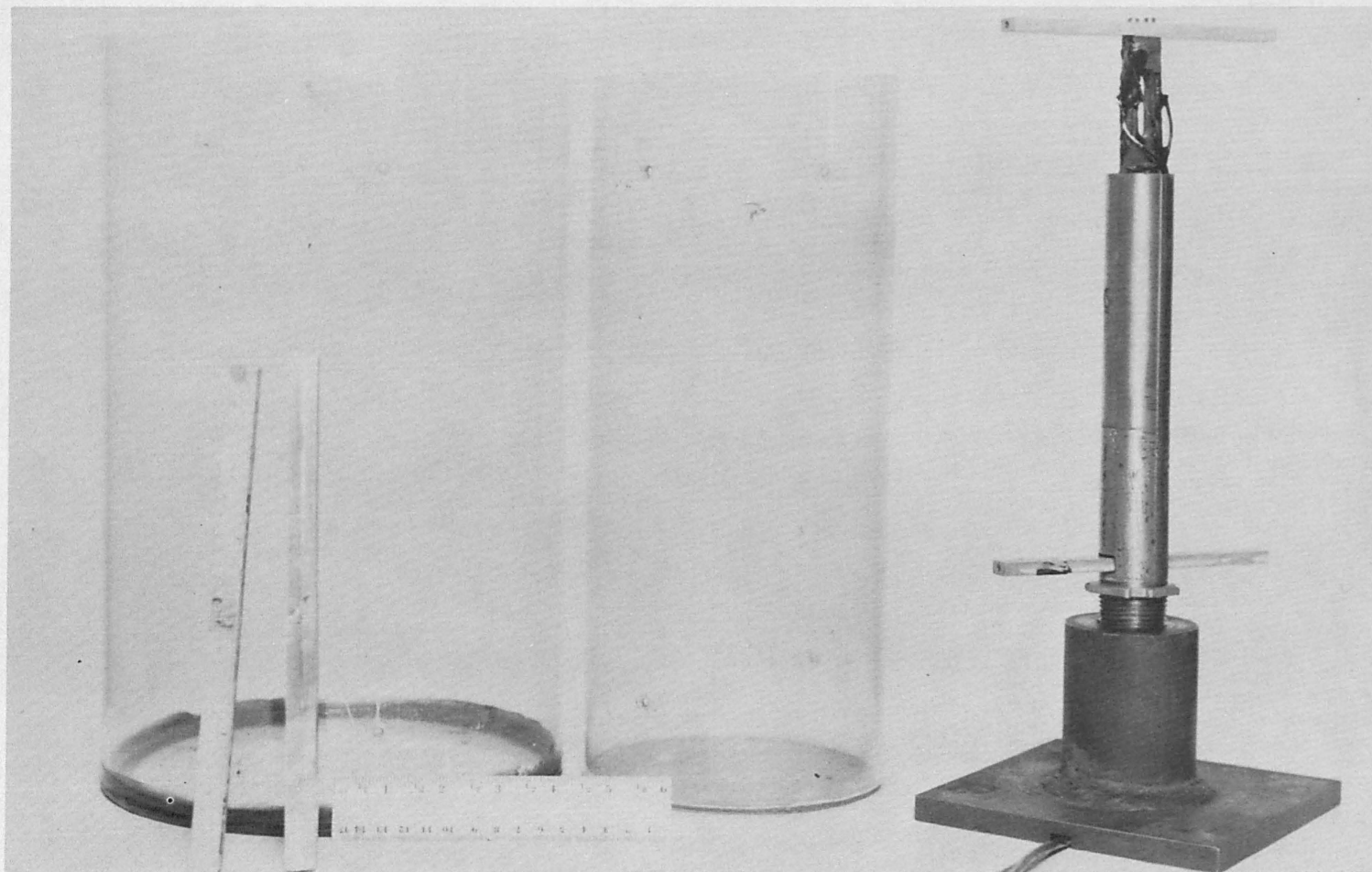
Figure 22. Force transducer and plastic cylinders.

elements as shown in Figure 23. The deformation of each load cell is picked up by the four strain gages shown in the figure; each gage acts as a resistance element of a full Wheatstone bridge. The output from each bridge passes through a preamplifier, the two outputs are summed and then passed through an amplifier to yield a pen deflection on the strip-chart recorder that is proportional to the total force.

The force transducer had to be sensitive and at the same time have a natural frequency that is high with respect to the oscillation frequency. The latter requirement is necessary to use the results of a static cali-bration to measure time-varying forces and to shift the noise to higher frequencies. The natural frequency was measured to be 43 cycles per second when the 0.50-foot O.D. cylinder was submerged to the maximum water depth of 1 foot; the corresponding value for the 0.75-foot O.D. cylinder was not measured but calculations based on the previous measured value and the theoretical added mass showed it to be about 35 cycles per second. The force transducer was assumed to respond statically because the meas-ured force data were for oscillation frequencies less than 2.5 cycles per second.

    f. Displacement Sensor. The carriage displacement, X_0, was measured by a linear potentiometer-type displacement sensor. Figure 24 shows the sensor. The motion of the rod changes the resistance in a manner that is linear with displacement. Figure 25 shows the sensor attached to the carriage.

    g. Wave Gages. Five resistance-type wave gages were used to measure the radiated waves. Each consisted of two stainless steel wires 0.50-foot long and 0.03 inch in diameter as shown in Figure 26 (the scale in the figure is in centimeters). The wave gage acts as a resistance element in a Wheatstone bridge network. The resistance is proportional to submergence and therefore the gage can be used to measure water level fluctuations.

    h. Amplifiers and Recorders. An eight-channel Brush amplifier-recorder system was used to record the force, carriage displacement, and wave data. Figure 27 shows the system in position for recording the forces and corresponding carriage displacement. The two amplifiers on the left side of the recorder were used to amplify and sum the outputs of the top-force and bottom-force load cells as previously described. The carriage displacement was measured by the bottom amplifier. Due to frequent break-downs all eight amplifiers could not be used continuously. Consequently, the waves and corresponding carriage displacement were recorded separately using any six of the amplifiers that were operational.

2. Measured Forces, Analysis, and Results.

One of the objectives was to verify the theoretical wavemaking forces for deepwater conditions in the vicinity of $F_0 = 1.4$ where C_W is maxi-mum. To do this accurately required that both the viscous and added-mass forces be small in comparison with the wavemaking forces. These require-ments restricted the experiments to stout cylinders for which $d/h \geq 0.50$
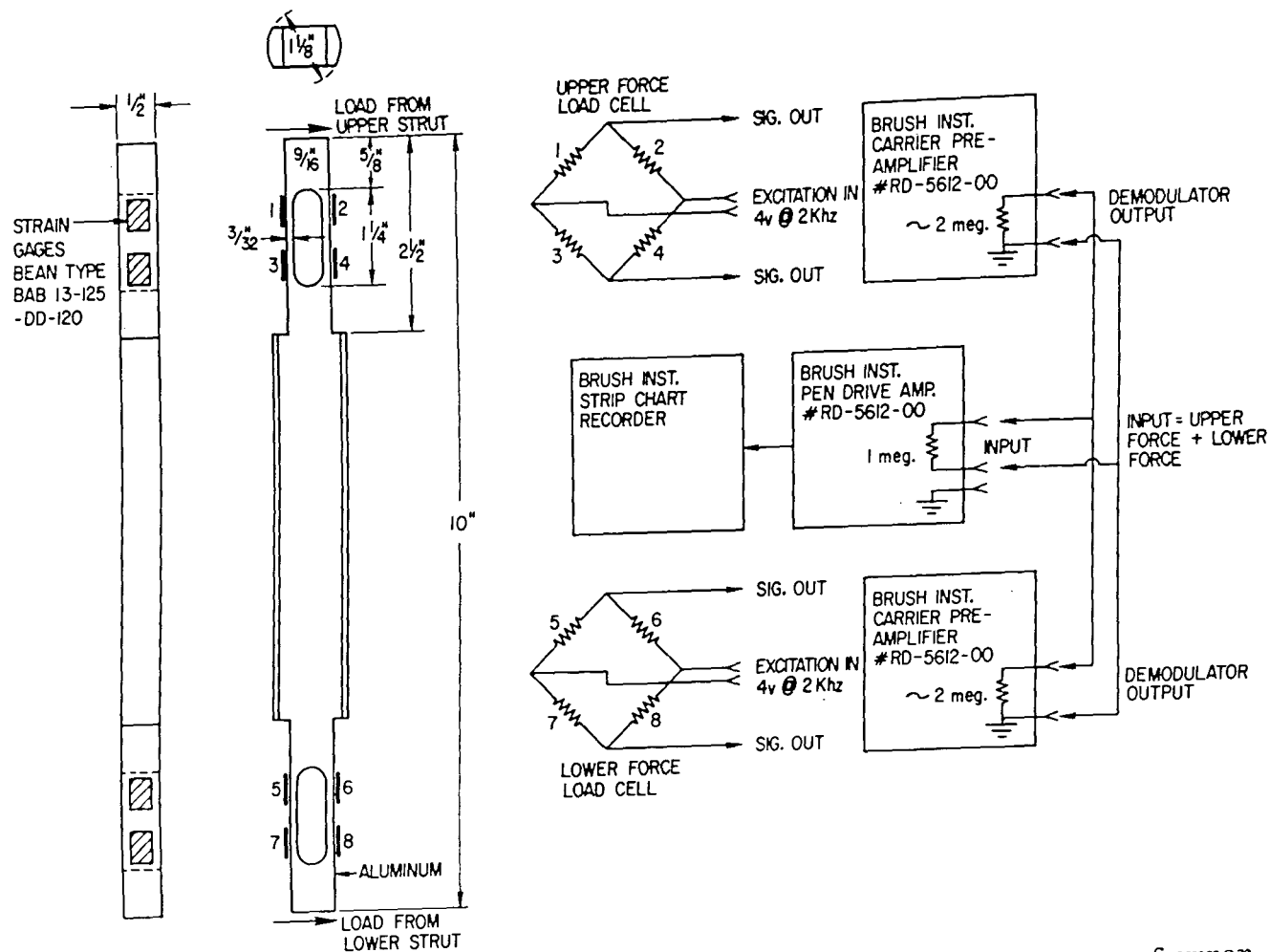
Figure 23. Wiring and instrument connection diagram for summing outputs of upper and lower force load cells.
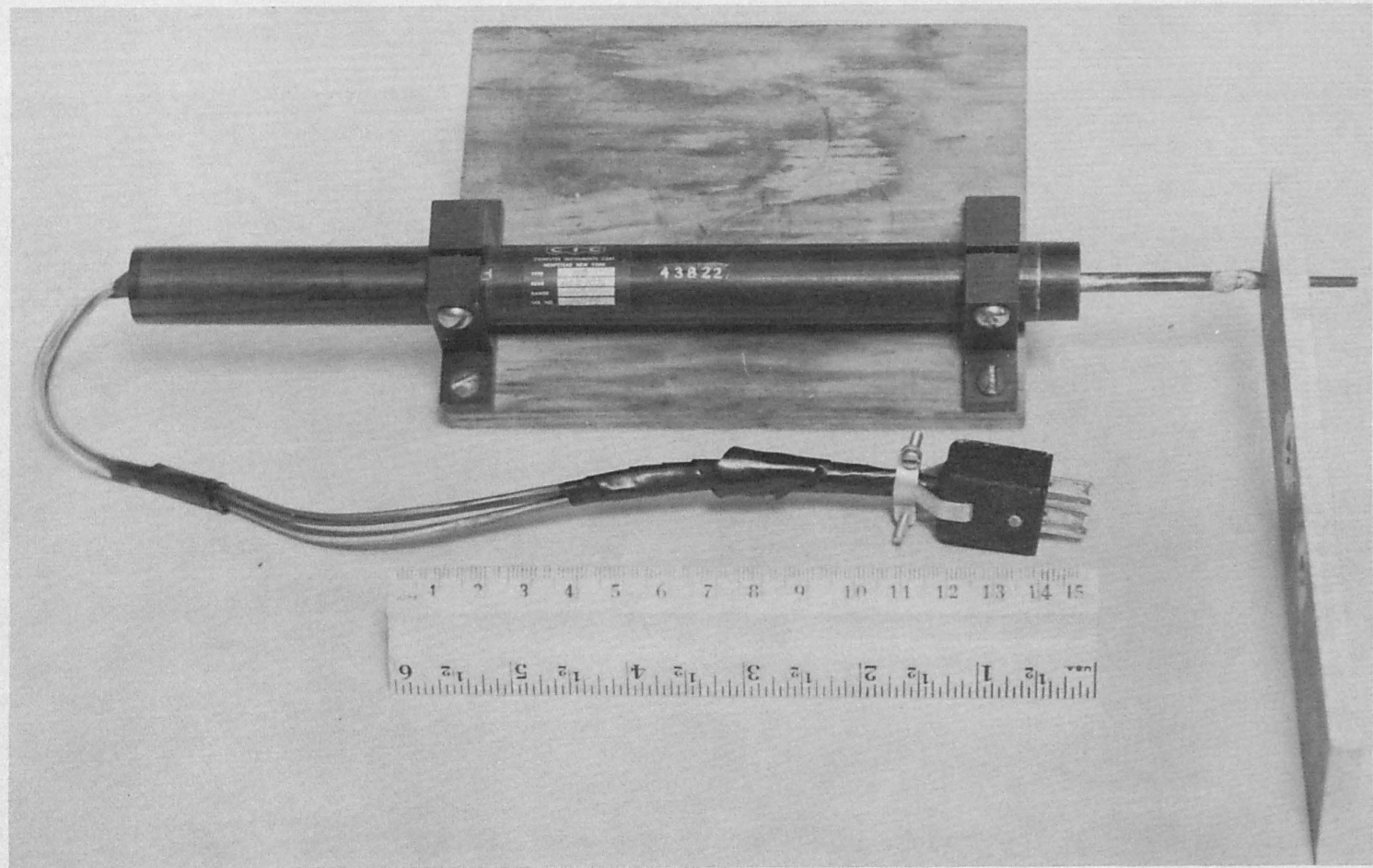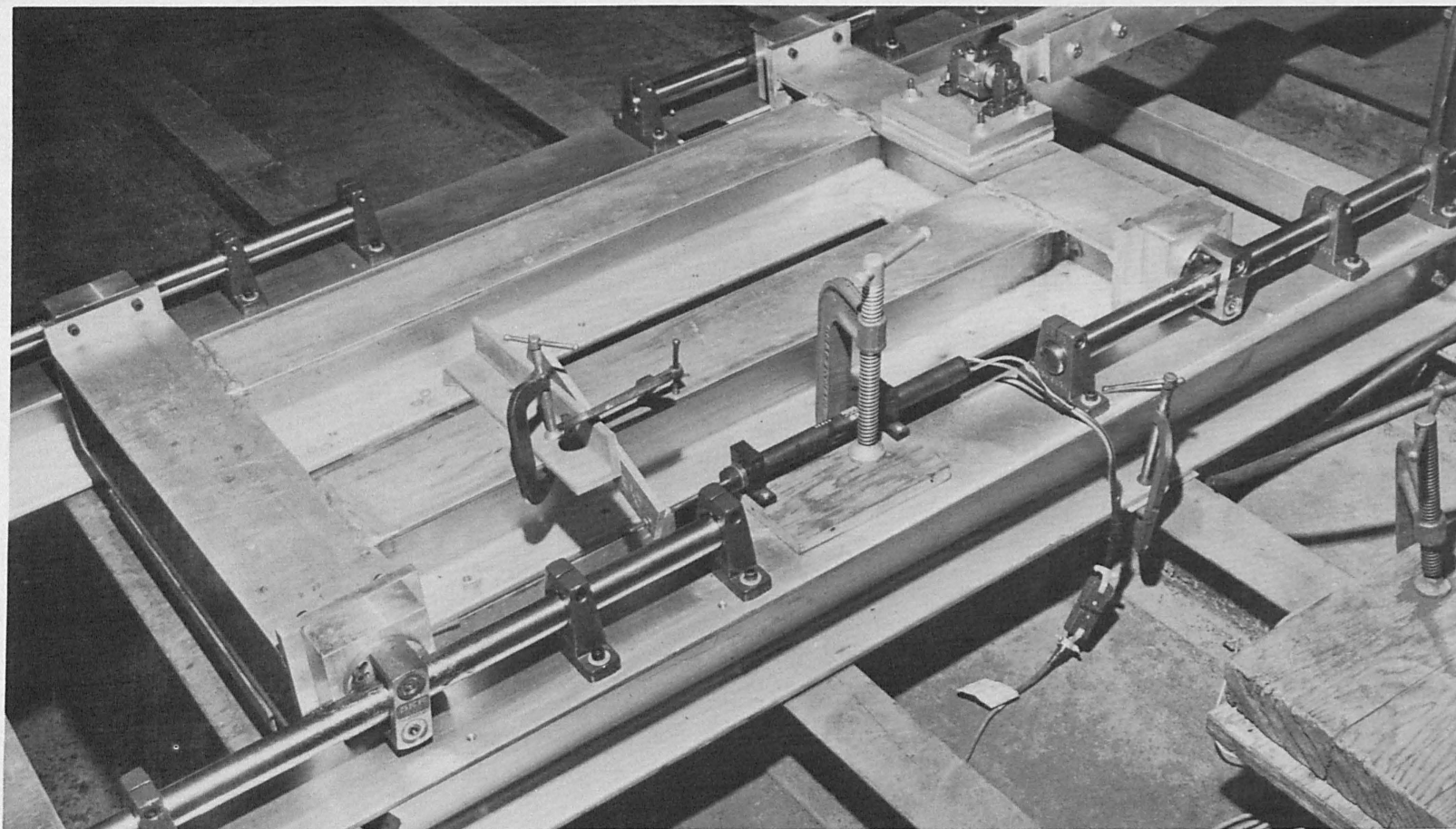
Figure 24. Carriage-displacement sensor.

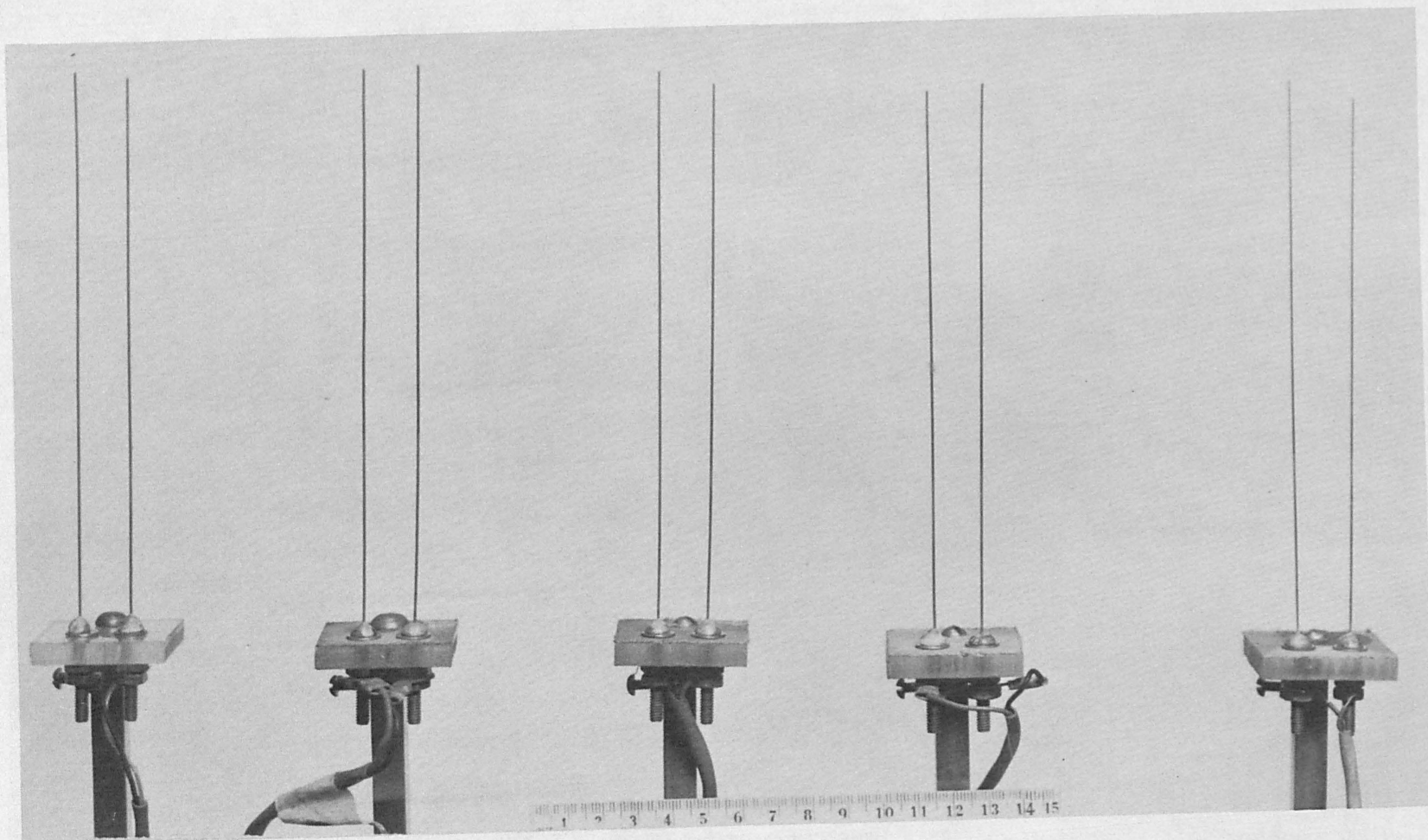Figure 25. Location and attachment of carriage-displacement sensor.

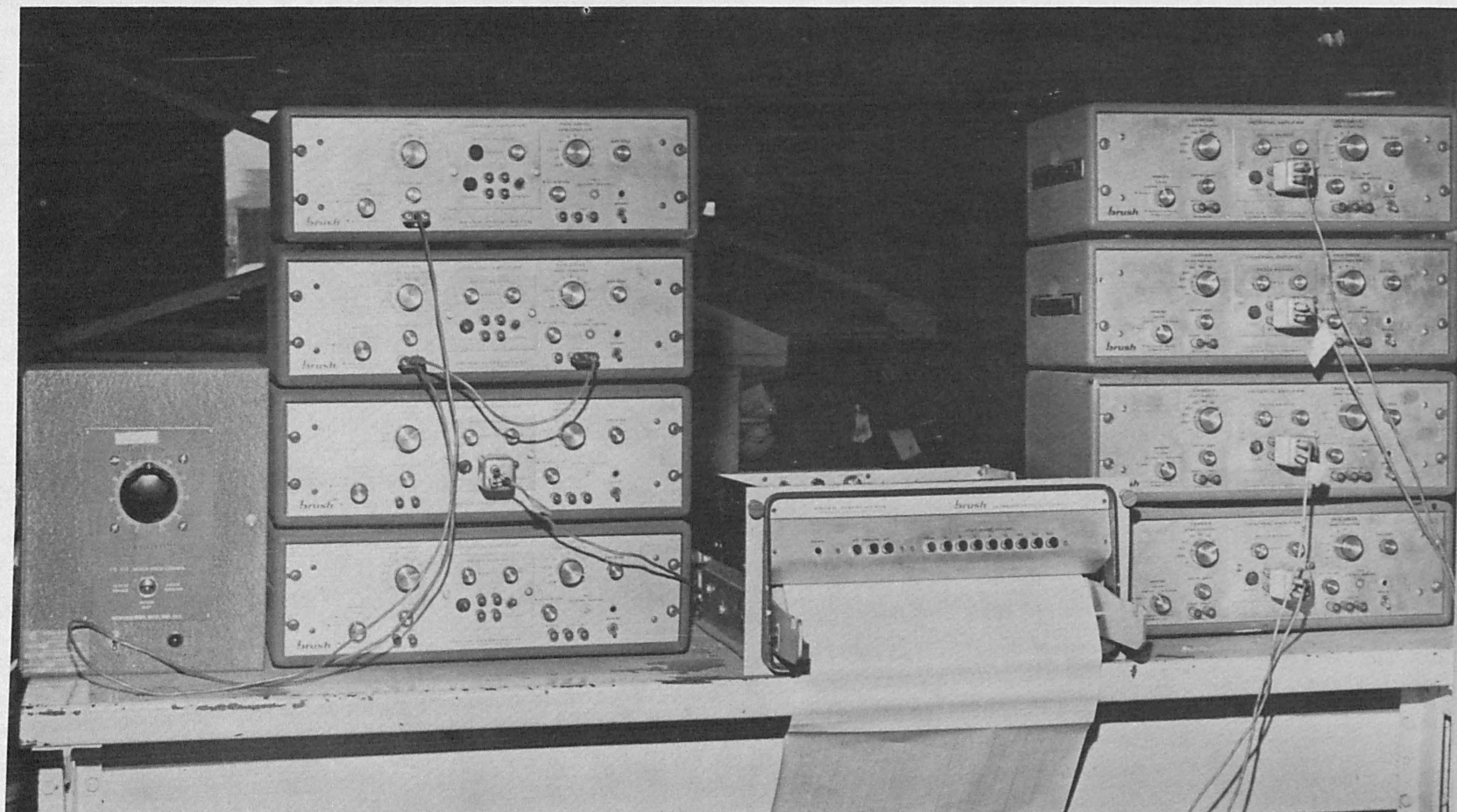Figure 26. Parallel-wire resistance-type wave gages.

Figure 27. Eight-channel recorder, amplifiers, and d.c. motor speed control.

and values of $\sigma^2 h/g < 8$; consequently, the added-mass forces, which depend on both parameters, were verified only in this range. The viscous-force requirement also restricted X_0/D to small values.

a. Ranges of the Variables. In order for the viscous forces to be small in comparison with the wavemaking forces it was important to prevent boundary-layer separation, otherwise the low pressure in the wake could produce drag forces that would not be possible to separate from the wavemaking forces. Separation can be prevented by using small values of X_0/D. Schlichting (1968) shows that for a cylinder starting impulsively from rest and then continuing with a constant velocity, separation begins only after the cylinder has traveled a distance of 0.175D. If the starting process is more gentle, then the distance traveled before separation occurs is larger, e.g., the distance is 0.26D for a motion defined by a constant acceleration. Consequently it is unlikely that separation will occur for an oscillating cylinder if X_0/D is less than 0.25.

In this case laminar boundary-layer theory can be used to obtain an estimate of the viscous forces. Batchelor (1967) obtains the viscous forces on an oscillating cylinder in a still fluid of infinite extent (no free surface) for the case that $X_0/D \ll 1$ and the Reynolds number, $\sigma D^2/\nu$, is large in comparison to unity. The part of the force that is proportional to velocity is due to two factors, each contributing 50 percent: (a) tangential stresses on the surface of the cylinder, and (b) normal stresses acting on a cylinder whose cross section is that of the cylinder plus a perturbation on the order of the boundary-layer thickness. His result for its amplitude, F_V, is shown plotted in Figure 28 as the ratio F_W/F_V versus oscillation frequency; F_W is the amplitude of the wavemaking force for the translation mode. This shows that if D/h is sufficiently large and the oscillation frequency is sufficiently small then F_V can be made insignificant in comparison with F_W.

The added-mass effects dictated that $\sigma^2 h/g$ be small so that F_W could be accurately isolated from the total measured force. The importance of $\sigma^2 h/g$ can be seen from the following relationship for the ratio F_W/F_{am} where F_{am} is the amplitude of the added-mass force:

$$F_w/F_{am} = C_w/(\hat{C}_{am}\ \sigma^2 h/g)$$

(67)

However, in order to measure C_w for deepwater conditions, $\sigma^2 h/g$ could not be smaller than π. Consequently, the experiment could not be designed such that F_w is very large with respect to F_{am}. Nevertheless, very accurate values of C_w were obtained by the analysis technique described previously.

Considering the simultaneous effects of viscous and added-mass forces it was decided to use the following ranges for the variables of the experiment:
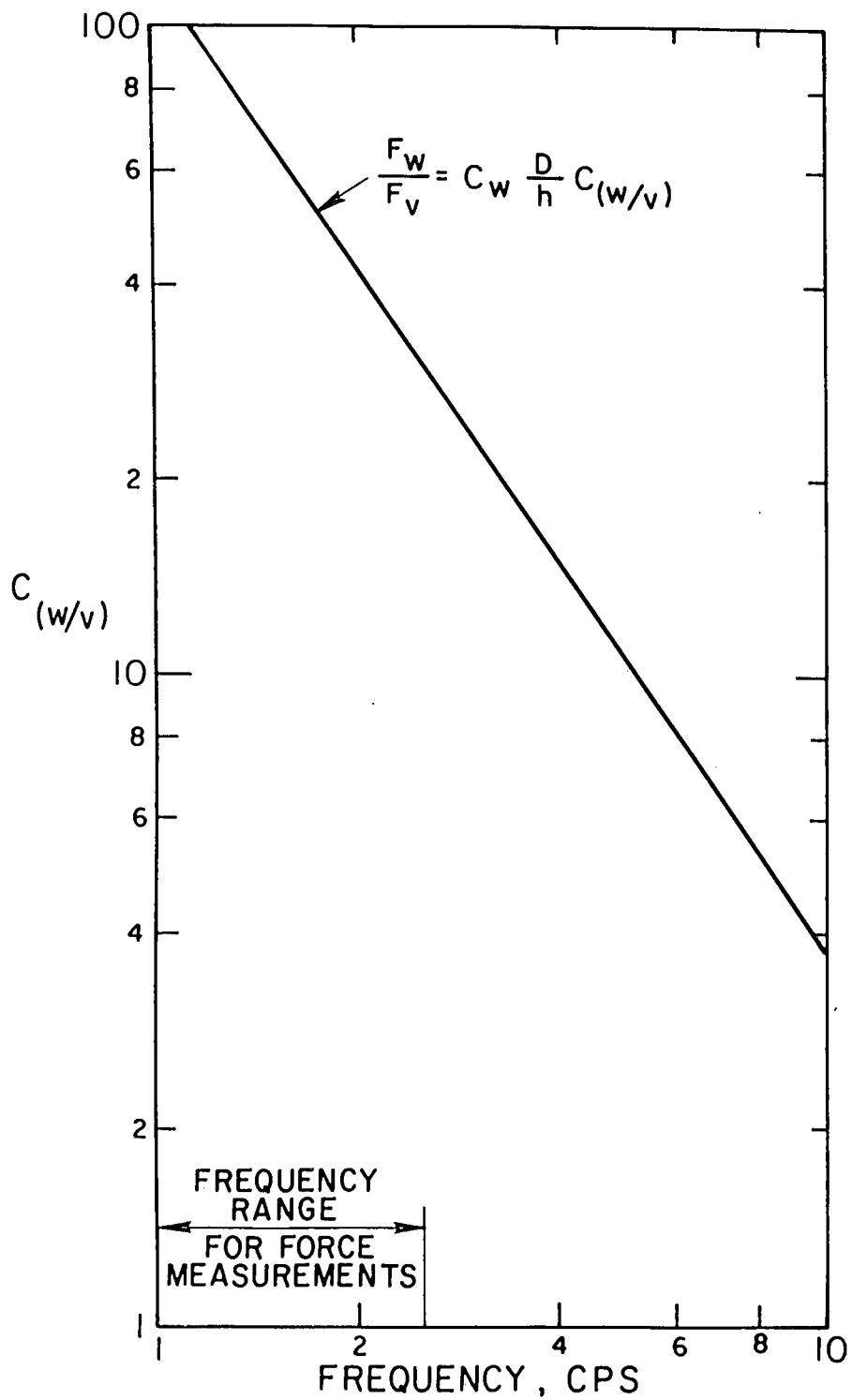
Figure 28. Effect of viscous force, F_V, in comparison with the wavemaking force, F_W.

X_0 = 0.025 foot,

D = 0.50 and 0.75 foot,

σ = 2π to 5π radians per second (1.0 to 2.5 cycles per second),

h = 0.67, 0.83, and 1.0 foot.

The corresponding ranges for the nondimensional variables were:

X_0/D = 0.05 and 0.033,

D/h = 0.50, 0.60, 0.75, 0.90, and 1.12,

$1.0 < \sigma^2 h/g < 8.0$,

$1.2 < F_0 < 2.2$ (for $\sigma^2 h/g > \pi$).

b. Experimental Procedure. Both static and dynamic calibrations were required for the force transducer. The static calibration determined the relationship between the total force on the cylinder and the deflection of the recorder pen. The method of imposing a known horizontal load on the cylinder is illustrated in Figure 29. The figure shows a string looped around the cylinder passing over two pulleys and supporting a 1,000-gram weight in a tin container; the cylinder is loaded at the upper-reaction point defined as the elevation at which no output is measured from the lower-force load cell. The procedure consisted of: (a) locating by trial the upper- and lower-reaction points, (b) setting the sensitivity on the amplifiers such that the pen deflection was the same for a given load whether the cylinder was loaded at the upper- or lower-reaction point, (c) engaging the summing circuit so that the pen deflection is proportional to the sum of the amplifier outputs, and (d) loading the cylinder with a series of loads at the two reaction points and midway between them to obtain three calibration curves of load versus pen deflection. This type of calibration was performed in air as well as water. The three calibration curves were nearly identical and therefore, it was assumed that the pen deflection will be proportional to the total force on the cylinder when it is forced to oscillate. The curves were also linear so that an incremental calibration was not required for each run; the pen deflection due to one load was sufficient. The dynamic calibration determined the mass-in-air that would have to be subtracted from the mass-in-water to arrive at the added mass due to the outside water. The procedure consisted of oscillating the cylinder in air with X_0 = 0.025 foot at five to six different frequencies in the range of 1.0 to 2.5 cycles per second. Using the results of the static calibration to calculate the oscillatory forces, the mass-in-air was obtained for each frequency and the average value used in the calculation of added mass as explained later in this section.

A run consisted of force measurements for a given diameter and water depth and covering the complete range of oscillation frequencies in seven to eight discrete steps. Preceding each run the force transducer was
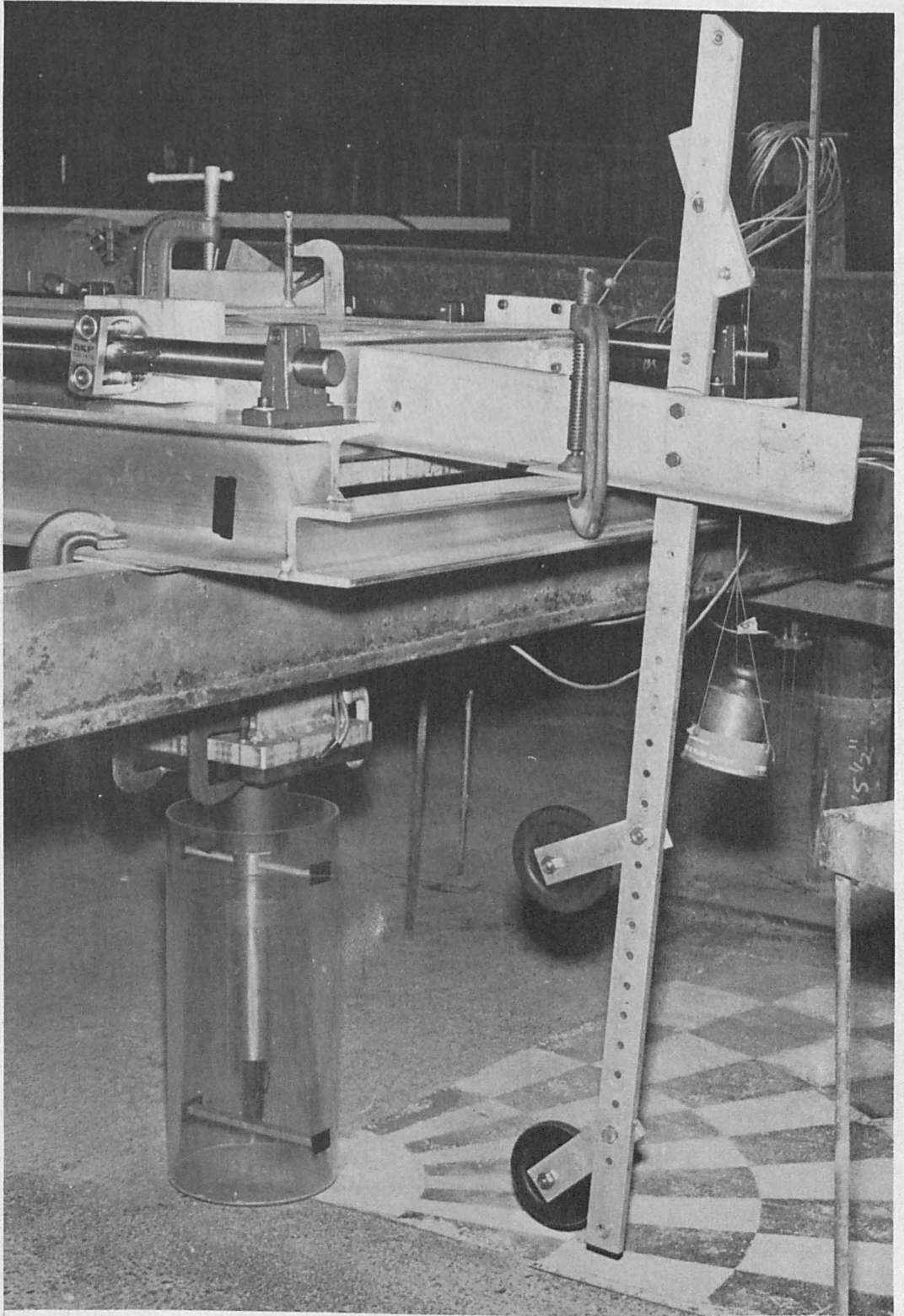
Figure 29. Force transducer calibration.

to eight discrete steps. Preceding each run the force transducer was calibrated statically in water using the procedure described above. Then forces and carriage displacements, corresponding to approximately the 5th through 15th cycle, were recorded.

c. Force Data. A sample of the force data for the 0.50-foot diameter cylinder is shown in Figure 30. The data represent approximately the 5th through the 15th cycle from the time the oscillations began in calm water. The carriage displacement is also recorded because the phase difference between the force and displacement records is required to separate out the wavemaking and added-mass forces. Similar records were obtained for each frequency and water depth. Some noise was still present in the force records; however, its level was not high enough to introduce significant errors in the analysis.

d. Analysis. To obtain the measured wavemaking and added-mass forces it was necessary to first resolve the total measured force into two components; one proportional to the velocity of the carriage, and the other proportional to its acceleration. Assuming that both the force and the carriage displacement signals are simple harmonic, two pieces of information were required from the recorded data: (a) the amplitude of the total force, F, and (b) the phase difference, ε, between the force and carriage displacement signals. The phase difference yields the ratio $F_{\dot{x}}/F_{\ddot{x}}$ where $F_{\dot{x}}$ is the amplitude of the force proportional to velocity and $F_{\ddot{x}}$ is amplitude of the force proportional to acceleration. The additional information provided by F was then used to calculate the magnitudes of the components by the following equations:

$$F_{\dot{x}} = F/[1 + 1/\tan^2 \varepsilon]^{\frac{1}{2}}, \tag{68}$$

$$F_{\ddot{x}} = F_{\dot{x}}/\tan \varepsilon. \tag{69}$$

F was defined as one-half of the peak-to-through value that appeared to be representative of the force record. ε was the average of approximately 15 values based on zero-crossings of the force and displacement records. The averaging process allowed accurate values to be obtained even though they were small, ranging from 10° to 40°, and the records still contained some noise.

C_w and $\hat{C}_{am}$ were calculated using the following equations:

$$C_w = F_{\dot{x}}/\rho g \frac{\pi D^2}{4} X_0, \tag{70}$$

$$\hat{C}_{am} = [(F_{\ddot{x}}/X_0 \sigma^2) - M_s]/\rho \frac{\pi D^2 h}{4}. \tag{71}$$

$F_{\dot{x}}$ was assumed due solely to wavemaking because the viscous forces for all the data were less than 5 percent of F_w. The calculation of C_{am} required the subtraction of the mass-in-air, M_s, which ranged from 10 to 50 percent of the added mass.
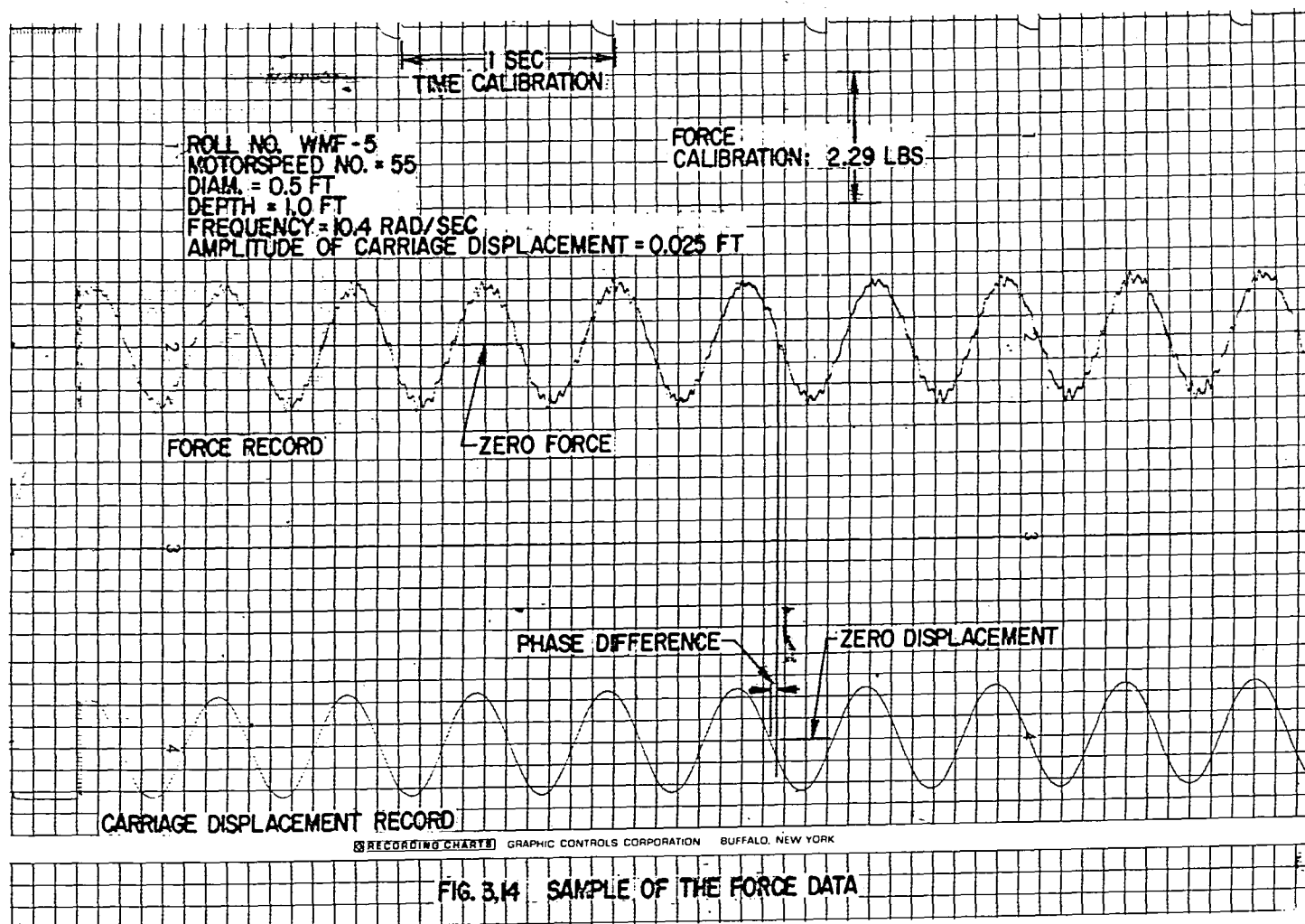
Figure 30. Sample of the force data.

e. Results and Comparison with Theory. The C_W calculated from the measured forces are compared with theoretical results in Figures 4 and 31. The first figure contains all the deepwater data plotted as a function of F_0. The measured values compare well with those predicted by theory and are shown to be independent of D/h. The second figure contains all the data. In this case C_W is plotted as a function of two parameters, $\sigma^2 h/g$ and D/h, because both are important for $\sigma^2 h/g < \pi$. The theoretical values were calculated using equation (40). The measured values compare well enough with the theoretical results that the effect of D/h is clearly shown. C_W for $D/h = 0.75$ is derived from forces measured for both diameters; no systematic effect of D is evident.

The $\hat{C}_{am}$ are shown plotted in Figure 8. Again the measured values compare well with the theoretical results. The decrease of $\hat{C}_{am}$ with increasing $\sigma^2 h/g$ is clearly shown. Some of the measured values that are past the $\sigma^2 h/g$ for which $\hat{C}_{am}$ is minimum shows the subsequent increase of $\hat{C}_{am}$.

f. Data of Other Investigators. Garrison and Berklite (1973) performed a series of experiments to measure the coefficient of added mass in stillwater for various bodies, one of which was a vertical circular cylinder. The objective was to verify their numerical solution for the case where $\sigma^2 h/g \to \infty$. Experimental values of $\hat{C}_{am}$ were obtained for the circular cylinder as a function of D/h for $\sigma^2 h/g$ in the range of 200 to 500; D/h ranged from 0.4 to 6.0. Their results for D/h of 0.50, 0.60 and 0.90 are shown plotted in Figure 8. The deviations of the experimental values from the corresponding theoretical ones are real because theoretical values in the figure agree with their numerical results.

The experimental work of Clough (1960) provides some verification of the theoretical mode-shape effects. The objective in one set of his experiments was to measure the effect of flexibility on added mass. This was done by using flexible hollow vertical cylinders of various cross sections that were fixed to the bottom of a tank and extended upward to the MWL. The experiments consisted of measuring the natural frequency in stillwater and then applying uniform weights along the cylinder until the same frequency was measured in air. The applied weight per unit length was then assumed to be proportional to the added mass after the effects of the water inside the cylinders were subtracted.

One of the cylinders was circular and had a diameter of 0.25 foot. Its natural frequency was 3 cycles per second in a water depth of 3 feet. This yields $\sigma^2 h/g = 23$ and $D/h = 0.125$. The average coefficient of added mass was measured to be 0.58. This measure of added mass is identical to R^*_{am} as defined by equation (55) and plotted in Figure 9 for the cantilever mode which approximates the first-mode shape of the cylinders tested by Clough. His result is shown plotted in the figure. The theoretical results show that low values of R^*_{am} can occur for certain combinations of D/h and $\sigma^2 h/g$. The primary effect is due to the nonuniform
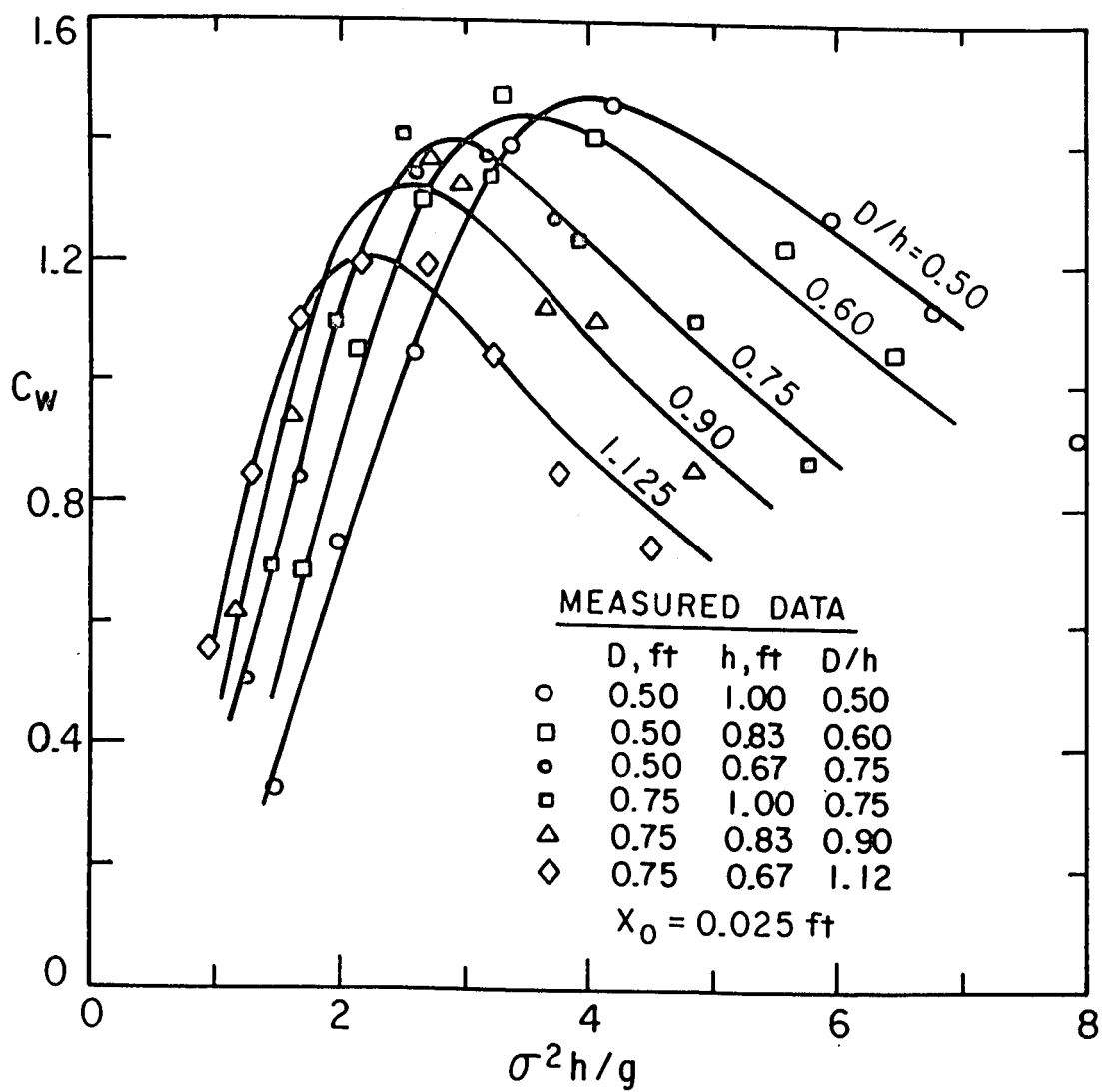
Figure 31. Coefficient of the wavemaking force for all force measurements.

distribution of added mass as illustrated by Figures 6 and 7. This appears to explain Clough's low value. Flexibility becomes important only for the higher mode shapes.

3. Measured Surface Waves, Analysis, and Results.

Surface waves, generated by oscillations of the cylinders, were measured in one quadrant at five different locations along a circular arc formed by a 3.5-foot radius (Fig. 18). At this radius the surface fluctuations are primarily due to the radiated waves; the nonprogressive surface disturbance due to added-mass effects is negligible. The objective of the measurements was to obtain C_W directly from the radiated waves.

a. Ranges of the Variables. The diameters and oscillation frequencies were the same as for the force measurements. Two additional water depths (<1.0 foot) were used for the 0.50-foot-diameter cylinder. X_0 was extended to larger values on the assumption that the viscous forces should not affect the generated waves. The water depths and X_0's were as follows:

For $D = 0.50$ foot,
$h = 1.00, 0.92, 0.83, 0.75,$ and 0.67 foot,
$X_0 = 0.025, 0.0375, 0.05,$ and 0.0625 foot;

for $D = 0.75$ foot,
$h = 1.00$ and 0.83 foot,
$X_0 = 0.0375, 0.0568, 0.075,$ and 0.0938 foot.

b. Experimental Procedure. Before any runs were made all five gages were checked for linearity over an elevation range of ±0.05 foot with respect to the MWL. This was done for the maximum and minimum water depths by performing a step calibration in increments of 0.01 foot. The procedure consisted of raising each gage to ±0.05 foot, lowering it to -0.05 foot, and then returning it to original position. The submergence of the gages proved to be linearly related to the pen deflection of the chart recorder.

A run consisted of surface wave measurements for a given water depth and diameter and spanning all pairs of X_0 and σ. Because an average of six σ's were used this resulted in approximately 24 wave records per run. Preceding each run a simplified calibration was made based on the linearity of the wave gages. All gages were calibrated simultaneously using a single increment equal to the maximum expected wave amplitude. The sensitivities of all gages were made equal by adjusting the amplifiers. Consequently, the recorded waves at each gage were of the correct height

with respect to the waves at any other gage. Next, the X_0 was set by adjusting the stroke of the eccentric and the first 10 to 20 waves were recorded for each σ. Approximately 5 minutes were required for the water to become still between changes in σ. The wave gage calibration was checked at the end of each run.

c. Surface Wave Data. Figure 32 shows a sample of the recorded wave data for the 0.75-foot-diameter cylinder. The wave height is maximum at $\theta = 0°$ (gage 5) and decreases with decreasing θ (see Fig. 18 for coordinate system). At $\theta = -90°$, which is perpendicular to the oscillation direction, the wave frequency is twice the oscillation frequency. This is an effect of nonlinearity because linear theory predicts no energy propagation in this direction. The amplitude of these waves was found to increase with increasing X_0 and decreasing σ, but it was too small to contribute significantly to the total radiated energy.

The characteristics of the waves at the other gages were also affected by X_0 and σ. Simple-harmonic surface fluctuations occurred only when deepwater waves were generated using the smaller values of X_0. A second harmonic became evident for the larger X_0's. For the smaller values of σ the waves were highly nonlinear; for the lowest σ the shape was asymmetrical. The asymmetry was found to be due to the generation of a second harmonic that propagates at its own phase speed rather than the speed of the fundamental component. This was determined by measuring the waves at five locations along the direction of oscillation. The records showed that the profile differed from gage to gage because the phase of the free-second harmonic with respect to the phase of the fundamental changed with distance. This phenomenon has been predicted and experimentally verified by Madsen (1971) for a flap-type wavemaker oscillating in a translation mode. He shows that in shallow water it occurs when $(H/2)/(kh)^2 > 1/6\pi^4$; it can be eliminated if a second harmonic of an appropriate amplitude is added to the simple-harmonic motion of the generator. An analysis of this phenomenon was outside the scope of this study. It is reported here because this effectively limited the measurements of C_W to deepwater waves.

d. Analysis. C_W can be calculated from the radiated waves by equating the average rate of energy flux through a circular boundary at a radial distance, r, with the average rate at which the cylinder does work on the fluid. Using this principle Wehausen (1971) derives the relationship between the damping coefficient, for an arbitrary body and the resulting amplitudes of the radiated waves. His result appears to have a typographical error that yields a damping coefficient that is twice the correct value. The correct result for C_W is given by:

$$C_w = \frac{32}{\pi} \frac{(r/D)}{F^2} \left[\frac{\sinh 2kh + 2kh}{\cosh 2kh + 1}\right] \int_0^{-\frac{\pi}{2}} \left[\frac{Y_0(\theta)}{2X_0}\right]^2 d\theta \tag{72}$$
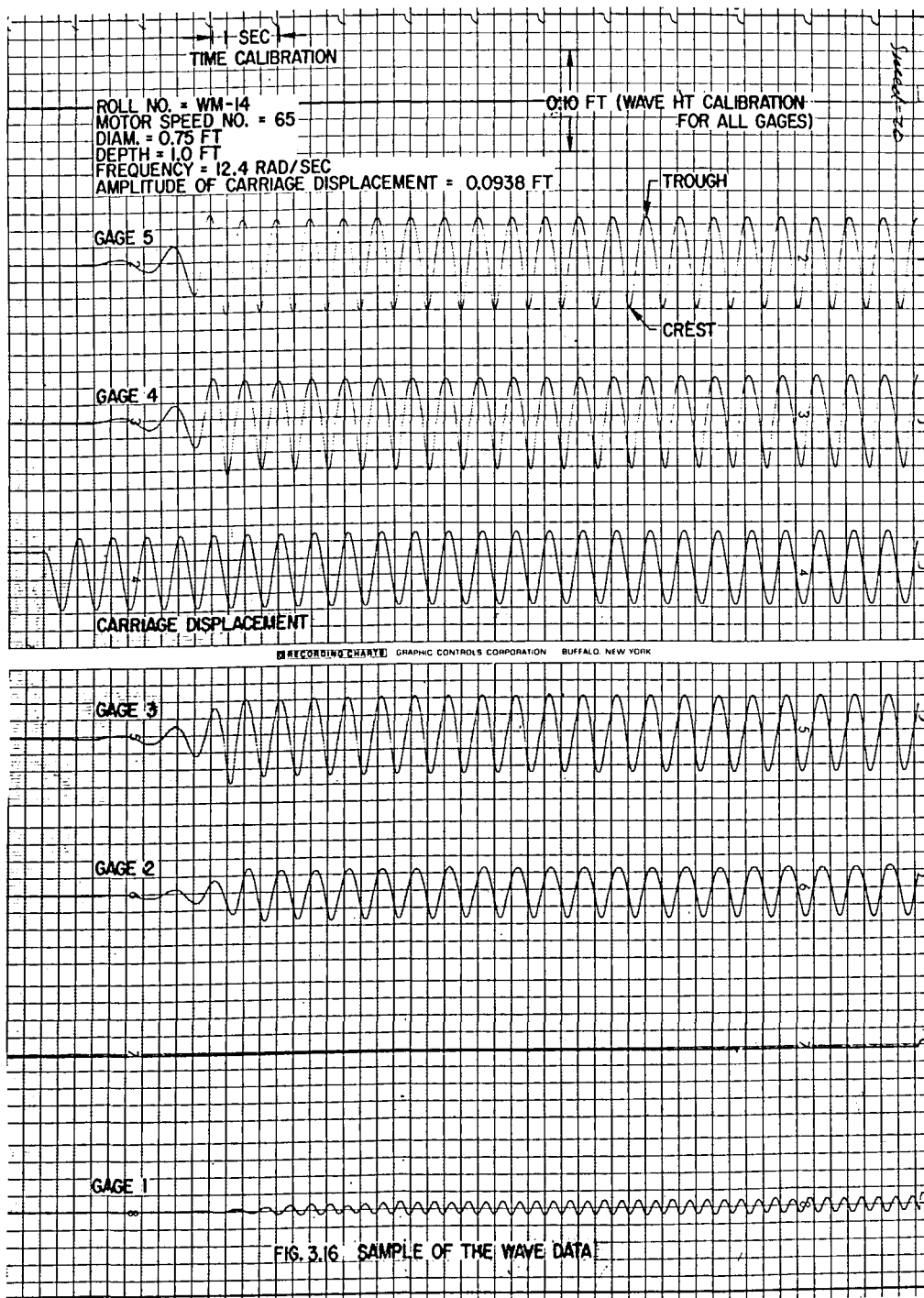
Figure 32. Sample of the wave data.

Due to symmetry, the integration extends over one quadrant. This result can also be derived from the following relationship:

$$4 \int_{0}^{-\frac{\pi}{2}} \frac{\rho g}{4} \frac{\sigma}{k} \left(1 + \frac{2kh}{\sinh 2kh}\right) \left[\frac{Y_0(\theta)}{2}\right]^2 r d\theta =$$

$$\frac{1}{T} \int_{0}^{T} C_w \rho g \frac{\pi D^2}{4\sigma} \dot{X}(t) \dot{X}(t) dt , \tag{73}$$

where the integrand of the left side is the linear-theory power for a plane simple-harmonic wave of amplitude $Y_0(\theta)$ and crest length $r d\theta$.

Y_0 was defined as one-half the difference between the measured crest and trough elevations. This definition yields the amplitude of the first harmonic provided the third and higher harmonics are negligible.

The measured Y_0's were assumed to be represented by:

$$Y_0 = a_0 \cos\theta + b_0 \cos 3\theta . \tag{74}$$

a_0 and b_0 were determined by a least-squares procedure using the measured values at three locations; $\theta = 0°$, $-22\frac{1}{2}°$ and $-45°$. This representation was chosen because it provided a better fit to the measured data than the theoretical variation defined by $\cos\theta$. These three locations were used because: (a) The measurements here were the most accurate due to the larger waves, and (b) the other locations contained energy at twice the oscillation frequency and therefore violated the linear-theory assumptions.

e. <u>Results and Comparison with Theory</u>. Although C_w was calculated for all values of $\sigma^2 h/g$ only those corresponding to deepwater conditions are plotted. The other values are not valid because in most cases the waves contained a free-second harmonic that made the waves asymmetrical as discussed earlier in this section. The results are plotted in two separate figures. Figure 33 shows C_w plotted as a function of F_0 for the variables of the experiments that correspond to the force measurements. Figure 34 shows all the deepwater results. It is evident that the theory forms an upper bound to the C_w's calculated from the measured waves. This is expected because energy is lost during generation and propagation. This was particularly evident for the larger X_0's because in some cases the wave crest at $\theta = 0°$ broke before it reached the wave gage. Sometimes this resulted in a wave amplitude at $\theta = 0°$ that was smaller than that at $\theta = -22\frac{1}{2}°$. On the average the measured C_w's were about 20 percent lower than the theoretical quantities.
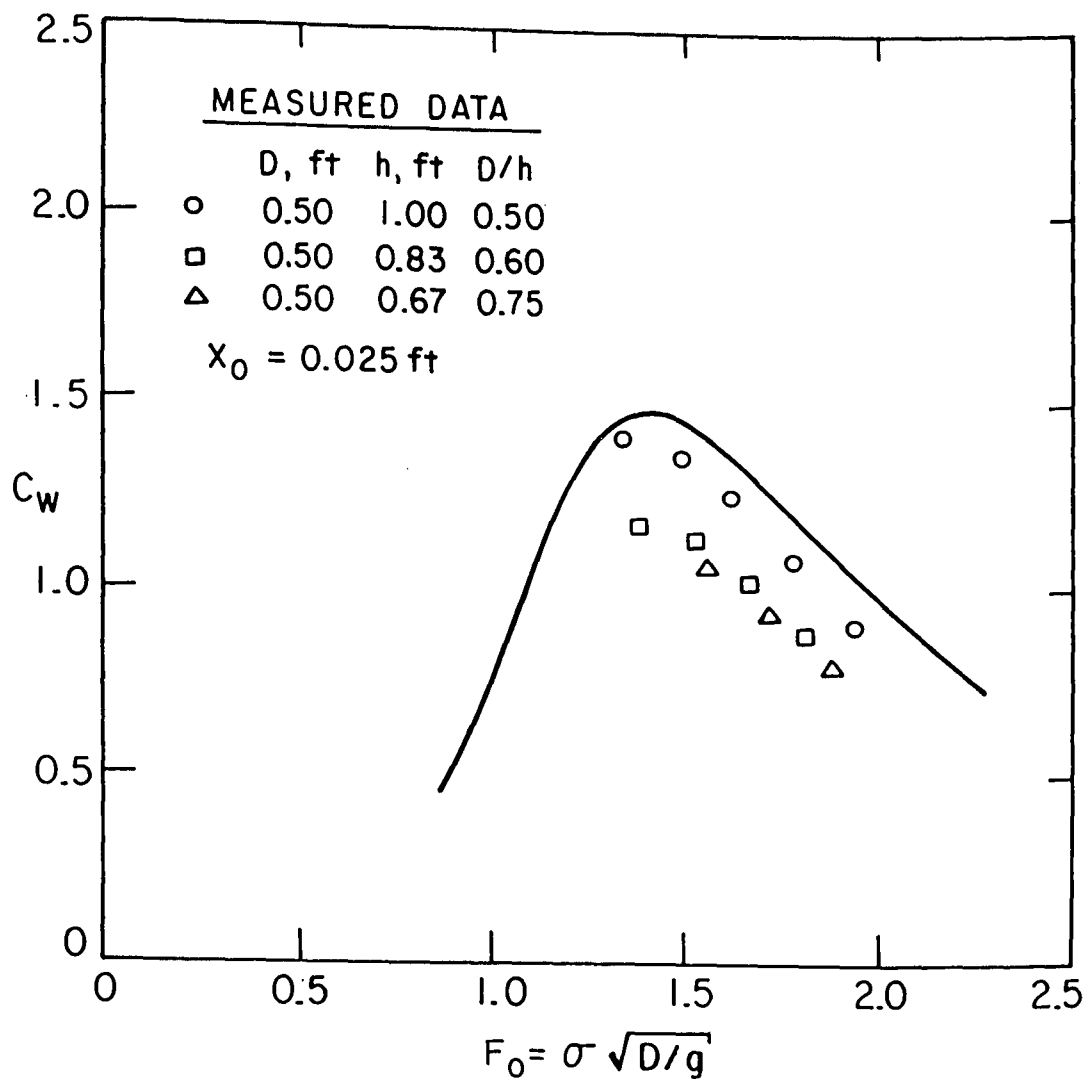
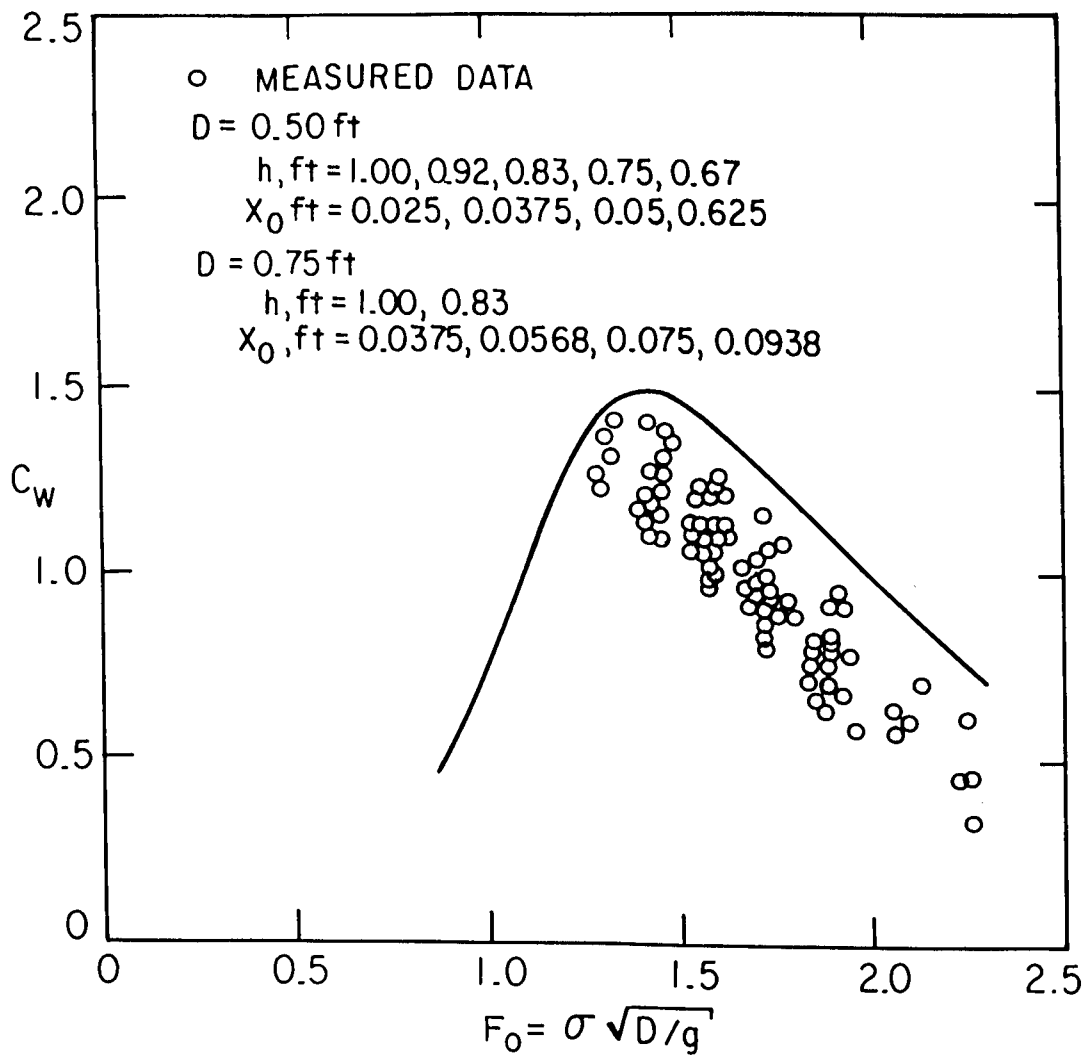Figure 33. Coefficient of the wavemaking force calculated from the measured radiated waves for $\sigma^2 h/g > \pi$.

Figure 34. Coefficient of the wavemaking force calculated from the measured radiated waves for $\sigma^2 h/g > \pi$.

IV. HYDRODYNAMIC DAMPING AND ADDED MASS
FOR CYLINDER OSCILLATING IN A CURRENT

It is shown in the introduction (Sec. I) that if the velocity of the structural members, $\dot{x}(t)$, is small in relation to the wave-induced water particle velocities, u, then the damping force due to the drag-force interaction term of the modified Morison equation can be represented by $C_D \rho D |u| \dot{x}$. The dominant contribution to this term will come from the highest waves in the spectrum. The average frequency of these waves during design-storm conditions will be much lower than the natural frequency of the structure so that a number of oscillation cycles will take place during the passage of the large waves. Consequently, as a first approximation, it is assumed possible to model this situation in a steady current.

The experiments discussed in this section used an elastically supported rigid cylinder instead of a system whereby the cylinder was forced to oscillate like for the wavemaking experiments. This was done because it was desired to obtain data in the range where the oscillation frequency was much higher than that of vortex shedding. The use of a forced-oscillation system in this frequency range would have made it impossible to extract the viscous forces that are proportional to velocity from the total forces because they would have been (on the basis of results in this section) less than 1 percent of the inertial forces in the range of the present experiments.

The experiments consisted of a series of tests in which the decay of vibrations with respect to time were measured when the cylinder was given an initial displacement and then suddenly released. The cylinder was completely submerged and its motion was constrained to be in the direction of the current. The corresponding damping values were compared with theoretical values that are predicted by the drag-force interaction term of the modified Morison equation. Coefficients of added mass were also measured.

1. Experimental Equipment and Arrangement.

Figure 35 is a schematic diagram of the major experimental equipment and its arrangement. A horizontal circular cylinder, having a diameter of 0.125 foot and a wall thickness of 1/32 of an inch is shown positioned in a 1-foot-wide open channel. Disk-type flanges of 0.167-foot-diameter were welded to the ends of the cylinder in an attempt to produce a predominantly two-dimensional flow over the cylinder so that it could be considered a section of an infinitely long cylinder. The flanges are welded to rigid struts that are in turn connected to H-shaped elements that act as elastic supports for the cylinder. All components are of aluminum. The system was positioned about 36 feet from the channel entrance.

The initial displacement was produced by weights which transmit their load to the cylinder via a string as shown in Figure 35. Because the

STRAIN GAGES

STRAIN GAGES
STRAIN GAGES

RIGID STRUT
$1'' \times \sqrt[3]{32}''$

O.D. = 0.125'

GAP = $\frac{1}{8}''$

1.0'

VIEW ALONG THE CHANNEL

CUT STRING
HERE

PULLEY

STRING

STRAIN
GAGES

WEIGHT
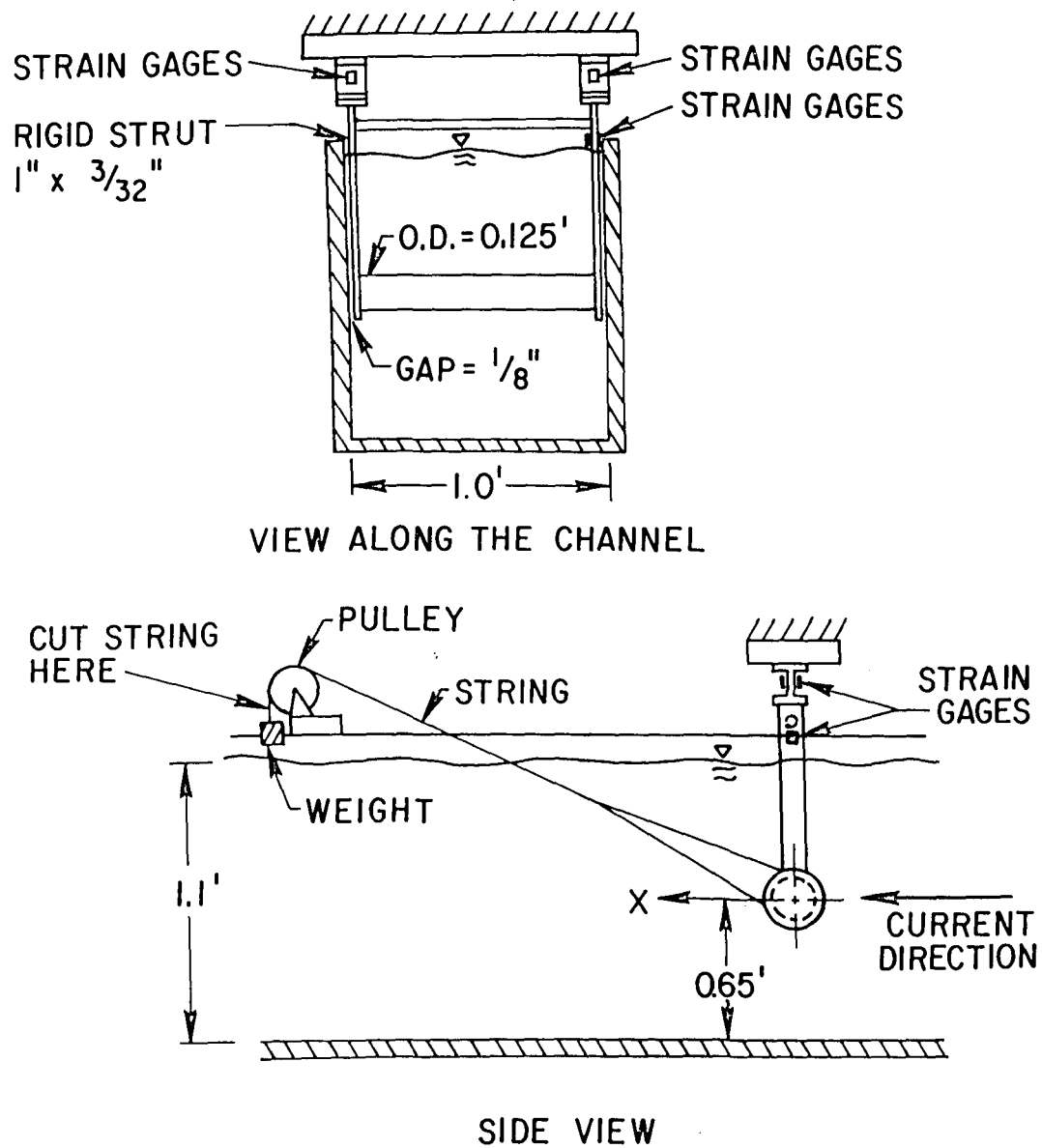
1.1'

X

0.65'

CURRENT
DIRECTION

SIDE VIEW

Figure 35. Schematic diagram of experimental arrangement and method
of producing initial displacement.

86

struts are stiff relative to the elastic supports, the initial displacement and subsequent dynamic response is constrained to be along an arc of a circle whose origin is at the elevation of the elastic supports. However, the motion was essentially a pure translation because the maximum amplitude in the x-direction was less than 1 percent of the length of the struts.

Strain gages mounted on the flanges of the H-shaped elements were used to measure the steady-state forces, initial displacement and dynamic response in the x-direction. The gages mounted on one of the struts was used to monitor the dynamic response of the cylinder along its axis. This later response was kept to a minimum by adjusting the position of the string along the cylinder so that no initial displacement was produced in the axial direction. The wiring diagrams for all the gages and dimensions of the H-shaped elements are shown in Figure 36.

The velocity of the current in the channel was limited by the available discharge. Values up to 2 feet per second were obtained with a 1.1-foot water depth. They were extended to 2.7 feet per second by using a water depth of 0.8 foot. The velocity was recorded by a Kent Mini-flow propeller-type current meter that had a propeller diameter of 0.032 foot. It was positioned 0.50 foot upstream of the cylinder at the elevation of the cylinder's axis along the centerline of the channel. The current meter was supported by a track spanning the width of the channel and was movable in the vertical direction so that velocity profiles could be measured.

2. Experimental Procedure and Ranges of Variables.

a. Calibration. The first step was to measure the damping of the elastically supported cylinder in air in order to extract the hydrodynamic effect on damping from the vibration-decay curves in water. This was done by tapping the cylinder, which was positioned in an empty channel as shown in Figure 35, and then measuring its response. The vibration-decay was found to be exponential with ξ_s (percent) equal to 0.096. The method of calculation is discussed later.

The second step was to perform a dynamic calibration whose results could be used to obtain the added mass from natural frequency measurements in water and to determine the generalized stiffness, K_s^*, of the dynamic system with respect to the generalized coordinate, X. The dynamic calibration was performed in air. Fifteen pieces of 1/16-inch lead lashing wire, each piece about 5 feet long and weighing about 0.10 pound, were wrapped around the outside of the cylinder. The natural frequency of the cylinder was measured without the wire and also after each piece was added. The measurements were obtained from the recorded dynamic response when the cylinder was tapped. Without the wire the natural frequency, σ_s, was 199 radians per second (31.7 cycles per second); with all the wire wrapped the natural frequency was 103 radians per second (16.4 cycles per second).
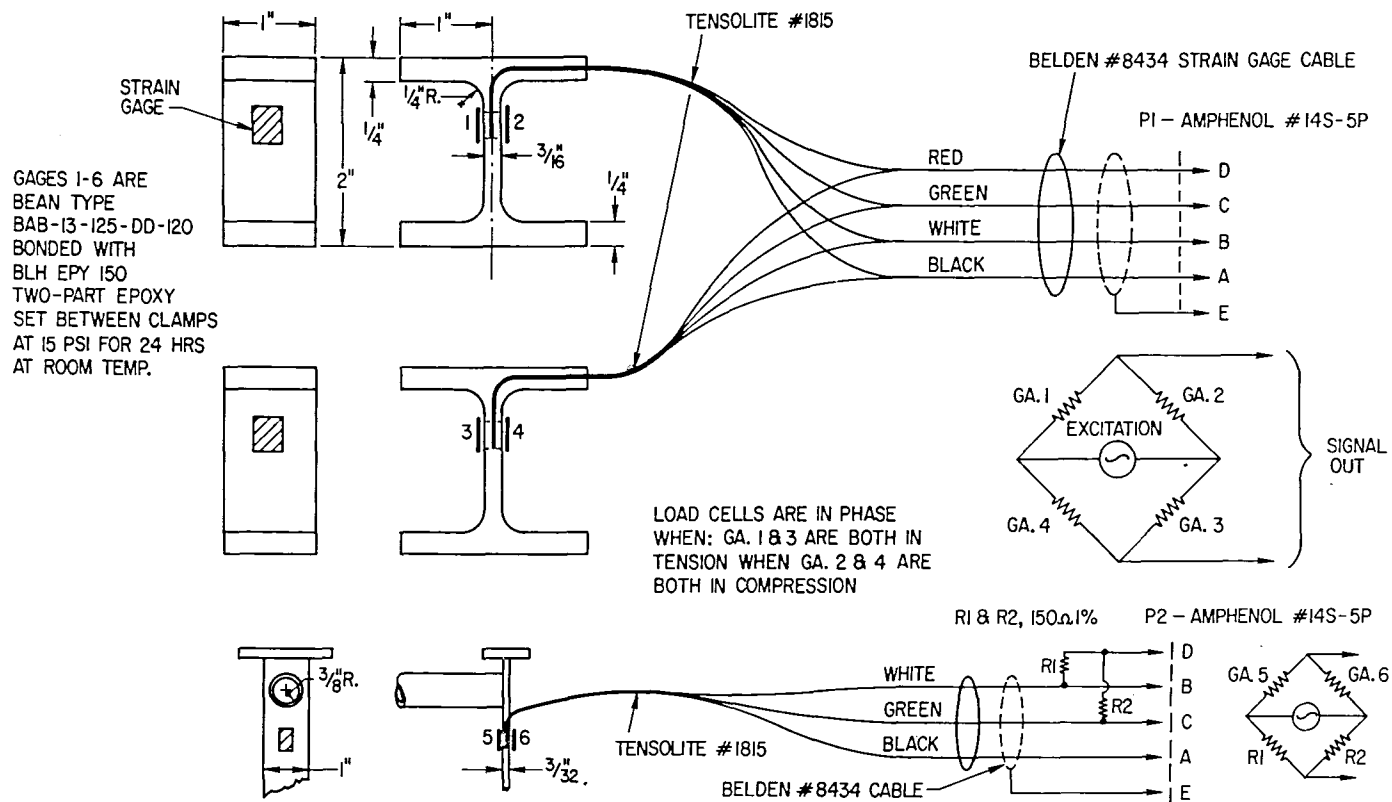
STRAIN GAGE

GAGES I-6 ARE BEAN TYPE BAB-I3-I25-DD-I20 BONDED WITH BLH EPY I50 TWO-PART EPOXY SET BETWEEN CLAMPS AT I5 PSI FOR 24 HRS AT ROOM TEMP.

1"   1"
1/4"R.
1/4"
2"
1/4"
3/16"

1   2

TENSOLITE #1815

BELDEN #8434 STRAIN GAGE CABLE

PI – AMPHENOL #14S-5P

RED — D
GREEN — C
WHITE — B
BLACK — A
— E

3   4

LOAD CELLS ARE IN PHASE WHEN: GA. I & 3 ARE BOTH IN TENSION WHEN GA. 2 & 4 ARE BOTH IN COMPRESSION

GA. I   GA. 2
EXCITATION
GA. 4   GA. 3

SIGNAL OUT

3/8"R.

5   6
3/32"

1"

TENSOLITE #1815

BELDEN #8434 CABLE

WHITE
GREEN
BLACK

RI & R2, I50Ω1%

RI
R2

P2 – AMPHENOL #14S-5P

D
B
C
A
E

GA. 5   GA. 6
RI   R2

Figure 36. Wiring diagram and strain gage connection for vibration decay measurements.

88

The theoretical relationship between the mass of the wire, M_ℓ, and the corresponding oscillation frequency, σ_ℓ, can be expressed by the following equation:

$$M_\ell^* = M_s^* \left[\left(\frac{\sigma_s}{\sigma_\ell}\right)^2 - 1 \right].$$ (75)

M_ℓ^* is approximately equal to M_ℓ because the diameter of the cylinder is small in comparison with the length of the struts. M_s^* includes the effects of the cylinder and its supporting struts.

A straight line was obtained when M_ℓ was plotted versus $(\sigma_s/\sigma_\ell)^2 - 1$; its slope M_s^* was measured to be 0.0159 slugs. This equation was then used to obtain the generalized added mass, M_{am}^*, by replacing σ_ℓ with the measured natural frequency, σ_n, in water. M_{am}^* is approximately equal to M_{am} because the added mass of the struts and flanges is small in comparison to that of the cylinder. K_s^* is equal to $\sigma_s^2 M_s^*$.

The final step was to perform a static calibration in water whose results could be used to measure the steady-state drag forces and the cylinder displacements. A series of known horizontal loads was applied to the cylinder under submerged conditions and then the corresponding pen deflections were recorded. This resulted in a straight line relationship between load, F, and pen deflection, Δ, defined by $F = k_0 \Delta$, that was used to measure the steady-state drag forces. The static and dynamic displacements, X, were obtained from:

$$X = (k_0/K_s^*) \Delta .$$

b. <u>Submergence of the Cylinder.</u> One of the requirements was that the experiments simulate conditions representative of an infinite fluid. Consequently, it was necessary to position the cylinder so that effects of the free surface and impermeable bottom be negligible.

The location of the cylinder with respect to the free surface was determined by measuring the coefficient of added mass, C_{am}, for different submergences as the channel was being filled. The procedure was to tap the cylinder and measure the resulting σ_n. M_{am} was obtained using the method explained previously and C_{am} was then determined by dividing M_{am} by the equivalent water mass of the volume of the cylinder between the struts.

The results are shown plotted in Figure 37. Beyond a submergence of three diameters, C_{am} remained at a constant value of 1.07. On the basis of these results a submergence of 4.2 diameters was used for all the tests. For the 0.8-foot depth the cylinder was closer to the bottom, 0.36 foot above it, but no change in C_{am} was detected. Consequently, it was assumed that the bottom had no influence.
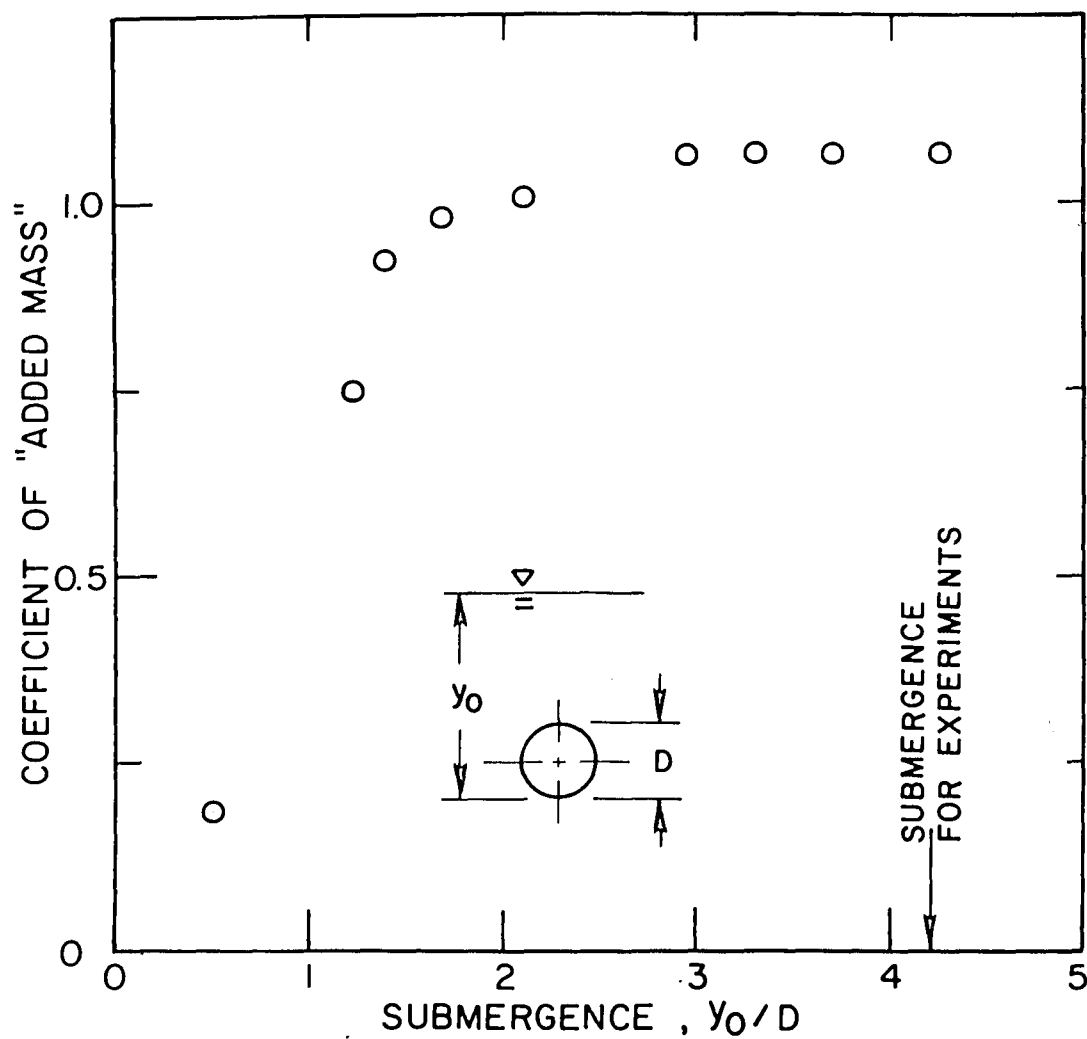
Figure 37. Effect of submergence on the measured coefficient of "added mass" in stillwater.

c. Measurement of Steady-State Forces. Steady-state forces were measured only for the 1.1-foot-depth case. Seven different centerline velocities, ranging from 0.40 to 2 feet per second were used. These corresponded to a Reynolds number range from 5.5×10^3 to 2.4×10^4 at a temperature of 74° Fahrenheit for which the kinematic viscosity, ν, is about 10^{-5} square feet per second.

d. Current-Velocity Profiles. Lateral and vertical profiles were measured for a centerline current velocity of 1.4 feet per second at a position of 0.5 foot upstream of the cylinder. The lateral variation was measured at 10 stations spanning the width of the channel. The results are shown plotted in Figure 38. They were used to correct the drag coefficients based on centerline velocities. The vertical profile was measured at the centerline of the channel. It was found to be uniform over the elevation range of $\pm 2.0D$ with respect to the axis of the cylinder.

e. Measurements of Vibration Decay. Vibration decay of the cylinder for the 1.1-foot depth was measured for three different initial displace-ments, X_0: 0.0015, 0.0030, and 0.0078 foot. This corresponds to X_0/D of 0.012, 0.024, and 0.0625, respectively. Only the maximum value was tested for the 0.8-foot-water depth. The initial displacement was pro-duced by a weight as shown in Figure 35. The string was cut at the weight by a pair of sharp scissors and the subsequent response was recorded.
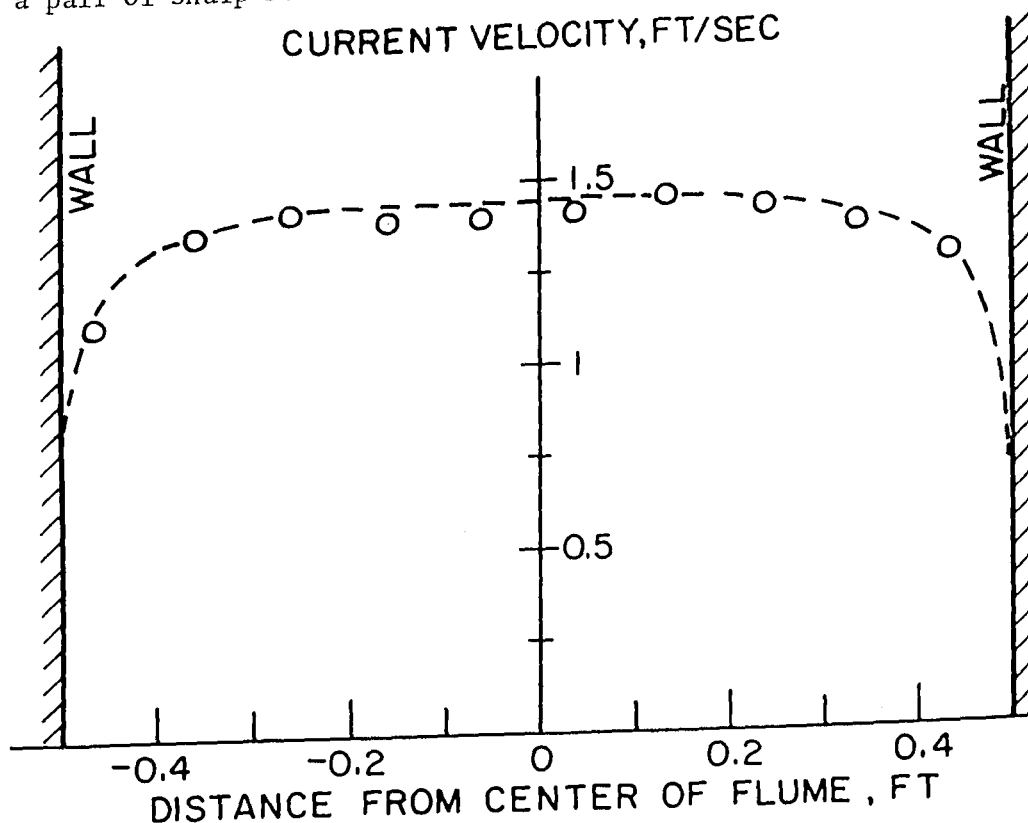

Figure 38. Lateral-velocity profile at centerline of cylinder.

Data were obtained in stillwater and flowing water. Eight different current velocities, up to 2 feet per second, were used for the 1.1-foot-water depth. Six values were used for the 0.8-foot-water depth, four of which were less than 2 feet per second and the other two reached up to 2.7 feet per second.

3. Analysis and Results.

    a. Steady-State Drag Coefficients. The steady-state force measurements were converted to drag coefficients, C_D, by the following equation:

$$C_D = \frac{F_D}{\frac{\rho}{2} A \, \overline{U}^2} \left(\overline{U}^2 \Big/ \overline{u^2} \right), \qquad (76)$$

where

A = projected area of cylinder and flanges,

$\overline{U}$ = centerline current velocity averaged over time,

$\overline{u}$ = current velocity at any lateral location averaged over time.

The term in the parentheses is the correction factor for C_D due to the nonuniformity of the current velocity across the width of the channel. $\overline{u^2}$ is the average value over the width of the channel of the square of the lateral-velocity profile of Figure 38 for $\overline{U} = 1.4$ feet per second. The correction was applied to all C_D's by assuming the velocity profiles for the other values of $\overline{U}$ were similar.

The resulting C_D's are shown plotted versus Reynolds number in Figure 39. The average value is about 0.9 up to a Reynolds number of 1.6×10^4 and about 1.0 for the rest of the range. The contribution due to wave resistance was estimated using equations presented by Wehausen and Laitone (1960) of Havelock's (1936) "first approximation". It was found to be less than 1 percent of the measured C_D's.

    b. Damping and Added Mass. Sample records of the vibration decay data for the 1.1-foot depth are shown in Figure 39. The upper two records were obtained in stillwater for the maximum and minimum initial displacements, respectively. The lower two records were obtained in flowing water whose velocity was 2 feet per second. Similar records were obtained for other velocities.

The records showed that the natural frequency in water was not affected by the velocity of the current and did not change as the amplitude of vibration decayed; it remained at the stillwater value of 126 radians per second (20 cycles per second). Consequently, the coefficient of added mass was also constant, equal to 1.07 that was measured during the submergence tests in stillwater.
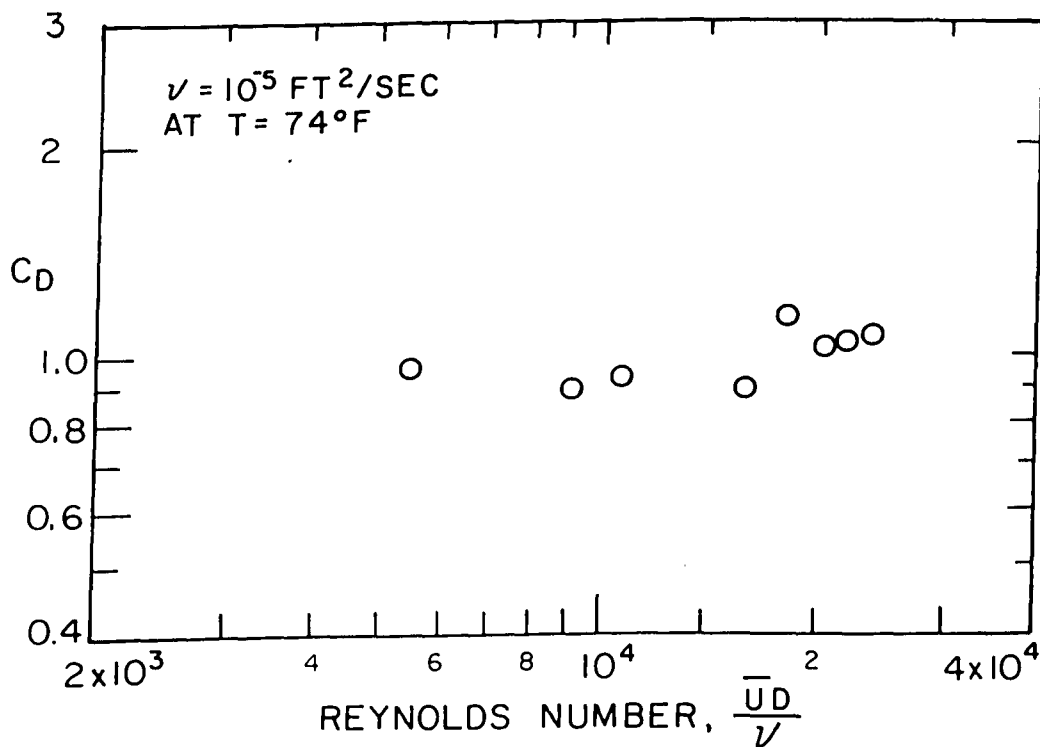
Figure 39. Drag coefficient for still cylinder.

An initial analysis indicated that the vibration-decay was exponential in time, implying that the damping is due to a force that is directly proportional to the velocity of the cylinder. This information, together with the results of the static calibration that showed the imposed force to be linearly related to displacement and the invariancy of the added mass with respect to the amplitude of vibration, imply a linear dynamic system whose equation of motion for free vibrations can be written as:

$$\ddot{X}(t) + 2\sigma_n \xi \dot{X}(t) + \sigma_n^2 X(t) = 0, \tag{77}$$

where

$$\xi = \xi_s M_s^* / (M_s^* + M_{am}^*) + \xi_{vi}, \tag{78}$$

ξ_s = structural damping measured in air; equal to 0.00096,

ξ_{vi} = hydrodynamic damping.

Using equation 75 and its subsequent discussion, ξ, can be expressed as:

$$\xi = \frac{\xi_s}{(\sigma_s/\sigma_n)^2} + \xi_{vi}, \tag{79}$$

where the first term is equal to 0.0004. ξ_{vi} was assumed to be equal to ξ because this first term was less than 5 percent of the measured values of ξ.

The calculation of ξ was based on the following well-known solution of the above differential equation for the initial conditions $X(0) = X_0$ and $\dot{X}(0) = 0$ (Biggs, 1964):

$$X(t) = X_0 e^{-\sigma_n \xi t} (\xi \sin \sigma_n t + \cos \sigma_n t). \tag{80}$$

For small values of ξ this reduces to:

$$X(t) = X_0 e^{-\sigma_n \xi t} \cos \sigma_n t. \tag{81}$$

If $t = 2\pi m / \sigma_n$ then $X(t)$ coincides with the m-th amplitude, X_m, $(m \leq 1)$ of the vibration-decay curve which is given by:

$$X_m = X_0 e^{-2\pi \xi m}. \tag{82}$$

This relation is also valid for the $(m + n)$-th amplitude that is scaled by an arbitrary constant and therefore can be used to obtain ξ for any part of the vibration-decay record using arbitrary units for the amplitude.

ξ was calculated for each record on the basis of the 16 cycles near the beginning of the records that are delineated by the arrows in Figure 40. The first few cycles were not used because of disturbances created by cutting the string. Equation (82) was assumed to represent the vibration-decay over these 16 cycles except that X_0 corresponded to the first amplitude preceding the 16 cycles. For this purpose X_0 will be denoted by X_0' in the following logarithmic version:

$$\ln X_m = \ln X_0' - 2\pi \xi m \tag{83}$$

ξ as well as $\ln X_0'$ were assumed unknown and solved for by a least-squared-error procedure. X_m was defined by one-half of the distance between a trough and the following crest. This eliminated effects of fluctuations whose time scale was larger than the natural period of the oscillations. For each initial displacement and $\bar{U}$ two records were available and consequently two values of ξ were calculated. These were averaged for plotting purposes.

The values of ξ are shown plotted in Figure 41 versus $\bar{U}$ and an oscillation Strouhal number, $\sigma_n D / 2\pi \bar{U}$. The values corresponding to $X_0 = 0.00030$ foot are not shown because they were essentially the same as for the other two X_0's except for the two largest values of $\bar{U}$. In this case, ξ plotted between those corresponding to $X_0 = 0.0015$ and 0.0078 foot.
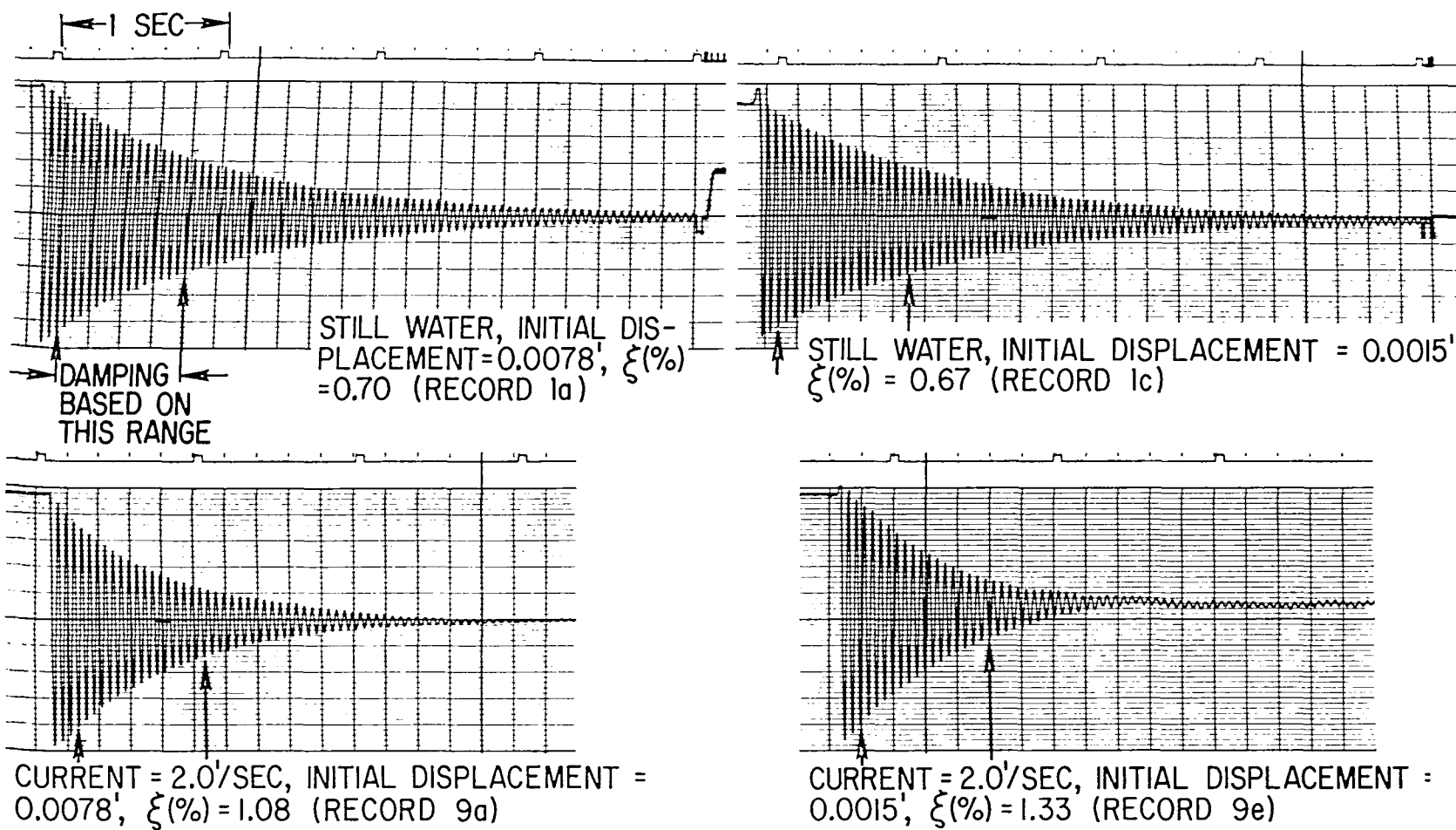
94

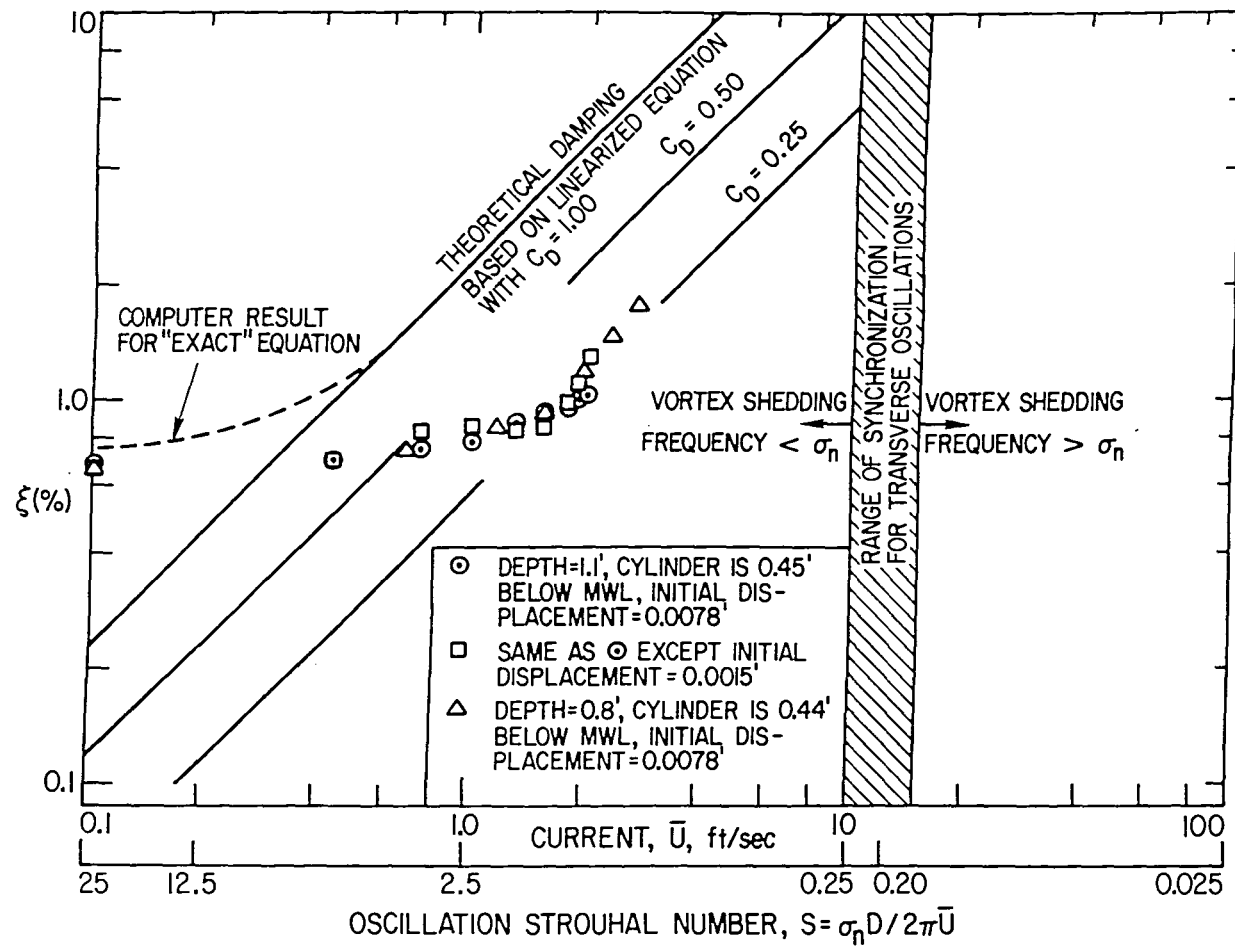Figure 40. Sample records of vibration decay in water (test VI-55).

Figure 41. Effect of current on damping.

4. Discussion of Results.

a. Comparison of Damping with Predictions Based on the Modified Morison Equation. The differential equation of motion for free vibrations of the cylinder in a steady current for the case where the viscous forces are represented by the drag-force interaction term of the modified Morison equation is given by:

$$\ddot{X} + \frac{C_D (\rho/2) A}{M^*} \, |\dot{X} - \bar{U}| \, (\dot{X} - \bar{U}) + \sigma_n^2 X = 0 , \qquad (84)$$

where

$$M^* = M_s^* + M_{am}^* .$$

(In this equation structural damping is not included.)
If $\dot{X} \ll \bar{U}$, the equation can be linearized to yield the following approximation:

$$\ddot{X} + \frac{C_D \rho A \bar{U}}{M^*} \, \dot{X} + \sigma_n^2 X = 0 . \qquad (85)$$

Comparing the damping force of this equation with that of equation (77) implies that

$$\xi = \frac{C_D \rho A \bar{U}}{2 \sigma_n M^*} . \qquad (86)$$

Assuming that the average C_D is equal to 1.0, as measured from the steady-state forces, this equation becomes equal to:

$$\xi(\%) = 2.48 \, \bar{U} . \qquad (87)$$

Figure 40 shows that the theoretical results overpredict the measured values. The measured values increase gradually to about 1.8 feet per second and then become asymptotic to the predicted results for which C_D is about 0.25.

The dotted line represents theoretical results obtained from a numerical solution of the "exact" equation (equation 84). A fourth-order Runge-Kutta technique (Hamming, 1962) was used with a time step equal to 1/20th of the natural period of oscillation. The accuracy of the numerical method was checked by applying it to solve equation (77) for which an analytical solution could be obtained. The numerical and analytical results were indistinguishable for this time step. Therefore, the numerical method was assumed valid for the exact nonlinear equation. The numerical solution showed that the vibration-decay was not exponential. Therefore, the dotted line does not have the same meaning as for the linear system; it simply indicates when the linearization becomes valid.

97

b. Interpretation of Comparison. It can be shown by use of dimensional analysis that the force acting on a submerged cylinder that is forced to oscillate with an amplitude X_0 in an oncoming current can be specified in terms of the following three parameters: (a) X_0/D; (b) $\sigma_n D^2/\nu$; and (c) $\sigma_n D/2\pi\overline{U}$.

The significance of the first two parameters can be understood best if they are interpreted for the case of no current. The first parameter is a measure of the ratio of the force due to the local acceleration of the fluid to that due to the convective acceleration. It can also be interpreted as a measure of the distance that vorticity, generated by the cylinder, is convected in relation to D during one cycle of oscillation. If it is small, then according to Batchelor (1967), the vorticity cannot be convected too far away from the cylinder before the convection velocity reverses thereby generating vorticity of the opposite sign. Consequently, no net vorticity is generated. Keulegan and Carpenter (1958) have shown experimentally that this parameter controls the generation of vortices in the wake of a fixed cylinder that is subjected to an oscillating flow field (in this case, X_0 is the amplitude of the water particle excursion). The second parameter is a type of Reynolds number. It is a measure of the distance that the generated vorticity of one sign diffuses with respect to D during one cycle (Batchelor, 1967). In order for the vorticity to be confined in a boundary layer this parameter must be much larger than unity (Wang, 1968).

For most practical situations in which the cylinder is oscillating (rather than the external flow) X_0/D will be significantly less than one and $\sigma_n D^2/\nu$ will probably be larger than 10^3. In that case the vorticity will be contained in a boundary layer. As a consequence separation of the boundary layer will be inhibited and the rest of the flow field will be irrotational. This implies that in still water the added-mass forces can be adequately predicted by potential theory and the viscous forces can be calculated by using linear boundary-layer theory in which the convective accelerations are neglected.

The results of the experiments in this section verify the latter conclusions regarding the forces in still water. Figure 37 proves that potential theory adequately predicts the measured coefficient of added mass for the case of large submergence. The viscous forces are also adequately predicted. Calculations using Batchelor's (1967) result for the viscous force yielded a value of $\xi_{vi}(\%) = 0.46$ which gives $\xi(\%) = 0.50$ when corrected for structural damping by use of equation (79). This latter value is close to the measured value of 0.70.

The effect of the current is defined by the third parameter, herein referred to as the oscillation Strouhal number, S_0. Lighthill (1954) and Pedley (1972) studied the importance of this parameter in defining the flow in the boundary layer for the case of a fixed cylinder in a current with superimposed fluctuations. The velocity of the fluctuations was taken to be always less than or equal to the mean current so that

flow reversal would not have to be considered. Their conclusions apply as well to the case where the cylinder oscillates in a steady current. They show that the quasi-steady assumption is approached as this parameter becomes small. But at the other extreme, when the parameter becomes large, the oscillatory boundary layer is contained within the boundary layer caused by the mean current and therefore the two flow fields may be considered independent.

According to the foregoing analysis, the present experimental results for damping, as plotted in Figure 41, are in the region for which the quasi-steady assumption is not valid. This appears to explain qualitatively the difference between the damping predicted by the drag-force interaction term and the measured values. The increase of ξ with decreasing S_o indicates that interaction of the oscillatory flow with the mean current becomes increasingly important and acts to increase the damping. The mechanism involved in causing the increase of ξ cannot be determined from this data; however, the gradualness of the increase suggests that it is due to increased shear stresses caused by the interaction.

The validity of the quasi-steady assumption for low values of S_o has been shown by Parkinson and Modi (1967) and Novak (1969). They present data on the transverse response of prismatic cylinders to steady wind and show comparisons with the quasi-steady predictions. Good agreement is found provided the vortex shedding frequency, σ_v, is sufficiently high with respect to the natural frequency of the cylinders. The required separation distance of the two frequencies depends on the shape of the cylinders.

The implications of the present data and current understanding of the interaction problem on damping of offshore platforms are not entirely clear. As stated at the beginning of this section the major part of the damping implied by the drag-force interaction term will occur during the passage of the largest waves. In that case, S_o could be calculated in order to see if the damping mechanism is operative. $\overline{U}$ could be assumed to be equal to the maximum water particle velocity at the MWL for a wave whose height and period is the significant height and significant period, respectively, corresponding to the design condition. If the resulting S_o is much lower than 0.20 (the value at which $\sigma_n = \sigma_v$) then the quasi-steady assumption may be valid and the damping mechanism operative. Otherwise vortex shedding may provide additional excitation energy if S_o is too close to 0.20 and the damping may be insignificant if S_o is much higher than 0.20.

c. Effect of Current on Added Mass. The coefficient of added mass was not affected by the current and was equal to the potential theory value. This was also discovered by Protos, Goldschmidt, and Toebes (1968) for forced oscillations of circular and triangular cylinders in the direction transverse to an oncoming current. Their experiments covered the range of σ_n/σ_v from 0 to 2.0; their relative oscillation amplitudes, X_o/D, were less than 0.072. It appears that potential theory is valid

for predicting coefficients of added mass provided the oscillation amplitudes are small in comparison to the cylinder diameter. The motion of the surrounding water does seem to influence the potential theory values.

V. SUMMARY AND CONCLUSIONS

A theoretical and experimental study was undertaken to investigate the "added mass" and hydrodynamic damping for offshore platforms.

Classical potential theory with linearized boundary conditions was used to formulate the steady-state dynamic response problem for a platform idealized by a vertical surface-piercing cylinder of constant diameter in finite water depth. The hydrodynamic forces due to wavemaking and added mass were investigated as a function of oscillation frequency, cylinder diameter, water depth, and mode shape. Importance of wavemaking as a damping mechanism was investigated for idealized and proposed platforms. The following findings were made:

1. The nondimensionalized wavemaking force and the coefficient of added mass are functions of only two parameters, kh and ka or alternatively, $\sigma^2 h/g$ and D/h, and the mode shape $\psi(y)$.

2. The wavemaking forces may be considered localized in the near-surface zone for most practical applications. In that case the force depends on only one parameter, $F_0 = \sigma\sqrt{D/g}$, and may be considered independent of mode shape.

3. The coefficient of added mass consists of two components: (a) a "local" component concentrated in the near-surface zone and (b) an "overall" component that extends over the total water depth. As a result the coefficient depends on both parameters and the mode shape and varies with respect to elevation. It ranges from values significantly greater than one all the way to negative values. A uniform value of 1 may be used over all elevations if D/h is less than 0.01.

4. The effectiveness of wavemaking as a damping mechanism, specified in terms of fraction of critical damping, ξ_w, depends on σ, h, D, $\psi(y)$ and the structural mass. Values of damping ranging from 2 to 4 percent of critical could be attained for platforms that have natural periods of about 4 seconds in a water depth of 600 feet provided the cylinder diameters are larger than 30 feet.

5. Damping for a number of proposed platforms proved to be negligible because the diameters in the near-surface zone were small.

Experiments were conducted to verify the wavemaking and added-mass forces predicted by the potential theory. Rigid vertical cylinders were

oscillated with simple-harmonic motion in a translation mode. The oscillations were performed in still water. Total forces and radiated waves were measured. The following findings were made:

1. The measured wavemaking forces compared very well with the theoretical predictions. In the range where deepwater waves were generated all the measured values plotted on one curve as a function of F_0 irrespective of the cylinder diameter and water depth.

2. The measured coefficients of added mass also compared very well with the theoretical predictions.

3. Wavemaking forces derived from the measured radiated waves were on the average underestimated by 20 percent.

4. External hydrodynamic forces on oscillating bodies can be reliably measured provided lightweight material is used for the bodies and great care is taken in designing the mechanical equipment so that all components are rigid.

An experimental study was made in an attempt to verify the hydrodynamic damping implied by the drag-force interaction term of the modified Morison equation. Decay of vibrations and the corresponding hydrodynamic damping were measured when an elastically supported circular cylinder was given an initial displacement and then suddenly released. The cylinder was completely submerged and its motion was constrained to be in the direction of an oncoming current. Coefficients of added mass were also measured. The following findings were made:

1. The drag-force interaction term predicted damping values that were about 4 times as large as the corresponding measured values. However, boundary-layer theory indicates that the quasi-steady assumption in the modified Morison equation is valid only when the oscillation Strouhal number, $S_0 = \sigma_n D/2\pi\overline{U}$, approaches zero. Consequently, the disagreement between measured and predicted values of the damping is probably due to the fact that S_0 was large for the experiments.

2. The measured coefficient of added mass corresponded to the potential theory value for all current velocities.

LITERATURE CITED

BARNETT, T.P., "Observations of Wind Wave Generation and Dissipation in the North Sea: Implications for the Offshore Industry," Paper No. OTC 1516, *1972 Offshore Technology Conference*, Houston, Texas, pp. I-44-I-48.

BATCHELOR, G.K., *An Introduction to Fluid Dynamics*, Cambridge University Press, 1967, 615 pp.

BIDDE, D.D., "Wave Forces on a Circular Pile Due to Eddy Shedding," HEL 9-16, University of California, Berkeley, June 1970, 141 pp.

BIESEL, F., and SUQUET, F., "Laboratory Wave Generating Apparatus," Translation of a series of articles from La Houille Blanche, Nos. 2-, 4-, and 5-1951; No. 6-1952, St. Anthony Falls Hydraulic Laboratory, University of Minnesota, 27 pp.

BIGGS, J.M., *Introduction to Structural Dynamics*, McGraw-Hill, New York, 1964, 341 pp.

BREWER ENGINEERING LABORATORIES, INC., "Final Report, Motion Analysis of Texas Tower No. 4," Contract No. AF30(635)--7317, June 1959.

BURKE, B.G., and TIGHE, J.T., "A Series Model for Dynamic Behavior of Offshore Structures," *Journal of the Society of Petroleum Engineers*, Vol. 12, No. 2, Apr. 1972, pp. 165-170.

CHOPRA, A.K., "Hydrodynamic Pressure on Dams During Earthquakes," *Journal of the Engineer Mechanics Division*, ASCE, Vol. 93, No. EM6, Dec. 1967, pp. 205-223.

CHOPRA, A.K., "Earthquake Behavior of Reservoir--Dam Systems," *Journal of the Engineer Mechanics Division*, ASCE, Vol. 94, No. EM6, Dec. 1968, pp. 1475-1499.

CHOPRA, A.K., "Earthquake Response of Concrete Gravity Dams," *Journal of the Engineer Mechanics Division*, ASCE, Vol. 96, No. EM4, Aug. 1970, pp. 443-454.

CLOUGH, R.W., "Effects of Earthquakes on Underwater Structures," *Proceedings of Second World Conference on Earthquake Engineering*, Vol. II, Japan, 1960, pp. 815-831.

DWIGHT, H.B., *Tables of Integrals and Other Mathematical Data*, Macmillan, New York, 1961.

FOSTER, E.T., Jr., "Model for Nonlinear Dynamics of Offshore Towers," *Journal of the Engineer Mechanics Division*, ASCE, Vol. 96, No. EM1, Feb. 1970, pp. 41-67.

GARRISON, C.J., and BERKLITE, R.B., "Impulsive Hydrodynamics of Submerged Rigid Bodies," *Journal of the Engineer Mechanics Division,* ASCE, Vol. 99, No. EM1, Feb. 1973, pp. 99-120.

HAMMING, R.W., *Numerical Methods for Scientists and Engineers,* McGraw-Hill, New York, 1962, 411 pp.

HAVELOCK, T.H., "Forced Surface-Waves on Water," *Philosophical Magazine,* Vol. VIII, Oct. 1929, pp. 304-311.

HAVELOCK, T.H., "The Pressure of Water Waves Upon a Fixed Obstacle," *Proceedings of the Royal Society of London,* Ser. A, Vol. 175, July 1940, pp. 409-421.

HOERNER, J.B., and JENNINGS, P.C., "Modal Interference in Vibration Tests," *Journal of the Engineer Mechanics Division,* ASCE, Vol. 95, No. EM4, Aug. 1969, pp. 827-839.

JACOBSEN, L.S., "Impulsive Hydrodynamics of Fluid Inside A Cylindrical Tank and of Fluid Surrounding a Cylindrical Pier," *Bulletin, Seismological Society of America,* Vol. 39, 1949, pp. 189-204.

KEULEGAN, G.H., and CARPENTER, L.H., "Forces on Cylinders and Plates in an Oscillating Fluid," *Journal of Research of the National Bureau of Standards,* Vol. 60, No. 5, May 1958, pp. 423-440.

LANDWEBER, L., "Vibration of a Flexible Cylinder in a Fluid," *Journal of Ship Research,* Vol. 11, No. 3, Sept. 1967, pp. 143-150.

LIGHTHILL, M.J., "The Response of Laminar Skin Friction and Heat Transfer to Fluctuations in the Stream Velocity," *Proceedings of the Royal Society of London,* Ser. A, Vol. 224, June 1954, pp. 1-23.

MacCAMY, R.C., and FUCHS, R.A., "Wave Forces and Piles: A Diffraction Theory," TM-69, Beach Erosion Board, Washington, D.C., Dec. 1954.

MADSEN, O.S., "On the Generation of Long Waves," *Journal of Geophysical Research,* Vol. 76, No. 36, Dec. 1971, pp. 8672-8683.

MALHOTRA, A.K., and PENZIEN, J., "Sochastic Analysis of Offshore Tower Structures," Earthquake Engineering Research Center, Report No. EERC 69-6, University of California, Berkeley, Calif., May 1969, 160 pp.

MALHOTRA, A.K., and PENZIEN, J., "Response of Offshore Structures to Random Wave Forces," *Journal of the Structures Division,* ASCE, Vol. 96, No. ST10, Oct. 1970, pp. 2155-2173.

MORISON, J.R., et al., "The Force Exerted by Surface Waves on Piles," *Petroleum Transactions,* Vol. 189, TP 2846, 1950, pp. 149-154.

NATH, J.H., and HARLEMAN, D.R.F., "Dynamics of Fixed Towers in Deep-Water Random Waves," *Journal of the Water and Harbor Division,* ASCE, Vol. 95, No. WW9, Nov. 1969, pp. 539-556.

NATH, J.H., and HARLEMAN, D.R.F., "Response of Vertical Cylinder to Random Waves," *Journal of the Water and Harbor Division,* ASCE, Vol. 96, No. WW2, May 1970, pp. 373-386.

NOVAK, M., "Aeroelastic Galloping of Prismatic Bodies," *Journal of the Engineer Mechanics Division,* ASCE, Vol. 95, No. EM1, Feb. 1969, pp. 115-142.

OGILVIE, T.F., "First- and Second-Order Forces on a Cylinder Submerged Under a Free Surface," *Journal of Fluid Mechanics,* Vol. 16, Part 3, July 1963, pp. 451-473.

PARKINSON, G.V., and MODI, V.J., "Recent Research on Wind Effects on Bluff Two-Dimensional Bodies," *Proceedings of the International Research Seminar; Wind Effects on Buildings and Structures,* Ottawa, Canada, Sept. 1967, Vol. I., pp. 485-513.

PEDLEY, T.J., "Two-Dimensional Boundary Layers in a Free Stream Which Oscillates Without Reversing," *Journal of Fluid Mechanics,* Vol. 55, Part 2, 1972, pp. 359-383.

PENZIEN, J., KAUL, M.K., and BERGE, B., "Stochastic Response of Offshore Towers to Random Sea Waves and Strong Motion Earthquakes," *Computers and Structures,* Vol. 2, 1972, pp. 733-755.

PHILLIPS, O.M., "The Equilibrium Range in the Spectrum of Wind-Generated Waves," *Journal of Fluid Mechanics,* Vol. 4, 1958, pp. 426-434.

PHILLIPS, O.M., *The Dynamics of the Upper Ocean,* Cambridge University Press, 1966, 261 pp.

PIERSON, W.J., Jr., and MOSKOWITZ, L., "Proposed Spectral Form for Fully Developed Wind Seas Based on Similarity Theory of S.A. Kitaigorodskii," *Journal of Geographical Research,* Vol. 69, No. 24, Dec. 1964, pp. 5181-5190.

PROTOS, A., GOLDSCHMIDT, V.W., and TOEBES, G.H., "Hydroelastic Forces on Bluff Cylinders," *Journal of Basic Engineering,* Sept. 1968, pp. 378-386.

ROSHKO, A., "Experiments on the Flow Past a Circular Cylinder at Very High Reynolds Number," *Journal of Fluid Mechanics,* Vol. 10, Part 3, May 1961, pp. 345-356.

SCHLICHTING, H., *Boundary-Layer Theory,* McGraw-Hill, New York, 1968, 747 pp.

SELNA, L., and CHO, D., "Resonant Response of Offshore Structures," *Journal of the Water, Harbor, and Coastal Engineering Division,* ASCE, Vol. 98, No. WW1, Feb. 1972, pp. 15-24.

SHUBINSKI, R.P., WILSON, E.L., and SELNA, L.G., "Dynamic Response of Deepwater Structures," *Proceedings of the ASCE Conference on Civil Engineering in the Oceans,* San Francisco, Calif., 1967, pp. 123-146.

TICK, L.J., "Differential Equation with Frequency-Dependent Coefficients," *Journal of Ship Research,* Vol. 3, No. 2, Oct. 1959, pp. 45-46.

VUGTS, J.H., Jr., "Cylinder Motions in Beam Waves," Netherlands Ship Research Center TNO, Report No. 1155, Dec. 1968, 23 pp.

WANG, CHANG-YI, "On High-Frequency Oscillatory Viscous Flows," *Journal of Fluid Mechanics,* Vol. 32, Part 1, 1968, pp. 55-68.

WEHAUSEN, J.V., and LAITONE, E.V., "Surface Waves," *Encyclopedia of Physics,* Vol. IX, Springer-Verlag, Berlin, 1960, pp. 445-777.

WEHAUSEN, J.V., "The Motion of Floating Bodies," *Annual Review of Fluid Mechanics,* Vol. 3, 1971, pp. 237-268.

WIEGEL, R.L., and DELMONTE, R.C., "Wave-Induced Eddies and 'Lift' Forces on Circular Cylinders," HEL 9-19, University of California, Berkeley, July 1972, 40 pp.

APPENDIX A

THE FUNCTIONS $P_1(x)$, P_2, AND P_3

Computer results for these functions are plotted in the figure to this Appendix. The following are approximate representations of these functions, accurate to within 1 to 2 percent, for large and small arguments. They are derived using a combination of computer results and expansions of Bessel functions as given by Dwight (1961).

(a) $P_1(x) = \dfrac{2/\pi x}{J_1'(x)^2 + Y_1'(x)^2}$

for $x < 5$; $P_1 \approx \dfrac{\pi}{2} x^3$

for $x > 2$; $P_1 \approx 1.0$

(b) $P_2(x) = - \left[J_1(x)J_1'(x) + Y_1(x)Y_1'(x) \right] / \left[J_1'(x)^2 + Y_1'(x)^2 \right]$

for $x < 3$; $P_2 \approx x$

for $x > 3$; $P_2 \approx 1/2x$

(c) $P_3(x) = - K_1(x)/K_1'(x)$

for $x < .2$; $P_3 \approx x$

for $x > \approx 20$; $P_3 \approx 1.0$
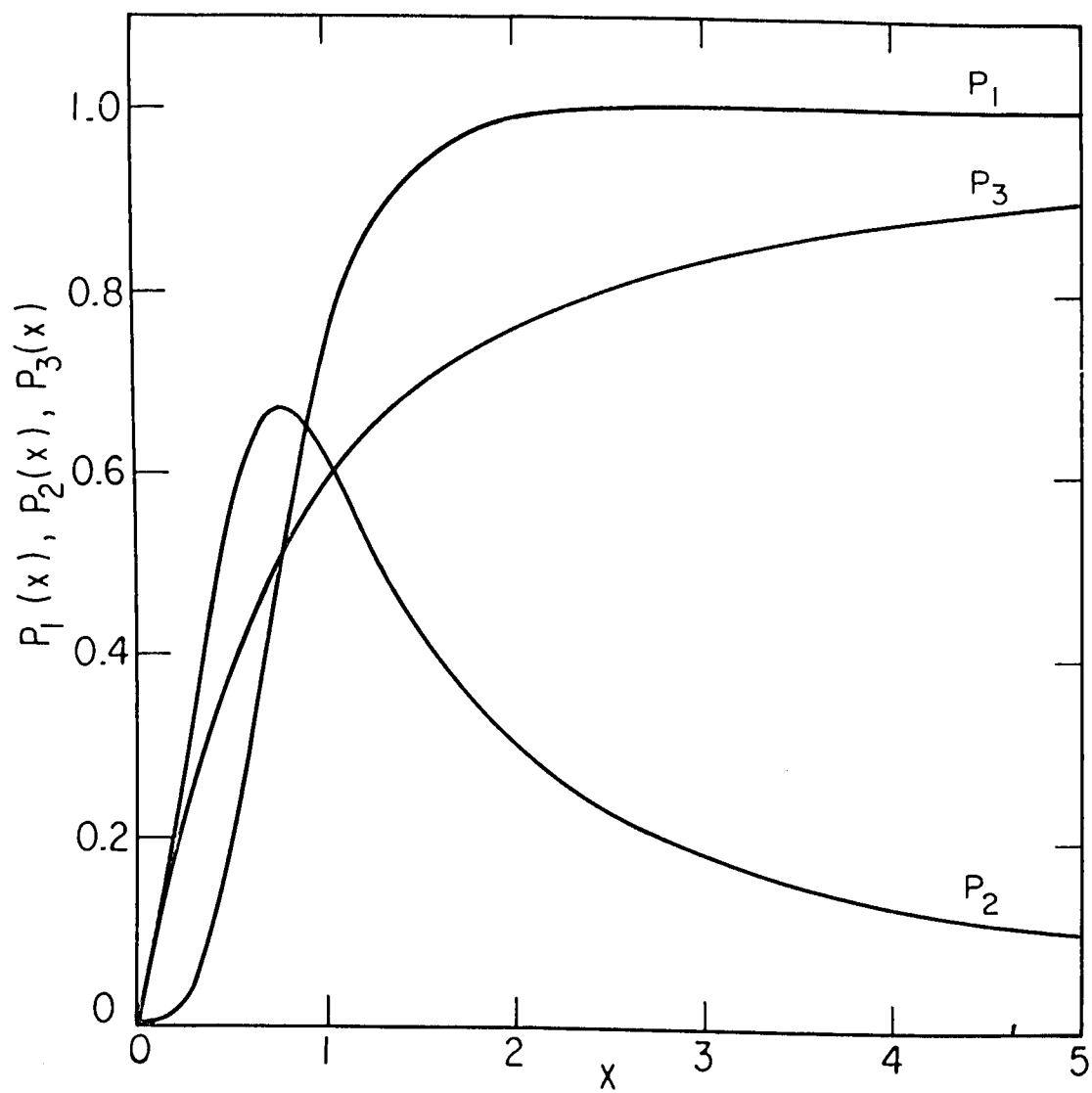
The functions $P_1(x)$, $P_2(x)$, $P_3(x)$.

APPENDIX B

EQUATIONS USED TO CALCULATE R_{am}^*

For any mode shape:

$$R_{am}^* = \left\{ \left(\frac{2}{h}\right)\frac{h}{a} \int_{-h}^{0} \left[G_0(kh)P_2(ka)\cosh k(y+h) \right.\right.$$

$$\left.\left. + \sum_{m=1}^{\infty} G(\alpha_m h)P_3(\alpha_m a)\cos\alpha_m(h+y) \right] \psi(y)dy \right\} \Bigg/ \left(\frac{1}{h} \int_{-h}^{0} \psi^2(y)dy \right).$$

1. Cantilever mode; $\psi(y) = 1 - \cos \pi/2(1 + y/h)$.

(a) $\quad \dfrac{1}{h} \displaystyle\int_{h}^{0} \psi^2(y)dy = \dfrac{3}{2} - \dfrac{4}{\pi} = 0.228$.

(b) $\quad R_{am}^* = (1/.228) \left\{ \dfrac{2\sinh^2 kh}{kh(\sinh kh\cosh kh + kh)} \left[1 - \dfrac{\pi(kh)}{2\tanh kh[(kh)^2 + (\frac{\pi}{2})^2]} \right]^2 \right.$

$$\dfrac{P_2(ka)}{ka} + 2\left(\dfrac{h}{a}\right) \sum_{m=1}^{\infty} \dfrac{\sin^2\alpha_m h}{(\alpha_m h)^2(\sin\alpha_m h\cos\alpha_m h + \alpha_m h)}$$

$$\left. \left[1 - \dfrac{\pi(\alpha_m h)}{2\tan\alpha_m h[(\frac{\pi}{2})^2 - (\alpha_m h)^2]} \right]^2 P_3(\alpha_m a) \right\}.$$

109

2. Higher modes; $\psi(y) = \sinh \pi/2(1 + y/h)$: n = 3, 5, and 7.

(a) $\dfrac{1}{h} \displaystyle\int_{-h}^{0} \psi^2(y) = \dfrac{1}{2}$.

(b) $R^*_{am} = \dfrac{4kh}{\sinh kh \cosh kh + kh} \left[\dfrac{n\frac{\pi}{2} + (-1)^{\frac{n+1}{2}} kh \sinh kh}{(kh)^2 + (\frac{\pi}{2} n)^2} \right]^2$

$\dfrac{P_2(ka)}{(ka)} + 4\left(\dfrac{h}{a}\right) \displaystyle\sum_{m=1}^{\infty} \dfrac{P_3(\alpha_m a)}{\sin \alpha_m h \cos \alpha_m h + \alpha_m h}$

$\left[\dfrac{n\frac{\pi}{2} - (-1)^{\frac{n+1}{2}} \alpha_m h \sin \alpha_m h}{(n\frac{\pi}{2})^2 - (\alpha_m h)^2} \right]^2$.

Petrauskas, Charles
  Hydrodynamic damping and ''added mass'' for flexible offshore plat-
forms / by Charles Petrauskas — Fort Belvoir, Va. : U.S. Coastal
Engineering Research Center, 1976.
  110 p. : ill. (Technical paper — U.S. Coastal Engineering Research
Center ; DACW72-69-C-0001) Also (Technical report — University of
California, Hydraulic Engineering Laboratory ; 9-23)
  Bibliography : p. 102-106.
  Dynamic responses of flexible platforms due to wind-generated waves
are an important design consideration. This study presents the theo-
retical and experimental study of hydrodynamic damping and
''added mass.''
  1. Damping. 2. Offshore structures. 3. Structural dynamics.
4. Wave forces. I. Title. II. Series : U.S. Coastal Engineering
Research Center. Technical paper no. 76-18. III. U.S. Coastal Engi-
neering Research Center. Contract DACW72-69-C-0001. IV. Series:
California. University. Hydraulic Engineering Laboratory. Technical
Report HEL-9-23.
  TC203   .U581tp   no.76-18   627   .U581tp